1987

A theoretical model for a volcanic column-plume

M. E. Giordano
San Jose State University

Order Number 1332027

A theoretical model for a volcanic column-plume

Giordano, Marco Evan, M.A.

San Jose State University, 1987

U·M·I
300 N. Zeeb Rd.
Ann Arbor, MI 48106

A THEORETICAL MODEL
FOR
A VOLCANIC COLUMN - PLUME

A Thesis

Presented to

The Faculty of the Graduate Program in Natural Science

in the

Department of Physics

Department of Meteorology

Department of Geology

San Jose State University

In Partial Fulfillment

of the Requirements for the Degree

Master of Arts

By

M. E. Giordano

May, 1987

Approved for the Graduate Program in Natural Science

Dr. Patrick Hamill

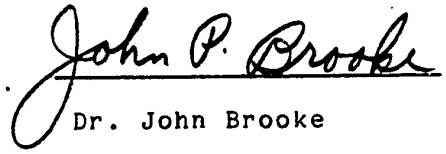

Dr. John Brooke

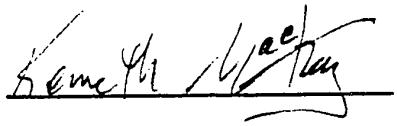

Dr. Kenneth MacKay

Approved for the University

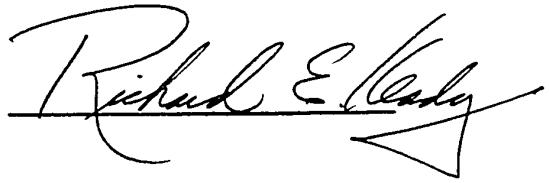

A THEORETICAL MODEL

FOR

A VOLCANIC COLUMN - PLUME

By

M. E. Giordano

May, 1987

Abstract of The Treatise

A THEORETICAL MODEL

FOR

A VOLCANIC COLUMN - PLUME

by

M. E. Giordano

Department of Physics

San Jose State University

1987

A set of simultaneous equations based upon the hydrodynamics and thermodynamics of a volcanic column-plume are derived and cast into the framework of a one-dimensional computer model. These equations were modified to account for the concentration of ash material, the drag forces resulting from larger-than-ash pyroclastic material, and the ratio of carbon dioxide to steam (H_2O vapor phase) in the gaseous effluent. Drag forces act on particulates of sizes down to one micron radius. Sub-micron particulates affect the buoyancy by increasing the mass of the plume gas.

Solutions to the set of dynamic equations give mean flow velocity, differential temperature above the

ambient environment, ash fraction, plume composition, plume radius, particulate size distribution, and particle velocities, all as functions of altitude above the vent. Numerical experiments were performed to examine the effect of changing the initial value conditions upon the resulting characteristic fields of the modeled flow. A series of sensitivity tests were run as a validation of the physical basis of the model. Results of these studies revealed the sensitivity of the model to changes in the flow parameters, solid particulate parameters, gaseous constituents, and environmental parameters. The effects of these changes on velocity, radius, differential temperature and maximum plume height are presented.

The model was used to simulate the La Soufriere (1979) volcanic event. The input parameters were obtained from observations cited in the literature; in cases of variables not measured, such as plume centerline temperature, the model was run using a range of reasonable values. The results obtained are shown to agree well with observations of the plume.

Table of Contents

List of Figures

The following figures appear in consecutive order displayed one figure per page starting at page 156:

Figure 77. Effect of the mode radius of the particulate distribution function with a_g = 250 microns. Velocity contours of the pyroclastic particulates within the sizes ranging below 10,000 micron radius. Each line represents a contour of velocities at equal height intervals of 500 meters along the length of the established VCP.

Figure 78. Effect of the mode radius of the particulate distribution function with a_g = 250 microns. Velocity contours of the pyroclastic particulates of the entire size distribution. Each line represents a contour of velocities at equal height intervals of 500 meters along the length of the established VCP.

Figure 79. Effect of the standard deviation of the particulate distribution function with σ = 1.25 microns. Velocity - height profiles of the pyroclastic particulates (all 50 bins).

Figure 80. Effect of the standard deviation of the particulate distribution function with σ = 1.25 microns. Velocity contours of the pyroclastic particulates within the sizes ranging below 1,000 micron radius. Each line represents a contour of velocities at equal height intervals of 500 meters along the length of the established VCP.

Figure 81. Effect of the standard deviation of the particulate distribution function with σ = 1.25 microns. Velocity contours of the pyroclastic particulates within the sizes ranging below 10,000 micron radius. Each line represents a contour of velocities at equal height intervals of 500 meters along the length of the established VCP.

Figure 82. Effect of the standard deviation of the particulate distribution function with σ =

values for each case within the 18 to 21 kilometer maximum range.

Figure 108. La Soufriere Simulation: Effect of ambient relative humidity for the 449 cases similar to the La Soufriere event. Number of occurrences plotted against the individual values for each case within the 18 to 21 kilometer maximum range.

Figure 109. La Soufriere Simulation: Effect of initial pyroclastic number concentration (particles per cubic meter) for the 449 cases similar to the La Soufriere event. Number of occurrences plotted against the individual values for each case within the 18 to 21 kilometer maximum range.

Figure 110. La Soufriere Simulation: Effect of initial mode radius of the particulate distribution for the 449 cases similar to the La Soufriere event. Number of occurrences plotted against the individual values for each case within the 18 to 21 kilometer maximum range.

List of Tables

Acknowledgements

The author wishes to express the sincere gratitude to Dr. Patrick J. Hamill for his teaching, challenging, and encouraging guidance throughout the duration of this project; without his efforts and continual proding this research would have reached its stage of completion much more slowly. Many thanks go to those of the faculty at San Jose State University who continue to support the interdisciplinary cooperation necessary to maintain the Graduate Program in the Natural Sciences.

With the extreme thanks which may defy mere verbal expression I mention the multi-dimensional support of my father Mr. John N. Giordano.

M. E. Giordano

I. INTRODUCTION

The ascent of volcanic plumes into the atmosphere is a phenomemon having significant environmental implications. In general the effect of any single volcanic event is related to its intensity of eruption (Tsuya, 1955; Newhall and Self, 1982). Eruption intensities may be expressed in terms of energy fluxes (kinetic and thermal) and mass fluxes from the vent (Hedervari,1963; Wilson, 1976; Settle, 1978; Walker, 1981a). This document shall present a mathematical model to predict the maximum altitude, profiles of velocity, momentum and temperature, and distribution of solid particulates within a singular volcanic plume.

A volcanic column has two regions, each with a source mechanism: an initial jet region dominated by impulse and momentum fluxing through the vent, and a buoyant plume region controlled by a convective driving force. Vertical motions of the column are due to the kinetic energy of the jet released at the vent,and to thermal energy transfer from the gases and pyroclasts to the environment in the plume region (Wilson, Sparks, Huang, and Watkins, 1978). The term volcanic column-plume complex (VCP) will be used to refer to the

entire region from that immediately above the vent up to the maximum height reached by the plume.

A. Volcanic Eruptions and Eruptive Event Types Producing VCP's

Eruptive events have been categorized according to "styles" of eruption and various geologic parameters. In general, there are five types of eruptive events (see Table 1). Each of these is subject to further subclassification. The descriptive approach to classification does not discriminate on the basis of composition and/or origin of magma source or by the type of resulting deposit formed.

TABLE 1

ERUPTIVE EVENT TYPES

Pelean	Eruptions of very viscous lavas characterized by nuees ardentes
Hawaiian	Eruptions characterized by steaming vents and seams usually in large calderas. Calderas exhibiting relatively low explosivity
Vulcanian	Eruptions characterized by long periods between eruptive events which are dependent upon the build-up of high gas pressures in high viscosity lavas yielding relatively high explosions
Strombolian	Periodic eruptions of low

	explosivity in moderately to highly viscous lavas which produce large, poorly fragmented particulates
Vesuvian	Extremely violent eruptions interrupting very long periods of quiessence - a result of very high gas pressures in highly viscous lavas (Plinian events being the most energetic)

By a critical assessment of some of the physical parameters of volcanic eruptions more quantitative classification schemes have been derived.

By using magma gas pressure and viscosity of the lava, Escher (1933) was able to define eight distinct categories for which historical examples were known. According to Escher, the types of Merapi, St. Vincent, and Perret events are distinct from those previously mentioned here. However, eruptions of the Merapi type are more likely to produce nuees ardentes than column-plume complexes - hence they are not directly within the scope of this research. Events of the St. Vincent type are generated from rather viscous lava sources which have plugged the actual vent until sufficient gas pressure explodes the plug into a moderately fragmented column of juvenile lithics. Small to moderate eruptive columns and weakly buoyant plumes combined with radially descending nuees ardentes are often produced. It is the opinion of this author that St. Vincent type events may be difficult to distinguish from stages of Vulcanian events. One may note that Escher did not distinguish between Vulcanian and Vesuvian events as evidenced by his classification of the actual events of Mount Vesuvius as Perret type.

Perret events are extremely significant in the problem of understanding large scale volcanic eruptions, but are actually Plinian to Ultra-Plinian events (given the name Escher prefered to use in honor of Frank Perret).

Another approach to the classification of volcanic events has been to define the eruptive event type based on the physical parameters of the resulting pyroclastic deposit (Walker and Croasdale, 1971, 1972; Walker, 1973; Walker, 1981b). Geologic data recorded in-situ often includes particle collection for size analysis and thickness mapping of the resulting ash (both airfall and flow) deposits. These two genre of information were used to develop criteria for two empirical parameters known as "dispersal" and "fragmentation." Since these are rather non-specific, Walker saw fit to quantify them by strict definitions from which data from various individual eruptive events could be compared (Walker and Croasdale, 1972). Dispersal was defined as "the area enclosed by an isopach which bears a fixed ratio to the maximum thickness of the deposit" (arbitrarily chosen as 0.01 of the maximum thickness). The fragmentation parameter was similarly difficult to define, but was stated to be the weight-weight percent of particles finer than 1.0 millimeters at the point where the 0.1 maximum

thickness isopach crosses the major axis of dispersal. (It would seem that the area of dispersal, kilometers by kilometers, would basically be some function of the maximum altitude reached by the volcanic plume complex and the strength of any prevailing winds, whereas the fragmentation could be dependent upon the overall particle distribution in the airfall ash of the VCP, its chemical composition and temperature history.) By plotting the fragmentation (in percent) versus the dispersal (in kilometers squared) attempts were made to distinguish the previously classified volcanic event types. The results provided quantitative (although numerically arbitrary) descriptions of the known types, some further sub-classifications, and a newly defined type - Surtseyan eruptions (Walker and Croasdale, 1972).

With regard to this research, the purpose for the discussion on the classification of volcanic event types is to specify which types have been historically better candidates for production of VCP's (see table 2). It is then required that any attempts at a valid and reasonable theory for a VCP would be generally applicable and adaptable to any of the "better candidate" types of events.

TABLE 2

EVENTS LIKELY TO PRODUCE VCP'S

event-type	characteristic(s)	example
Strombolian	Mildly to moderately eruptive discrete explosions involving juvenile magma and lithics resulting from near-surface bursting of large gas bubbles in the magma pool.	Stromboli Mt. Etna (1943,52) Paricutin (1973) Hiemaey
Surtseyan	Moderately explosive continuous erruption of balsatic magmas through overlying lacustrine or oceanic bodies of water.	Surtsey (1963) Capelinhos (1957,58) Hekkla (1964,80)

Vesuvian	The most violent eruptions producing well established columns and plumes to extreme altitudes (often into the stratosphere). These events carry large amounts of pumice and ash to maximum altitude.	Taupo Quiozapu (1932) Vesuvius (1944) Agung (1963) El Chichon (1982)
Vulcanian	Frequent discrete high explosivity eruptions from deep in the volcanic vent, exiting with great force and large ejection velocities (hundreds of meters per second). These events often produce nuees ardentes.	Bezymianny (1956) Arenal (1968) Ngaruhoe (1975) Soufriere (1979) St. Helens (1980)

B. Volcanic Mechanisms

> "Explosive volcanic eruptions are so varied in their products and effects that it is difficult to generalize on the processes that produce them."
>
> A. R. McBirney

At certain locations within the earth's planetary crust, zones of preferentially accumulated magma exist (Decker and Decker, 1980). Due to structural weakness and tectonically generated deformations in the crust, these magma zones are often overlain by zones of crustal fracture. These fractures generally are not evidenced by surface features but remain beneath the earth's exterior prior to periods of active volcanism. Through time these fractures may become enhanced by the effects of the local temperature, pressure, and stress field histories.

Without focusing on specific composition and concentration of the gas-magma mixtures (for general

references on composition see Krauskopf, 1967; Tazieff, 1970; and Sigvaldason, 1974) certain interactions will occur between the magma source and the overlying rock which eventually result in volcanic eruption. Consider a magmatic gas at depth which has a certain natural head pressure. When this pressure is exerted on some non-regular body above the magmatic source material, the magmatic gas will pursue voids in the fracture zones and will extend them into more and/or greater cracks. The gas flows vertically toward lower pressure. This upward motion due to gaseous expansion scours the cracks and channels toward the surface in preparation for further vertical intrusion of magma. Any irregular shape along the surface of or extending from these channels will be subject to thermal and mechanical stress weakening the walls. Objects in the channel decompose and fracture into smaller objects which are abraided in the gas flow. Hence the particulate mass portion in the gas-magma streams increases throughout the flow, promoting further scouring on the channels en-route to the surface. In the initial stages of development the channels from the magma source conduit up to the surface vicinity of the present or not-yet-present vent may be asymmetrical in form. Scouring processes will widen and produce

cylindrical forms which flare into funnel shapes at the near-surface region (Ollier,1974; Wilson, 1980). Lithostatic overpressures (and lateral pressures) acting on the rock and hydrostatic pressure on the magma-gas mixtures are less near the surface than at depth; the combination of these coetaneous conditions increases the ease and rate of rock erosion in the near-surface region by the rapidly expanding gases. Due to the relatively low critical temperature of water with respect to the local magmatic temperatures, the likelihood of flashing any available interstitial water is great - thereby its explosivity will further enhance the erosional scouring process (Mcgetchin and Ullrich, 1973; Kieffer, 1977; Wilson, 1980). Locations where the scoured conduit passages emerge on the crustal exterior then become the preliminary vent sites of volcanic activity.

Interactions between the source magma and the surrounding rock serve only as the preliminary events leading to the establishment of a volcanic conduit and vent. Through time the magma rises surface-bound along the established fractures and channels, expanding as pressure on the gas-fluid mixture decreases. At some point in the pressure-temperature space, magmatic gases exolve rapidly blowing magma apart. If this explosion

is in the near-surface vent, eruption occurs. An understanding of the temperature-pressure-depth history of the souce magma is necessary to explain the mechanism(s) of volcanic eruption. Attempts at revealing the mechanism(s) of eruption are based upon a synthesis of the information collected through various networks throughout the scientific community (observational, experimental, and theoretical). Direct observation of actual eruptions, the ensuing emplacement of ejecta and the resulting landforms can be combined with studies of past geologic events. Collected data from exposures of volcanic craters, vents, and deposits, at historical sites can be interpreted in light of theoretical studies (Ollier, 1974).

As a body of magma approaches its saturation with gases and available groundwater it may still remain as a stationary column. In the upper portion of the column, volatiles seeking lower pressures will vesiculate upward; some of these bubbles may actually penetrate through the overlying layers of country rock or pre-existing solidified lava encrusting the actual surface vent. This process resembles geyser and "crustal boiler" activity by producing pulsating eruptions (Elder, 1976; Keiffer, 1977). Since magmatic

gases are pressurized in solution, the tendency to relieve pressure on the top level of a stationary magma column can cause exolution and expansion without initiating upward movement of the fluid body itself (champagne phenomenon). A mechanism such as this may be triggered by cap rock fracture and/or sudden lowering of the local groundwater level. If the gaseous expansion is maintained long enough, the magma column will itself rise buoyantly (seeking pressure compensation) to the level where the exolution was initiated; hence, stationary magma columns can rise toward the surface even without explosive eruption.

Rising magma moves upward until it reaches a depth at which the pressure directly above it is low enough to allow vesiculation. In some cases magma rises into shallow pools where temporarily high pressures may be produced which are sufficient to drive water vapor into surrounding fractures in the rising magma itself (McBirney, 1973). If the magma is relatively viscous and the permeability of the surrounding materials relatively low, gas pockets could explosively relieve their pressure further up in the column.

Another mechanism of eruption has been presented based upon sudden releases of pressure in gas-rich

saturated magmas (Bennett, 1971; Keiffer, 1977): it is postulated that the very rapid release of pressure in one direction (upward) will generate a decompressional wave propagating with a velocity near the local speed of sound (in the magma-gas fluid) in the direction opposite the pressure release (downward); the magma will continue to expand into a mixture of gas and liquid forcing the liquid portion to move upward as a piston in a cylinder.

Further details of the eruption mechanisms are to be found throughout the literature and need not be discussed in this document. Of the magma-gas-rock interactions mentioned here, models have been proposed to clarify the observed patterns and causal interrelationships of these characteristic ocurrences. The basic mechanisms of eruption have been used to explain the various eruptive styles previously mentioned. Table 3 includes descriptions of some of the most commonly modeled mechanisms.

TABLE 3

COMMONLY MODELED VOLCANIC MECHANISMS

1. "Firehose"	Ejecta is moving in a high velocity, low pressure flow of expanding gas. Smaller fragments are locked to the gas motion and are carried further than larger pieces (McBirney, 1973).
2. "Projectile propulsion"	Fragments are propelled by a high pressure gas, accelerated and carried ballistically further than smaller particles (Fudali and Melson, 1972; McBirney, 1973).
3. "The tap"	The formation of the conduit occurs such that lava is

extruded (on the surface) without interaction of groundwater. Magma then descends back into the conduit and groundwater filters down into the conduit zone and the resulting steam scours out the fissures into a funnel-shaped crater. The column of magma rises again, but the steam has either been depleted and/or the pressure gradient forces the groundwater out of the conduit proper such that the eruption only produces scoria type ejecta (Singleton and Joyce, 1969). This is very similar to geyser models.

4. "Big Bang" — Magma ascends into a local groundwater source, rapidly

	produces high pressure steam, then violently explodes in a single blast (Ollier, 1974).
5. "Fluidization"	A stream of solid particles suspended in a turbulent gas-liquid mixture will behave with fluid flow characteristics. Such a mechanism may involve combustion of steam, and gaseous and liquid magma above their respective critical points. This is evidenced in nuees ardentes and pyroclastic flows (Ollier, 1974; Wilson, 1980; Wilson, Sparks, and Walker, 1980).

All of the mechanisms mentioned have at least one common phenomenon - the interaction of magmatic gases with a rising liquid column. The rate and degree of gaseous expansion in a rising magma body will control two very important characteristics of an explosive volcanic eruption: the pressure of the gas released at the surface, and the vent ejection velocity of the gas-magma fluid (McBirney, 1973). Based on gas pressures, ejection velocities, and other physical considerations) various sequences and combinations of the eruption mechanisms have been used to describe in detail the intricacies of the volcanic event types for VCP production (Blackburn, 1977; Blackburn, Wilson, and Sparks, 1976; Wilson, 1980; Wilson, Sparks and Walker, 1980). Via any mechanism, once magma has reached the planetary surface, eruption may occur in one or more of three basic modes: lava flows and showers, pyroclastic flows, and airfall dispersal (Francis, 1984). It is the later mode (airfall dispersal) that concerns this research, as an event could not possibly produce even a small VCP without being involved in the dispersal of airfall material. The problem is to develop a reasonable model for a VCP associated with an airfall producing eruption.

C. Statement of the Problem

In considering the problem of adequately describing a VCP, this work has incorporated a basic fluid dynamic approach to find the fields of pressure, density, and velocity within the VCP. This is predicated upon the flow being due to the action of external forces. More specifically, descriptions of the fields of the state variables must be derived for the fluid whose motion results from the force of an explosive volcanic eruption and for the ambient fluid through which it moves. Properly expressed descriptions must be related in such a way that solutions can be derived which result in values for the magnitude of the field variables as functions of coordinate space. Since the problem really does not involve an ideal incompressible fluid nor an ideal barotropic fluid, the system of equations must include equations of state for both the ambient fluid (the atmosphere) and the VCP with respect to their interdependency of motion, energy, and continuity. However, "ideal" conditions are frequently a convenient starting point for development of the forms of the

necessary functional relationships, and have been used as such.

A fluid model applicable to the VCP phenomenon should attempt to incorporate the most important physical parameters of a volcanic event. It should consider the velocity of the larger block-type pyroclasts leaving the vent, the velocity of the eruption column exiting the vent, the mass and temperature of the gaseous component of the VCP, the total mass of the pyroclastic material erupted and its areal distribution around the vent, and the shape and height of the VCP (after Wilson, 1972).

II

MATHEMATICAL DEVELOPMENT

II. MATHEMATICAL DEVELOPMENT

One may begin to model the VCP with a much simplified problem - that of a pure jet-plume exiting from a circular vent in the absence of internal friction. Such a condition may be aptly handled in the manner of the axially-symmetric jet (see Hinze, 1959; Tennekes and Lumley, 1972). If the motion of the jet is due solely to the impulse supplied at some original source, the resulting motion of the fluid out of the vent is momentum governed. At downstream distances within six to ten jet vent diameters the initial axial exit velocity is not significantly decayed and the flow is mainly laminar (Corrsin and Uberoi, 1950). Beyond this downstream "length" the motion of the flow along its surface boundaries is turbulent and the resulting attenuation of the axial exit velocity serves to retard the jet. For a fluid of identical composition and temperature to the ambient fluid through which it passes there will be no buoyancy effects. Without the addition of the buoyant force, the jet decays rapidly due to the net dissipation of mechanical energy. Such

a model for the VCP based solely upon the momentum driven jet would not be sufficient to produce geophysical scale plumes.

Buoyant jets or forced plumes (as they are also called) are flows arising from sources of continuous momentum and buoyancy (Morton, 1959a). Since the VCP producing event is defined as one with distinct flows resulting from momentum and buoyancy dominated phenomena, the buoyant jet would be a plausible analog for the upward eruptive flow. Before pursuing the mathematical problem, it is necessary to discuss the conditions and assumptions associated with our preliminary model. The locus of all points continuously tangent to the velocity vector in a flow of a uniform fluid with a constant density may be defined as a streamline. We shall define all of the streamlines passing through any finite fixed cross-sectional area within the horizontal plane in which the coordinate system may be expressed by the variables r, ϕ, z as a streamtube. Upon any single horizontal sheet the variable r radiates from an origin where $r = 0$. The positive z axis extends vertically upward through all positions of $r=0$, defining the vertical axis of symmetry. Assuming all motions to be axisymmetric, changes with respect to ϕ are equal to

zero. One may define a ring elemental surface $d\sigma$ as the surface on any horizontal sheet covered by the area equalling the product $2\pi r dr$ as the radial position extends from r to r plus the infinitesimal dr. Thus the cross-sectional area of the flow upon any horizontal sheet is the integral of the element $d\sigma$ upon the interval r to r + dr.

The streamtube concept is useful in expressing the basic fields (velocity, density, pressure, etc.) of the flow. By examining the physical conditions of the fluid within a control volume bounded by a control surface (a streamtube) the fields may be examined as functions of their space and time coordinates. For any control surface S (defined as the integral of $d\sigma$ upon the interval r to r plus dr) composed of a streamtube, application of the appropriate forms of mass, momentum and energy conservation laws will lead to the necessary field equations. The conservation laws are: the conservation of mass, momentum and energy fluxes through the control surface (Morton, Taylor and Turner, 1956; Morton, 1959b; Fox, 1970; Morton, 1971).

A. Conservation of Mass

The law of conservation of mass states that the influx of mass into the surface must be equal to the efflux of mass from the surface. The continuity equation expresses the principle of mass conservation at all points within the field. For the initial discussion of the VCP model, a form of the continuity equation was used which states that the mass flux is non-divergent through any control surface.

$$\nabla\cdot(\rho V) = 0 \qquad (2.1)$$

where ρ is the fluid density and V is the total fluid velocity vector.

B. Conservation of Momentum

The mass flowing through a bounded surface $d\sigma$ in unit time into or out of a given unit volume V is equivalent to the time rate of change of mass through the surface,

$$(dm/dt)_\sigma = \rho v \, d\sigma. \qquad (2.2)$$

Defining the momentum P as the product mv, the momentum flowing through the surface in a unit time may be expressed as $d(mv)/dt$, equivalent to $\rho v^2 d\sigma$, taking on the physical meaning of the product of momentum per unit volume and the volume flow through the surface. Therefore, the total momentum flowing in a given volume V in unit time is defined as the momentum efflux from the top surface per unit time less the momentum influx through the bottom surface per unit time. In this case the lateral surfaces must be fixed.

$$dP/dt = \dot{P}(\text{out the top - efflux}) - \dot{P}(\text{in through the bottom - influx}). \quad (2.3)$$

Equation 2.3 may be explained as follows: Given a volume V of finite dimensions $d\sigma(\Delta z)$ between the horizontal levels (z)and $(z+\Delta z)$, the momentum flux contained within this volume is equated with the difference between the momentum efflux at the upper surface and the influx through the lower surface. Hence, the total momentum flux within the "volume" is equal to

$$\int \rho u^2 d\sigma_{z+\Delta z} - \int \rho u^2 d\sigma_z = dP/dt \text{ (total)} \quad . \qquad (2.4)$$

Previous discussion concerning the mechanics of eruption should support the author's assertion that the production of a VCP is the result of the external force of the volcanic explosion process. The use of the forced plume model demands a source of continuously supplied momentum flux. This continuously supplied momentum flux from an externally applied force can be treated by invoking the impulse form of Newton's Second Law:

$$dP/dt = F.$$

So

$$P = \int_0^t F dt$$

where F is the net force acting on a known body.

In this initial analysis the sum of the forces ΣF is the resultant of the two dominant forces - the weight force of the plume and the buoyant force acting upon it. Taking the upward buoyant force as positive and employing Archimedes' Principle gives:

$$\Sigma F = \text{Buoyant} - \text{Weight} \qquad (2.5)$$

$$= (\text{mass of displaced fluid} \times g)$$

- (mass of body fluid x g)

where g is the local gravitational acceleration.

Definitions of the weight and buoyant forces are as follows:

$$B=g\int \rho_o dV; \qquad \text{where } dV=d\sigma\Delta z; \tag{2.6a}$$

$$W=g\int \rho dV. \tag{2.6b}$$

The densities ρ_o and ρ represent the local values of the ambient and the body fluids respectively.

$$\Sigma F= g\int \rho_o d\sigma\Delta z \; - g\int \rho d\sigma\Delta z \tag{2.7}$$

(over the volume from z to $z+\Delta z$)

which can be re-arranged as

$$F= g\int [\rho_o d\sigma]\Delta z \; - \; g\int [\rho d\sigma]\Delta z \tag{2.8}$$

$$= g\Delta z\{\int [\rho_o 2\pi r dr - \int \rho 2\pi r dr]\} \; . \tag{2.9}$$

Further rearranging yields the following form:

$$F = 2\pi g \int (\rho_o - \rho) r dr \Delta z.$$

Equating dP/dt with ΣF results in:

$$\int \rho u^2 d\sigma_{z+\Delta z} - \int \rho u^2 d\sigma_z = 2\pi g \int (\rho_o - \rho) r dr \Delta z; \tag{2.10}$$

which upon dividing both sides by Δz yields

$$(1/\Delta z)\{\int \rho u^2 d\sigma_{z+\Delta z} - \int \rho u^2 d\sigma_z\} = 2\pi g \int (\rho_o - \rho) r dr. \tag{2.11}$$

Using the definition of the derivative by evaluating in the limit as Δz approaches zero, the expression becomes:

$$d/dz \int [\rho u^2 d\sigma] = 2\pi g \int (\rho_o - \rho) r dr; \tag{2.12}$$

where $d\sigma = 2\pi r dr$

such that

$$V = \int dV = \int d\sigma \Delta z = \iint 2\pi r dr dz \ .$$

The mixed form of equation (2.12) can be evaluated by integrating the elemental areas over the region from 0 to r. This results in (see Morton, Taylor, and Turner, 1956):

$$d/dz\ [\pi r^2 u^2 \rho] = \pi r^2 g(\rho_o - \rho). \qquad (2.13)$$

With further rearranging the momentum equation can be placed into another common form. Replacing $(\rho_o - \rho)$ with $\delta\rho$ and dividing each side of the equation by some constant reference density will yield (see Baum and Mullholland,1979):

$$d/dz \int [u^2 r dr] = - g \int (\delta\rho/\rho) r dr \ . \qquad (2.14)$$

Note: this reference density is often taken as the density of the ambient fluid at the height of the source of the jet phase. This is not the case described here, but is common enough to deserve mention.

The use of this reference density in the momentum and heat conservation equations does in some cases imply a subtle assumption: the ratio of the jet/plume fluid density to the reference density approaches unity and is considered negligible in the left-hand side of equations 2.13 and 2.14 .

C. Conservation of Thermal Energy

It can be demonstrated that simultaneous conservation of mass and momentum within the fluid body is sufficient for conservation of mechanical energy. A remaining condition is the conservation of thermal energy between the jet/plume fluid and the ambient environment.

As the fluid body rises adiabatic lifting reduces the plume temperature; mixing of plume fluid with ambient fluid likewise reduces the plume temperature. Both of these distinct temperature reductions play important roles in expressing the conservation of thermal energy.

A form of the general heat equation should be:

$$Q = mc\Delta T; \qquad (2.15)$$

where: Q is the thermal energy,
m is the mass of the fluid,
c is the specific heat capacity at constant pressure,
ΔT is the temperature change.

By making use of the mass-flux concept as developed in the streamtube model, the mass term m in equation 2.15 may be replaced with the appropriate mass flux term $\dot{m}$ and result in the equation for the heat flux $\dot{Q}$. Conservation laws then demand that the sum of all of the heat fluxes interacting in the plume/ambient fluid system be equal to zero. In simplest terms, the heat given off from the hot VCP must be equal to the heat acquired by the surrounding environment.

$$\dot{Q} = \dot{m}\, c\, \Delta T. \qquad (2.16)$$

$$\dot{Q}(\text{plume}) + \dot{Q}(\text{environment}) = 0. \qquad (2.17)$$

Making use of a general property of a quantity in a conserved field (similar to eq. 2.1) the divergence of the net heat flux is zero:

$$\nabla \cdot (\dot{Q}) = 0. \tag{2.18}$$

By further assuming that the local variations in Q with respect to radial and azimuthal coordinates are small compared with vertical changes, equation 2.18 may be simplified as follows:

$$d/dz\ (\dot{Q}) = 0, \tag{2.19}$$

and, if equation 2.17 is employed, one may rearrange to yield the following:

$$\dot{m}\ c\ dT/dz\ (\text{plume}) = -\ \dot{m}\ c\ dT/dz\ (\text{environment}). \tag{2.20}$$

The term on the left-hand side (l.h.s.) of equation 2.20 contains the expression for the total change in temperature of the plume fluid with height. This change in the plume fluid with height is the change due to both the adiabatic lifting of the thermally hotter plume, and the horizontal mixing of the plume fluid with the ambient environmental fluid.

$$d/dz(T_{plume})net = d/dz(T_{plume})mixing + d/dz(T_{plume})lifting \ . \qquad (2.21)$$

By invoking the assumption that the specific heat capacities (at constant pressure) of the plume fluid and the ambient fluid are equivalent,one may once again return to the conservation equation:

$$-\dot{m}_p c(dT/dz)dz_{plume} = \dot{m}_e c(T_{out}-T_{in})environment. \qquad (2.22)$$

Defining the differential temperature from outside to inside the convecting plume as the difference in temperature $\theta = \theta(z,r)$ the expression is given by equation 2.23 .

$$\dot{m}_p c_p (dT/dz)_{horizontal}\, dz = - \dot{m}_e c_{pe} \theta \quad . \tag{2.23}$$

From the equations 2.1 and 2.7 we have the following:

$$\dot{m}\ (plume) = \int_0^\infty \rho u r dr \tag{2.23b}$$

$$\dot{m}\ (envir) = d/dz \int_0^\infty [\rho u r dr] \Delta z \quad . \tag{2.23c}$$

The horizontal mixing equation now takes the form:

$$c_p (dT/dz)_H \int_0^\infty [\rho\ u\ r\ dr]\ \Delta z = -\{d/dz \int_0^\infty [\rho u r dr] c_p \theta\} \Delta z \tag{2.24}$$

which upon dividing by ($\Delta z c_p$) and rearranging may be used to express the horizontal mixing term of the heat equation.

$$(dT/dz)_{horizontal} = \{-\int_0^\infty [\rho u r dr]\}^{-1} \{d/dz \int_0^\infty [\rho u r dr]\} \theta \quad . \tag{2.25}$$

After obtaining the horizontal mixing term for the change in plume temperature with height, one can then make use of equation 2.21 again by replacing the

adiabatic lifting term $(dT/dz)_{vertical}$ with an expression for the adiabatic temperature lapse rate for a stably stratified fluid where

$$(dT/dz)_{lift} = -g/c_p \quad . \tag{2.26}$$

This results in an expression for the total vertical change in temperature of the convecting fluid as a function of height.

$$dT/dz\ (net) = dT/dz(horizontal\ mixing) + dT/dz(adiabatic\ lifting).$$

$$(dT/dz)_{net} = \{-\int_0^\infty [\rho u r dr]\}^{-1} \{d/dz \int_0^\infty [\rho u r dr]\}\theta + (-g/c_p) \ , \tag{2.27}$$

multiplying through by $\int_0^\infty \rho u r dr$ and rearranging yields

$$(dT/dz)_{net} \int_0^\infty [\rho u r dr] = - \{d/dz \int_0^\infty [\rho u r dr]\}\ \theta - (g/c_p) \int_0^\infty \rho u r dr \quad . \tag{2.28}$$

Both sides of equation 2.28 may be multiplied by the specific heat of the convecting fluid term c_p to obtain equation 2.29.

$$c_p(dT/dz)_{net}\int_0^\infty [\rho u r dr] = -\{d/dz\int_0^\infty [\rho u r dr](\theta c_p) - g\int_0^\infty \rho u r dr \ . \qquad (2.29)$$

This may be arranged as follows:

$$\{-d/dz\int_0^\infty [\rho u r dr]\}\ \theta c_p - g\int_0^\infty \rho u r dr \ - c_p dT/dz\int_0^\infty \rho u r dr = 0 \ , \qquad (2.30)$$

$$\therefore \quad \{d/dz\int_0^\infty [\rho\ u r dr]\}\ \theta c_p + (g + c_p dT/dz)\int_0^\infty \rho u r dr = 0 \ . \qquad (2.31)$$

Evaluating r between 0 and ∞ will give the expression (eq. 2.32) where c_p is the specific heat at constant pressure of the Column-Plume Complex mixture and $(dT/dz)_{net}$ represents the net vertical temperature gradient inside the convecting Column-Plume Complex. The "thermal energy" equaton as derived from the principle of heat conservation, should be integrated and rearranged to solve for the temperature as a function of height within the VCP at any given height z.

$$\theta c_p d/dz[\int_0^\infty \rho u r dr] + [g + c_p(dT/dz)_{net}]\int_0^\infty \rho u r dr = 0 \ . \qquad (2.32)$$

The $(dT/dZ)_{net}$ term is the vertical temperature gradient inside the VCP. The differential temperature was defined such that a new expression for the vertical temperature gradient is given in terms of the differential temperature gradient ($d\theta/dZ$) and the ambient vertical temperature gradient $(dT/dZ)_{env}$.

$$d\theta/dZ = (dT/dZ)_{net\ vcp} - (dT/dZ)_{environmental}. \quad (2.31i)$$

$$(dT/dZ)_{net} = d\theta/dZ + (dT/dZ)_{environmental}. \quad (2.32ii)$$

Replacing the appropriate factor on the l.h.s. of equation 2.32 and rearranging according to the product rule for exact differentials yields a simplified form of the heat conservation equation (2.34). This manipulation requires that the value of the specific heat of the plume fluid remain constant inside and outside the plume boundary, or be known as an explicit function of the variable r. The specific heat of the plume must also be identically equivalent to that of the ambient environment. For the case of constant specific heat, c_p may be divided through equation 2.35 to further rearrange this equation.

$$c_p\theta d/dz[\int_0^\infty \rho u r dr] + [c_p\int_0^\infty \rho u r dr](d\theta/dz)$$

$$+ [c_p\int_0^\infty \rho u r dr](dT/dz)_{env} + g\int_0^\infty \rho u r dr = 0 \ . \qquad (2.34)$$

$$d/dz[\int_0^\infty \theta c_p \rho u r dr] + [c_p(dTdz)_{env} + g]\int_0^\infty \rho u r dr = 0 \ . \qquad (2.35)$$

From the first law of thermodynamics for an adiabatic process in a perfect gas, combining Poisson's equation and the hydrostatic equation results in the following expression:

$$dT/dz = -g/c_p(RT\rho/p) \qquad (2.35i)$$

but, $RT\rho/p$ approaches unity for an ideal gas, and a first approximation may be used :

$$dT/dz = -g/c_p \ , \qquad (2.35ii)$$

where c_p is the specific heat at constant pressure of the VCP fluid.

A quantity, Δ, defined in the fashion of Baum and Mullholland, (1979) is:

$$\Delta = -c_p/g(dT/dz) \ . \qquad (2.35iii)$$

For the case of a dry adiabatic atmosphere, Δ will equal unity. In this model Δ will not be assumed constant, but will be functionally calculated as the specific heat of the convecting plume is calculated. The physical significance of Δ is related to the ability of a verticallly displaced parcel of fluid to accelerate positively or negatively. It is to some degree a measure of the buoyant restoration of the fluid mass [for more detailed discussions see Hess, 1959; Haltiner and Martin, 1957; and Iribane and Godson, 1981]. Delta may now be placed in the leading factor of the second term of equation 2.35 to yield equation 2.36 .

$$d/dz[\int_0^\infty \theta\rho ur dr] + (g/c_p)(1 - \Delta)\int_0^\infty \rho ur dr = 0 . \quad (2.36)$$

Up to this point a set of equations has been derived for the conservation of mass flux (2.1), conservation of momentum flux (2.14), and the temperature as a function of height for a pure plume rising adiabatically through an ambient fluid of similar composition and specific heat capacity (2.36). This "model" will be further developed by expressing

the conditions characteristic of an actual VCP more realistically.

$$\nabla\cdot(\rho v) = 0 \ . \tag{2.1}$$

$$d/dz\int_0^\infty [\rho u^2 r dr] = - g\int_0^\infty \delta\rho/\rho_1 r dr \ . \tag{2.14}$$

$$d/dz[\int_0^\infty \theta\rho u r dr] + (g/c_p)(1 - \Delta)\int_0^\infty \rho u r dr = 0 \ . \tag{2.36}$$

D. Further Thermodynamical Considerations

The model of the plume fluid has been restricted to a homogeneous incompressible fluid undergoing no axial rotation nor viscous dissipation within the fluid body. An actual VCP carries a large amount of solid particulates which are contributors to the actual composition of a VCP. Gaseous constituents of the volcanic effluent likewise contribute to the composition of a VCP. It is obvious that the composition of a VCP is dissimilar to that of the ambient environment. [See for example, Tazieff, 1970; and Krauskopf, 1967.] Further discussions will not be as to the nature and history of gaseous effluents presented herein. This study has been concerned with

gaseous composition as it affects the model equations. Gaseous effluents of volcanic eruptions are not incompressible, nor are they of identical composition and density with that of the ambient environment as has been assumed to this point.

The existing equations may be altered as follows: the actual non-solid particulate portion of the effluent in a VCP event is found to be of liquid and gaseous phases and should be modeled as such (Kieffer, 1977; Pai, Hsu, and O'Keefe, 1978; Housley, 1978); the density of the VCP as used in the mass conservation equation and hence in the momentum equation must be that of a mixture of gases, liquids, solid particulates, and any included ambient atmosphere; the thermal properties of this mixture must account for any interactions involving condensation, precipitation and evaporation.

Consider the case of a non-chemically interacting binary mixture of gases. Volcanic effluents commonly have a gaseous composition the greater portion of which is a mixture of steam (H_2O vapor phase) and carbon dioxide (CO_2) (Tazieff,1970; Wilson, 1976). Since the respective specific heat capacities at constant

pressure of these substances differs by a factor ranging from two to three, the ratio of steam to carbon dioxide can contribute significantly to the value of the specific heat capacity of the VCP fluid. The difference in their respective molecular weights will also insure that their densities differ at any pressure; this density difference will have an effect on the net density of the plume fluid as a result of the ratio of their mixing. This study does not include the chemistry of liquid droplet condensation, precipitation, or evaporation.

Before modifying the existing model equations a brief treatment of the ambient fluid is necessary. For an approximation one can assume that the specific heat capacities at constant pressure of water vapor, dry air, and moist air comprising the ambient environment are to be taken as independent of temperature. Consider a unit mass of moist air absorbing a quantity of heat δQ at a constant pressure as its temperature is increased by an amount dT. The heat absorbed by this mass may then be expressed in the following manner:

$$\delta Q = m_d \delta q_d + m_v \delta q_v \qquad (2.36i)$$

where δq_d and δq_v are the amount of heat per unit mass absorbed by the dry air and water vapor portions respectively; the expression m_d and m_v are those representative of the masses of dry air and water vapor within the moist air parcel mixture.

Let specific humidity be defined as the ratio of water vapor mass to the total mass of the fluid..

$$sh = m_v/m_{total} \qquad (2.36ii)$$

By the definition of specific humidity, the change in the heat absorbed by the unit mass of moist air may be restated as follows:

$$\delta Q = (1-sh)\delta q_d + sh\ \delta q_v\ . \qquad (2.36iii)$$

Upon dividing by the temperature increase dT, one can obtain an expression for the specific heat at constant pressure of the moist air.

$$c_{pm} = (1-sh)c_{pd} + sh\ c_{pv} = c_{pd}[1+((c_{pv}/c_{pd})-1)sh]\ , \qquad (2.36iv)$$

where the subscipts d, and v represent quantities for that of dry air and water vapor respectively. Using

the values for the specific heat of dry air (1005 Joules per Kilogram per Kelvin) and that of water vapor (1870 Joules per Kilogram per Kelvin), equation 2.36iv may be re-expressed as:

$$c_{pm} = c_{pd}(1 + 0.87sh) \ . \qquad (2.36v)$$

Equation 2.36v can now calculate values for the specific heat of the ambient fluid as a function of the mass fraction of water vapor content per unit mass. Values calculated from this relationship will be used for the appropriate term in the heat energy equation.

The assumption of temperature independence for the specific heat of the ambient fluid may serve well the purposes of this model, but is hardly reasonable for the gas mixture within the VCP. Further treatment to the heat energy conservation equation is necessary. Development will be along the following lines: to adjust the equation for the varying specific heat capacities of the ambient and convecting fluids, and to incorporate a method of accounting for the composition of the gaseous effluents. Returning to equation 2.32, replacing the general specific heat term with the appropriate terms for both the ambient and the plume fluid values will eliminate the assumption of a single

specific heat both inside and outside the VCP. This results in the following adaptation:

$$\theta c_{pe}\{d/dz[\int_0^\infty \rho u r dr]\} + [g + c_{pp}(dT/dz)_{net}]\int_0^\infty \rho u r dr = 0 \qquad (2.37)$$

where c_{pe} is the specific heat of the ambient fluid, c_{pp} is the specific heat of the plume fluid, and dT/dZ is the net vertical temperature gradient inside the convecting plume. Since the specific heat of the ambient fluid is a function of specific humidity only, its value will be considered as a constant and may be extracted from behind the integral in the leading term of the left-hand side of equation 2.37. The total fluid density, ρ, may be extracted from the integrals and divided out from equation 2.37 since at any vertical position z the value of the density within the plume boundary is constant as summed over the domain of the plume radius r. This adaptation renders equation 2.38 :

$$\theta c_{pe}\{d/dz[\int_0^\infty u r dr]\} + [g + c_{pp}(dT/dz)_{net}]\int_0^\infty u r dr = 0 \quad . \qquad (2.38)$$

Note: forming an exact, total differential as in equation 2.36 may not be used here since c_{pe} and c_{pp} are neither equivalent, constant in z, nor independent of r.

As previously mentioned the term dT/dZ expresses the vertical temperature gradient inside the VCP. One may assume that the process is adiabatic, but certainly it will be more complex than that of the ambient fluid's vertical temperature lapse. Therefore dT/dz inside the convecting fluid is not a constant, as often taken for the ambient fluid, but must be functionally obtained. The specific heat of the mixture of gases within the VCP must now be determined on the basis of the gaseous composition. From similar arguments used in the derivation of equation 2.33iv, the specific heat of a binary mixture (without phase changes) will be as follows:

$$c_{p12} = (m_1 c_{p1} + m_1 c_{p2})/m_1 + m_1 \quad , \qquad (2.39i)$$

where c_{p1} and c_{p2} are the specific heats at constant pressure for gas species one and two, and m_1 and m_2 are the masses of each species contained in some volume of the mixture.

Let C_1 and C_2 equal the concentration fractions of gas species one and two expressed in fraction per unit volume of the total gas volume such that the total concentration of all species is unity as per equation 2.39ii . The total gas density of the convecting fluid will then be the sum of the products of the individual concentration fractions and the total density as per equation 2.39iii .

$$\sum_{i=1}^{n} C_i = C_1 + C_2 + \ldots = 1 \quad . \qquad (2.39ii)$$

$$\rho = \sum_{i=1}^{n} C_i \rho_i = C_1\rho_1 + C_2\rho_2 + \ldots \quad . \qquad (2.39iii)$$

In equation 2.39iii , $C_1\rho$ and $C_2\rho$ represent the mass per unit volume of each gas species. The total specific heat of the binary mixed gas may now be expressed in equation 2.39iv where ρ_{o12} represents the initial gas density of the plume fluid effluents prior to entraining ambient fluid.

$$c_{p12} = (C_1\rho_{o12}c_{p1} + C_2\rho_{o12}c_{p2})/(C_1\rho_{o12} + C_2\rho_{o12}) \quad . \qquad (2.39iv)$$

As the plume rises it entrains air from the ambient environment thereby diluting the original concentrations of gaseous species and volcanic ash. This dilution of the gas species' concentration not only alters the density of the gaseous portion of the plume fluid but changes the specific heat value of the plume gas mixture. In accordance with the derivation of equation 2.39iv for the binary non-diluted gas mixture, the specific heat of the plume fluid as it mixes with the ambient environment is given by equation 2.39v .

$$c_{p123} = (m_3\, c_{p3} + (m_1+m_2)c_{p12}\,)/(m_1+m_2+m_3)\ . \qquad (2.39v)$$

In equation 2.39v, m_3 is the mass of the entrained air into any volume of the plume at a specific altitude z; c_{p3} is the value of the specific heat capacity of the entrained air which is identical to that expressed for the moist air given by equation 2.33vi. The summation of masses one, two, and three is equivalent to the total mass of the gaseous portion of the plume in a volume element at an altitude z.

The specific heat capacity at constant pressure is the derivative of the enthalpy with respect to

temperature [$dH = c_p(T)dT$]. If the change in enthalpy is taken over a range of temperatures in a constant pressure process, the specific heat is not to be considered a constant over large changes in temperature. It could be understood that in a constant pressure process this consideration would also be necessary for all of the species involved in the mixture. The specific heat at constant pressure is often expressed in a power series in the absolute temperature T, using empirically determined coefficients. This study will use the following equation (2.39vi) for the temperature dependence of heat capacities where the coefficients are expressed in combinations of Joules, kilograms, and Kelvins (see Atkins, 1978 table 4.3).

$$c_p(T) = a + bT + cT^{-2} \quad . \qquad (2.39vi)$$

Equation 2.39vi was employed to calculate the temperature dependent specific heat of each individual gas species where a is expressed in Joules per kilogram per Kelvin, b is expressed in $(10)^{-3}$ Joules per kilogram per Kelvin squared, and c is expressed in $(10)^5$ Joules-Kelvin per kilogram. The temperature dependence of the mixed gas was considered of primary importance for the binary mixture of water vapor and

carbon dioxide within the plume as it mixes with the entrained ambient moist air. The following values were employed:

	a	b	c
H_2O vapor	1695.254	571.191	0.0
CO_2	1004.999	199.727	-195.865

With these latest alterations the heat-energy conservation equation may be considered appropriately modeled for the purpose of this study. The preceding modifications now leave the hydrodynamic conditions of the VCP specified by equations 2.1, 2.14, and 2.38.

E. Effects of Solid Particulates

An objective of this study was to include the effects of both volcanic ash materials and larger clastics in the VCP model. The ash portion of the ejecta is considered to move with the gaseous constituents in a coupled, and non-interacting manner. For consideration of the ash portion within the plume, the mass of the entire plume and hence its density will be affected. No resulting dissipative forces (i.e. drag) will be attributed to the individual ash particles. The particulate ash fraction, $\times$, is defined as the ratio of masses of the volcanic "dust" to that of the entire plume (equation 2.40). The initial value of chi diminishes as the plume entrains the "dustless" ambient fluid with increasing altitude. The total amount of ash in the plume however remains constant. Since the dust fraction of the plume's total mass is a scalar function of the plume's mass itself, the form of the equation for its conservative nature will be similar to that of the VCP's mass. Given that equation 2.1 holds true where ρ is the total density, one may imply equation 2.41 .

$$\chi = (\text{mass of ash})/(\text{total plume mass}) \quad . \tag{2.40}$$

$$\nabla\cdot(\chi\rho v) = 0 \quad . \tag{2.41}$$

Converting from generalized coordinates to a cylindrical system in z and r, equation 2.1 for the mass flux conservation and equation 2.40 for the particulate conservation may now be replaced with equations 2.42 and 2.43 respectively.

$$d/dz(\rho v) = 0 \quad . \tag{2.42}$$

$$d/dz(\chi\rho v) = 0 \quad . \tag{2.43}$$

Arguments similar to those presented in the derivation of the momentum conservation equation (2.14) will allow the total density and the upward axial velocity vector, u, to be used in the expressions for the conservation of mass (2.44) and conservation of particulates (2.45).

$$d/dz\left\{\int_0^\infty \rho u r dr\right\} = 0 \quad . \tag{2.44}$$

$$d/dz\left\{\int_0^\infty \chi\rho u r dr\right\} = 0 \quad . \tag{2.45}$$

As previously asserted, the density ρ remains constant summed over the radius r for any volume element at altitude z. Hence it may be extracted from the integral and divided out from the above equations. The resulting equations express the conservation of total mass and particulate mass respectively.

$$d/dz\{\int_0^\infty urdr\} = 0 \quad . \tag{2.46}$$

$$d/dz\{\int_0^\infty xurdr\} = 0 \quad . \tag{2.47}$$

Particulates contribute to the overall bulk density of the VCP. In equation 2.14, the fractional density difference ($\delta\rho/\rho$) is dependent upon both the temperature difference $\theta(r,z)$ and the mass of particulates inside the plume. For the case of a hot plume comprised of gases having the same composition within and without, the density difference and the fractional density difference may be dealt with according to ideal gas laws. Equation 2.48i defines the density difference, where the subscript i denotes the inside values and o denotes those for the ambient environment. Equation 2.48i may be derived using the following relations:

$$p = \rho RT$$

$$\rho_i = p_i/RT_i$$

$$\rho_o = p_o/RT_o$$

$$\delta\rho = \rho_i - \rho_o = (p_i/RT_i) - (p_o/RT_o) \; . \qquad (2.48i)$$

We assume that the mixing process occurs at a constant pressure which is equivalent inside and outside the plume's boundary. Equation 2.48i may be now rearranged as follows:

$$\delta\rho = (p/R)[(1/T_i) - (1/T_o)] = \rho_o T_o[(T_o - T_i)/T_i T_o] \; ,$$

$$\delta\rho = (\rho_o T_o/T_i T_o)(-\theta) \; ,$$

$$\delta\rho = \rho_o(-\theta/T_i) \; . \qquad (2.48ii)$$

Dividing equation 2.48ii by the ambient density (at height z), ρ_o, will result in the fractional density difference due to temperature differences between the mixing fluids. As stated, the total density difference, and hence the fractional difference, results from two factors - "dustiness" and temperature. The following expression may be used:

$$\delta\rho = (\delta\rho)_{temperature} + (\delta\rho)_{ash} \; . \qquad (2.48iii)$$

Without a temperature difference the change in the VCP density would be due only to the addition of the ash portion of the plume to the existing gas portion. Defining the ash fraction (mass per unit mass) as the ratio of ash to gas ($\times = m_d/m_g$), the density changes would be:

$$\rho_o = m_g/V \qquad (2.48iv)$$

$$\rho_i = (m_g + m_d)/V \qquad (2.48v)$$

$$\delta\rho = (m_g + m_d)/V - m_g/V = m_d/V \qquad (2.48vi)$$

$$\delta\rho = \times m_g/V \qquad (2.48vii)$$

$$\delta\rho = \rho_o \times \qquad (2.48viii)$$

$$\delta\rho/\rho = \times \quad . \qquad (2.48ix)$$

The density difference is the sum of the expressions in equations 2.48ii and 2.48ix. Dividing by the ambient density ρ_o, the fractional density difference may be expressed as in equation 2.48xi.

$$\delta\rho = \rho_o[-\theta/T_i + \times] \quad . \qquad (2.48x)$$

$$\delta\rho/\rho_o = -\theta/T_i + \times \quad . \qquad (2.48xi)$$

The preceding adaptation of the density difference and fractional density difference equations may be only used to replace the corresponding terms in the momentum

conservation equation (2.14). Chi may be redefined as necessary to account for the various individual constituents of the VCP's total mass. By similar arguments and use of the ideal gas law assumption, an appropriate form of the fractional density decrease may be derived as per the specific gaseous composition of the plume. The intention of the alteration is to account for the density changes in the VCP due solely to the ash portion of the mass as it affects the upward momentum of the VCP. A modified definition of the ash mass fraction may be described as follows:

$$M_{total} = m_{rx} + m_{gas} + m_{ash} , \qquad (2.48xii)$$

$$\chi = m_{ash}/M_{total} . \qquad (2.48xiii)$$

In the preceeding equations m_{rx} is the mass of the non-ash volcanic ejecta as pyroclasts (to be discussed later), m_{gas} is the combined mass of each gaseous specie in the model (H_2O and CO_2 herein), and m_{ash} is the mass of the volcanic ash and dust in the VCP. The mass of the ash, and hence its mass fraction chi, is diluted as the rising plume entrains ambient fluid. By the nature of the solution of the hydrodynamic equations, chi will be decrease as the model marches

the plume upward. The mass of the ash portion may be calculated using equation 2.48xiv where m_1 and m_2 are the masses of the gaseous species 1 and 2 respectively, and m_{rx} is the mass of the pyroclastic material of sizes greater than the ash in the VCP.

$$m_{ash} = (x/1 - x)(m_1 + m_2 + m_{rx}) \quad . \qquad (2.48xiv)$$

The drag forces on the pyroclasts cause the other major effect of the solids moving inside the VCP. As the plume fluid moves upward, pyroclasts of a predetermined size distribution are subject to drag forces dependent upon a particle's size, velocity, and the velocity of the fluid through which it moves. These drag forces must be summed and added into the momentum conservation equation (2.14).

The model assumes the volcanic pyroclasts are spheres. Some studies have shown that volcanic particulates more realistically have the dynamic behavior of solid cylinders moving within a fluid (Walker, Wilson, and Bowell, 1971; Walker, 1972). The model uses a Stokesian form for the drag due to an individual spherical particle (eq. 2.49). Each particle has a drag force F_D unique to its radius and velocity. By summing the individual drag forces over

the entire distribution of particles, a term which expresses the total drag will be obtained. Such a term would give the drag force for each discrete particle size, particle velocity and each VCP velocity at all points in the VCP.

$$F_D(n,v_{rx},a_i) = \int n(a_i)6\pi\eta a_i[v(a_i) - u(r,z)]d\sigma dz, \quad (2.49)$$

where $\int_0^\infty d\tau = \iint d\sigma dz = \int_0^\infty \int_z^{z+\Delta z} 2\pi r\,dr\,dz$

is the volume of a finite portion of the VCP. This technique invokes two assumptions: firstly that the distribution function is known and predetermined as a parameter for input to the model; secondly assumption is that the drag force exerted on the plume fluid by the particles is of equal magnitude to that exerted upon the particles by the plume fluid. The sum of the individual drag forces may be expressed as:

$$F_D = \sum_{i=1}^{n} N_i[6\pi\eta a_i(v_i - u(z))] \quad . \quad (2.50)$$

The distribution is assumed to be of the form shown in equation 2.51 where N_i is the number of particles within a specific range of particle sizes, a_i is the particle radius, a_g is the geometric mode of the distribution function hence the mode radius, and sigma (σ) is the standard deviation of the distribution. (See Pinnick et al., 1976). The sizes of the particles in each characteristic bin and the characteristic particle radius are listed in Table 4.

$$dN_a/da = (N_o/a\sqrt{2\pi}\ \ell n\sigma)\ \exp(-\ell n(a_i/a_g)/\sqrt{2}\ \ell n\ \sigma)^2 . \tag{2.51}$$

The momentum equation may now be modified to include the effect of dragging due to pyroclastic material in the VCP. Equation 2.52 now represents the momentum conservation equation.

$$d/dz[\int_0^\infty u^2 r dr] = -g\int_0^\infty (-\theta/T_i + \times)r dr + \sum_{i=1}^{n} n(a_i)6\pi\eta a_i(v(a_i) - u(z,r))r dr. \tag{2.52}$$

Making use of the distribution function, the mass of pyroclastic material may be calculated as a function

of the number of rocks with a specific radius and the density of the pyroclastic material. The sum of the masses as a function of radius represents the total rock type pyroclastic material at any point in the developing plume. By summing the mass of the ash and the mass of the rocks at each step, the total solid mass at any height may be calculated as per equation 2.55.

$$m_{rxi} = n(a_i)(4/3)\pi a_i^3 \rho_{rx} \quad . \tag{2.53}$$

$$m_{rx} = \sum_{i=1}^{n} m_{rxi} = \sum n(a_i)(4/3)\pi a_i^3 \rho_{rx} \quad . \tag{2.54}$$

$$\text{mass solids} = \sum m_{ash} + \sum m_{rxi} \quad . \tag{2.55}$$

TABLE 4

PARTICULATE SIZES AS DISTRIBUTED

BIN	RADIUS in microns	BIN	RADIUS in microns
1	1.000	26	322.539
2	1.259	27	406.375
3	1.587	28	512.000
4	2.000	29	645.079
5	2.520	30	812.749
6	3.175	31	1.024E03
7	4.000	32	1.290E03
8	5.040	33	1.625E03
9	6.350	34	2.048E03
10	10.079	35	2.580E03
11	12.699	36	3.251E03
12	16.000	37	4.096E03
13	20.159	38	5.161E03
14	25.398	39	6.502E03
15	32.000	40	8.192E03
16	40.317	41	1.032E04
17	50.797	42	1.300E04
18	64.000	43	1.638E04
19	80.635	44	2.064E04
20	101.594	45	2.601E04

21	128.000	46	3.277E04
22	161.270	47	4.129E04
23	203.187	48	5.202E04
24	256.000	49	6.554E04
25	322.540	50	8.257E04

F. Further Dynamical Considerations

Now, the model has been developed to account for effects due to gaseous species in the plume, pyroclasts, and ash. The complete set of hydrodynamic equations is repeated here:

$$d/dz\{\int_0^\infty urdr\} = 0 \quad , \tag{2.46}$$

$$d/dz\{\int_0^\infty \varkappa urdr\} = 0 \quad , \tag{2.47}$$

$$d/dz[\int_0^\infty u^2 rdr] = -g\int_0^\infty (-\theta/T_i + \varkappa)rdr + \sum_{i=1}^{n} n(a_i)6\pi\eta a_i(v(a_i) - u(z,r))rdr, \tag{2.52}$$

$$\theta c_{pe}(d/dz[\int_0^\infty urdr]) + [c_{pp}(dT/dz)_{net} + g]\int_0^\infty urdr = 0. \tag{2.38}$$

This set of equations specifies five unknowns in four equations. A solution can only be obtained by providing a method of closure to the system. The motion of the VCP is by nature turbulent and not laminar. A standard technique for closing this open

system is to linearize this dynamically non-linear behavior by invoking an entrainment assumption (Morton, Taylor, and Turner, 1956; Wilson et al., 1976; Baum and Mullholland, 1979; Turner, 1979). These researchers have made used slightly different forms of the same method for closure. A common form of the entrainment assumption is to relate the upward axial velocity to the radial component of the mean flow velocity in a linear proportion with respect to the lateral boundary of the plume (i.e., its radius). By defining a vector potential function such that the mean mass flux through any horizontal section of the VCP at radius r and height z is the product $2\pi\rho\psi$, equation 2.46 can be altered to express the conservation of mass in terms of the vertical gradient of the upward mass flux and the vertical gradient of the stream function ψ.

$$d/dz\left\{\int_0^\infty ur\,dr\right\} - d/dz\ \psi(\infty,z) = 0\ . \qquad (2.56)$$

Here $d/dz\ \psi(\infty,z)$ is the vertical gradient of the stream function. The vertical gradient of the stream function $\psi(\infty,z)$ is equated to the product of some characteristic

radius function, a characteristic axial velocity function and a coefficient of entrainment.

$$d/dz\ \psi = \alpha R(z)U(z)\ , \tag{2.57a}$$

where α represents the entrainment coefficient empirically determined for various flow conditions (Turner, 1979; List and Imberger, 1973; Crapper, 1977); the terms U(z) and R(z) are the mean axial velocity and the mean plume radius as functions of the vertical position z. With the entrainment hypothesis modifying the mass conservation equation, the system of hydrodynamic equations now appears as follows:

$$d/dz\{\int_0^\infty urdr\} = \alpha R(z)U(z)\ , \tag{2.57b}$$

$$d/dz\{\int_0^\infty xurdr\} = 0\ , \tag{2.47}$$

$$d/dz[\int_0^\infty u^2rdr] = -g\int_0^\infty(-\theta/T_i + x)rdr + \sum_{i=1}^{n} n(a_i)6\pi\eta a_i(v(a_i) - u(z,r))rdr, \tag{2.52}$$

$$\theta c_{pe}(d/dz[\int_0^\infty urdr]) + [c_{pp}(dT/dz)_{net} + g]\int_0^\infty urdr = 0. \tag{2.38}$$

The system may be characterized by defining a set of conditions having variable fields of the plume differential temperature, centerline velocity, and particulate mass fraction assigned similar horizontal profiles. If the assumption of strict similarity of the fields can be applied such that the normalized fields adhere to identical dimensional profiles in the vertical coordinate, a characteristic shape may be selected. Previous researchers (both experimental and theoretical) have applied primarily two characteristic horizontal shapes (dimensional profiles) - "top-hat" and Gaussian. Morton, Taylor, and Turner, 1956 discuss both forms. It has been demonstrated experimentally that neither assumed profile appears to yield more significantly accurate results over the other with respect to the modelling problem (Turner, 1979); either form may be suitably applied. Here we adopt a Gaussian profile such that the variables u, θ, and χ as functions of the cylindrical coordinates z and r become redefined as functions of z and a new variable called the mean characteristic radius R(z). Instead of the VCP fields being constant inside the lateral boundary and having values of the ambient fluid outside of the radius r, the characteristic variables decay by a factor of 1/e to the appropriate ambient values over a

characteristic length scale R(z). Substituting the characteristic variables into the set of hydrodynamic equations and performing the necessary integrations over the variable r will result in a new set of equations (eq. 2.59 to 2.62). This new set of equations expresses the characteristic mean field variables as they have been "averaged" over the domain of R(z).

$$u(r,z) = U(z)\exp[-(r/R(z))^2] \quad . \qquad (2.58i)$$

$$\theta(r,z) = \theta(z)\exp[-(r/R(z))^2] \quad . \qquad (2.58ii)$$

$$\chi(r,z) = \chi(z)\exp[-(r/R(z))^2] \quad . \qquad (2.58iii)$$

$$d/dz(R^2U) = 2\alpha RU \quad . \qquad (2.59)$$

$$d/dz(R^2U\chi) = 0 \quad . \qquad (2.60)$$

$$d/dz(R^2U^2) = 2gR^2(\theta/T_i - \chi) + \sum_{i=1}^{n} n(a_i)(R_o/R)^2\, 6\pi\eta a_i(v(a_i) - U) \quad . \qquad (2.61)$$

$$\theta(z)\exp[-(r/R(z))^2]c_{pe[d/dz)R2_U)]} + c_{pp}R^2U(dT/dz)_{net} + gR^2U = 0 \quad . \qquad (2.62)$$

Note that the Heat Conservation Equation (2.62) is not of the exact form of the other dynamic equations. Retaining the individual identities of the specific heat capacities of the ambient and convecting fluids introduces another variable into the equation. The total net vertical temperature gradient inside the VCP $(dT/dz)_{net}$ may be expanded as follows:

$$(dT/dz)_{net} = d\theta/dz + (dT/dz)_{environmental} \quad . \qquad (2.63)$$

Such an expansion modifies equation 2.62 to:

$$\theta(z)\exp[-(r/R(z))^2]c_{pe}[(d/dz)R^2U)]$$

$$+c_{pp}R^2U[d/dz(\theta(z)\exp[-(r/R(z))^2)]$$

$$+ c_{pp}R^2U(dT/dz)_{env} + gR^2U = 0 \quad . \qquad (2.64)$$

Analogously let us rewrite the first two terms of equation 2.64 as

$$A\ c1\ d(BE)/dz\ +\ c2\ BE\ d(A)/dz$$

where A, B, and E are variable fields. In this case, because of the two different constants c1 and c2, it is not possible to form an exact differential of the form d(ABE)/dz . Hence the more realistic Heat Conservation Equation may not be compatible with the forms of the other dynamic equations. This may adversely affect finding a unique solution to the set of coupled equations. Therefore an approximation method will be employed. Returning to the Heat Conservation Equation as expressed in equation 2.36, a modified treatment may be applied. Once again the density may be extracted from the equation as previously demonstrated, the suitable characteristic variables utilized, and integration over r from zero to infinity may be performed. The result is now equation 2.65 where c_p is now c_{pp} as given by the effective equations for the specific heat as a function of temperature and gaseous concentration (2.36v).

$$d/dz\left\{\int_0^\infty \rho\theta u r dr\right\} + (g/c_p)(1 - \Delta)\int_0^\infty \rho u r dr = 0 \quad . \qquad (2.36)$$

$$d/dz(R2_{U\theta}) + 2(g/c_p)(1 - \Delta)R2_U = 0 \quad . \qquad (2.65)$$

Delta takes on the functional form:

$$\Delta = -(c_{pp}/g)(dT/dz)_{environment} \cdot \qquad (2.66)$$

The assumption in this revised method is that one is allowed to collect the two leading terms making an exact differential from the equation 2.65. This implies that C_{pe} and C_{pp} must be equal - which they are not. This slight assumption allows one to retain the same form for all of the dynamic equations. This similar form enhances the ability to solve the set of simultaneous equations. The model accurately calculates the specific heat of the VCP and places it appropriately back into the equation so as to avoid any further equivalence with that of the ambient environment.

G. A Model Solution

The model employs the following method of solution: each equation in the set of hydrodynamic equations was expressed as the total differential of a combination of the characteristic variables plus some constant multiplied by the step change in the axial direction dz. Each total differential was then

expressed as the sum of its partial differentials with respect to the characteristic variables R, U, θ, and χ . The result is a set of four equations in the four characteristic variables being equated to a product of a constant and the size step dz. This set (equations 2.67i to 2.67iv) is:

$$(2RU)\, dR + (R^2)\, dU + (0)\, d\theta + (0)\, d\chi = [A']\, dz \quad ,$$

$$(2RU\chi)\, dR + (R^2\chi)\, dU + (0)\, d\theta + (R^2U)\, d\chi = [B']\, dz \quad ,$$

$$(2RU^2)\, dR + (2R^2U)\, dU + (0)\, d\theta + (0)\, d\chi = [C']\, dz \quad ,$$

$$(2RU\theta)\, dR + (R^2\theta)\, dU + (R^2U)\, d\theta + (0)\, d\chi = [D']\, dz \quad ,$$

(2.67i - 2.67iv)

where

$A' = 2\alpha RU$

$B' = 0$

$C' = 2gR^2(\theta/T_i - \chi) + \sum n(a_i)(R_o/R)^2 6\pi\eta a_i(v(a_i) - U)$

$D' = -2(g/c_p)(1 - \Delta)R^2U$.

A computer solved for the values of the field variables as they are incremented from some initial value at any given point z to their new values at the points $z + \Delta z$.

The matrix of the spatial differential coefficients is subjected to manipulation via a least pivotal divisor elimination routine. This method of quadrature results in the numerical solution of the equations given the appropriate boundary values.

III

MODEL VALIDATION AND SENSITIVITY STUDIES

III. MODEL VALIDATION AND SENSITIVITY STUDIES

A. Introduction

This section considers model validation; that is, the results of running the model for a variety of different input parameters to see if it responds reasonably. For example, one would expect a large, hot plume to achieve a greater altitude than would a cooler, smaller plume. The model is sufficiently complex that it is not clear that such a result would actually occur, or to which parameters it would be due. Consequently, it is neccesary to carry out model validations. The model results are scrutinized for sensitivity to some choice of input parameters.

Before describing the model validations and sensitivity tests, we discuss the model framework and parameters. Then we will describe the validation and sensitivity runs and summarize the results.

B. Model Framework and Parameters

The model is encoded as a computer program which simultaneously solves the differential equations (2.67i-iv) by diagonalizing the matrix of coefficients using a least pivotal divisor elimination method. The result of this matrix technique is to output values of the difference quantities dR, dU, $d\chi$, and $d\Theta$ for the given step dZ. This allows us to step the developing VCP upward from height Z to height Z + dZ. For most cases the model is run with the value of dZ equal to one meter, and we obtain new values of radius, upward velocity, ash fraction, and differential temperature (hence VCP temperature) at each meter of altitude. At each step upward along the flow direction a variety of required ancillary calculations are carried out. For example, the calculated concentration of gaseous species in the VCP is also used to calculate the resulting specific heat capacity. Similarly, when the rock velocity of a specific particle size is negative the rocks are assumed to fall out of the plume, and the number of rock particles having that specific particle radius is set to zero; this eliminates the contribution to the net drag force due to particles moving downward. Another important ancillary calculation is the value

of the ambient temperature as a function of height determined from the altitude and the environmental lapse rate.

The model parameters used in an arbitrarily configured "standard case model" were the following (see Table 5): The initial altitude was set at 3000 meters above ground zero. This was selected because we wished to be above the jet portion of the VCP. Reasons for starting our model beyond the major portion of the jet region were based upon the following criteria: 1) the jet phase is an impulse and momentum dominated phenomenon which represents only the lower regions of a volcanic VCP event; 2) although the physics and hence the descriptive equations are of similar form for jets and plumes, the scaling factors for such equations are not identical - adjusting the model for such factors has not been part of this study; 3) the value of the entrainment constant for jet models is numerically different from that for a "forced plume" as it becomes functionally dependent upon the local Froude Number and cannot be assumed linearly proportional to the main flow velocity as we have done herein. This would present a problem with the method of closure adopted in this model; although such a problem can be handled, it was not deemed to be a

necessary part of this research. In the model validation runs the tropopause height was set to 10 kilometers. The density of the individual pyroclasts in the VCP was assumed to be 2500 kilograms per cubic meter; this value is not very reasonable for volcanic ash ejecta but is often used to calculate "dense rock equivalent" of the total ash ejecta material. The convecting fluid was initially taken to be air, although later the gaseous VCP was set with a composition of 65% H_2O and 35% CO_2 (by weight) at the vent. The radius of the VCP at the initial point of calculation was 250 meters, and the upward velocity at this point was set to 400 meters per second. This velocity value was selected arbitrarily and allowed to vary as discussed in the section on experiment 2. The temperature of the plume was assumed to be 100 degrees greater than that of the surrounding air at the initial height. The ash fraction was set at 0.35 by weight. We allowed the entrainment coefficient to be 0.07 which is considered a reasonable value based upon empirical evaluations (Turner, 1979).

The rock particulate parameters were chosen as follows: The mode radius of the log-normal particle distribution was taken to be 60.0 microns with a standard deviation (sigma) value of 1.60. For

numerical purposes the rocks were distributed into 50 size "bins", the smallest bin containing rocks of radius 1 micron. Each bin contains rocks with an individual volume twice that of the rocks in the preceding bin. Given an initial number density (the concentration of particulates as total number per cubic meter), the distribution function will distribute into the separate bins the number of particles in the apropriate radius range for each bin. The sum of the particles in each bin is equal to the actual number of particles per cubic meter of the VCP that have the radii in the range characteristic of that specific bin. As the VCP moves upward, its radius and hence its volume increases, thereby diluting the plume by entrainment of ambient fluid. This dilution, along with the dropping-out of pyroclasts will decrease the number of total particles per cubic meter of VCP fluid. The original number concentration was set at 1.25E8 particles per cubic meter at the start of the VCP motion.

TABLE 5

STANDARD CASE MODEL: PARAMETER VALUES

U START	400.00	m/s
R START	250.00	m
θ START	100.00	Kelvin
χ START	0.35	
α	0.07	
AMBIENT PRESSURE	101.325	KPa
AMBIENT TEMPERATURE	288.00	K
AMBIENT TEMPERATURE LAPSE	-6.5	K/Km
TROPOPAUSE HEIGHT	10.0	Km
RELATIVE HUMIDITY	0.25	
STEAM / CO_2 RATIO	0.65/0.35	
PARTICULATE CONCENTRATION	1.25E8	m^{-3}
PARTICULATE MASS DENSITY	2500	Kg/m^3
MODE RADIUS	60.00	micron
STANDARD DEVIATION	1.60	micron

The Standard Case Model produces a VCP reaching a maximum altitude of 10.12 kilometers.

C. Validations and Experiments

i. Experiment 1 - the effect of the iterative step size

The model in its executable form steps upward along the verticle axis by a step size dz. A suitable size step is a necessary control upon the stability of the numerical solution. If the step size is too large, the variables will change greatly but there is no assurance of linear continuity between the solution values at each successive step. If, on the other hand, the step size is too small the number of iterations required to march the VCP upward becomes very large and computer processing time is greatly increased. One desires a model which produces stable solutions with a reasonable execution time.

Initial experiments run with step sizes of 25 and 50 meters showed that the resulting values of the field variables at specified spatial positions varied greatly between the two sets of data. This observation indicated that step size should be reduced to the order of meters. The standard case, previously described, was run using the step sizes of : 10.0, 5.0, 2.0, 1.0,

0.5, and 0.1 meters. In each case the model executed until the maximum height for the VCP was reached.

Table 6 shows that the step size parameter affects the model in the following ways: 1) changes of one order of magnitude show insignificant changes upon the maximum height obtained; 2) a decrease of one order of magnitude in step size slightly increases the mean upward axial velocity and slightly reduces the characteristic radial length; 3) and, the mean velocity at the maximum height approaches zero as the step-size decreases.

Consequences of the step-size sensitivity may be considered as important factors in model use. For example, if one were interested only in the maximum altitude obtainable with a given set of initial conditions, the step-size could be increased from its suggested value of 1.0 meter to use less computer processing time. However, if one is interested in velocity dependent information associated with the VCP behavior a suitably small size step must be retained to insure accurate results.

TABLE 6

SUMMARY OF THE EFFECTS OF THE ITERATIVE STEP SIZE

		Distance From The Source		
DELZ	H_{MAX}	10 Km	8 Km	6 Km
(m)	(kilometers)		(velocity m/s)	
	(velocity m/s)		(radius in m)	
10.00	10.0500	12.2 m/s	94.4 m/s	159.0 m/s
	-3.0 m/s	3063.9 m	1014.6 m	658.6 m
5.0	10.0900	18.1 m/s	96.0 m/s	161.0 m/s
	-3.5 m/s	2569.6 m	1009.3 m	656.0 m
2.00	10.1120	21.0 m/s	97.0 m/s	162.1 m/s
	-1.6 m/s	2403.0 m	1006.2 m	654.5 m
1.00*	10.1190	21.9 m/s	97.3 m/s	162.5 m/s
	-0.5 m/s	2358.4 m	1005.2 m	654.1 m
0.50	10.1225	22.3 m/s	97.5 m/s	162.7 m/s
	-0.2 m/s	2337.7 m	1004.7 m	653.8 m

* Standard Case

ii. Experiments With The Characteristic VCP Variables as summarized in TABLE 7

TABLE 7

SUMMARY OF EXPERIMENTS PERFORMED

EFFECT OF	RANGE	# CASES
INITIAL UPWARD VELOCITY	50-1000 m/s	20
INITIAL STARTING RADIUS	25-1000 m	40
INITIAL TEMPERATURE DIFFERENCE	25-1000 K	40
INITIAL ASH FRACTION	0.00 - 0.95	20
TROPOPAUSE HEIGHT	6.0 - 20.0 Km	28
AMBIENT TEMPERATURE GRADIENT	4.0 - 20.0 K/Km	32
SPECIFIC HEAT OF GASEOUS EFFLUENT (RELATED TO THE STEAM/CO_2 RATIO)	1/0 to 0/1	40
PARTICULATE NUMBER DENSITY	1.25E4 - 1.25E10/m^3	10
MODE RADIUS OF THE DISTRIBUTION	25 - 500 μm	20
STANDARD DEVIATION	1.25 - 10.0 μm	20
MASS DENSITY OF PYROCLASTS	1000 - 2500 Kg/m^3	7

a. Experiment 2 - the effect of the initial upward velocity

The purpose of this experiment was to determine the general relationship between the initial upward velocity and each of the characteristic mean fields of the VCP. the model was run at its standard conditions while changing the initial upward velocity. ets of biaxial graphs depicted the profile of each characteristic field with height as a function of the variably changing initial condition. Each value of the test parameter will generate a line on the biaxial graphs. In the same fashion, each parameter tested has been so analyzed.

Figure 1 shows the vertical profiles of the characteristic mean VCP velocity field for values of the initial velocity ranging from 50 to 1000 meters per second in 50 meter per second increments. As expected, the magnitude of the velocity field decreases with height. The shape of the velocity field with height is similar for all values of initial velocity. Any given initial velocity should then show the VCP velocity decreasing with height in similar fashion. Note that the velocity decrease with height is rapid within the first 500 meters above the starting

elevation then passes into a region of more moderate decrease, then decreases more rapidly with height as the VCP approaches its maximum altitude.

Figure 2 shows the vertical profile of the characteristic radius field (length scale) for each initial value of the upward velocity. The radial profiles all appear to be of the same form. With an increasing initial upward velocity a greater maximum height may be obtained; and, with a taller plume, the radius will be greater. Changing the upward velocity does not affect the cross-sectional shape of the VCP. One must be careful not to impute a direct correlation between the characteristic radial profile and the actual plume boundary. This radial boundary has two traits as far as use in this model is concerned: 1) the shape has been adopted as a consequence of our choice of a similarity assumption for the sake of closure of the hydrodynamic system of equations (experiments justify the appropriateness of this assumption Morton, Taylor, and Turner, 1956), and 2) by defining the characteristic radius, it may have little discernable correlation to the visible lateral boundary of the VCP.

Vertical profiles of the differential temperature (Theta) and ash fraction (Chi) as respectively shown in

figures 3 and 4 reflect no change with initial upward velocity. Since no effective change occurs as a consequence of the velocity, one may consider the shape of these vertical field profiles as a standard. The characteristic differential temperature decreases rather parabolically with height to the tropopause (10.0 kilometers), after which it decreases linearly by virtue of the environmental stratospheric lapse rate used. Notice that for cases in which the upward initial velocity was at least of magnitude equal to that of the standard case (400 m/s), the VCP reached into the stratosphere as reflected in the linear decrease of differential temperature (see figure 3).

The decrease of the ash fraction with altitude shows virtually no response to changes in the initial upward velocity. All field lines appear to have the same shape and lie on the same path. This indicates that the decrease in ash with increased altitude is not a velocity-dependent phenomenon but perhaps due solely to dilution as a consequence of our entrainment-mass conservation assumption (see figure 4).

A graph depicting the maximum altitude obtained (above the starting elevation) as a function of the initial upward velocity is presented as figure 5. This figure shows the low-trajectory positively curved

increase in maximum height obtained with increased initial velocity. Larger upward velocities cause the VCP to reach greater maximum heights. This increased size of the plume has a larger radius.

b. Experiment 3 - the effect of the initial starting radius

Values of the starting radius for the VCP were changed from 25 to 1000 meters in increments of 25 meters. Figure 6 shows that the velocity field profile does not change shape with changes in the starting radius. This continual spectrum of field lines shows that decreasing the radius will result in a lower resulting height but the velocity will decrease with the height in similar fashion for all starting radius values. The starting radius has slight effect upon the characteristic VCP radial profile showing only an increased radius field with height as the the larger starting radius produces a taller, wider plume (see figure 7).

The profiles of differential temperature (figure 8) are more or less parabolic to the value of Theta at the tropopause, after which they decrease linearly to

the maximum height. For increasing values of the initial radius the field lines become steeper, upward curves which once again follow a linear path from the tropopause to the maximum height. This indicates that the differential temperature decreases more rapidly with height for an event with a narrower starting radius.

The vertical profiles of the ash fraction, (figure 9), follow paths of a similar nature to those of the differential temperature with the exception of not departing from their trajectories above the tropopause. This indicates that the ash fraction may not be dependent upon the ambient temperature lapse, but steadily decreases by dilution as the entraining VCP ascends.

Tests of initial radius on the maximum altitude of the VCP showed a steadily increasing trend for increasing values. For all values tested from 25 to 1000 meters an increase in the starting radius produced a corresponding positively increasing non-linear dependency of the maximum height upon the starting radius (see figure 10).

c. Experiment 4: effect of the initial differential temperature

These tests examined the effect of changing the initial differential temperature on the VCP characteristic fields. Values of the initial initial differential temperature were ranged from 25 to 1000 Kelvin in 25 degree increments. A summary of the results of this experiment are as follows: The shape of the velocity profiles as a function of differential temperature appeared non-linear (see figure 11). As the value of Theta initial was increased, the rate of velocity decrease with altitude was less severe. In each case the velocity decrease is initially rapid (greater deceleration) passing into a period of less rapid decrease with height (less deceleration) and finally decreasing more rapidly again (increased deceleration) as the VCP approaches its maximum altitude (as its mean velocity approaches zero). As the initial value of Theta is increased, the plume reaches a greater altitude and hence aquires a greater radius. The radial profiles as a function of the initial value of the differential temperature show a pattern consistent with those of the previous

experiments (see figure 12) except that the correlation is more positive in the height axis (compare figure 12 with figure 2). Varying the initial differential temperature indicates that Theta will decrease more rapidly with altitude for cases with greater initial values, then decrease gently toward the maximum altitude (see figure 13). Once again, in cases where the tropopause is penetrated, the decrease in Theta with height becomes more linear. Changes in the initial value of Theta show no effect upon the profile of the ash fraction (see figure 14). Increasing the initial differential temperature increased the maximum height reached by the VCP in a constant, positively-curved fashion (see figure 15).

d. Experiment 5: the effect of the initial ash fraction chi

The standard model was run using initial values of the ash fraction from 0.00 to 0.95 incremented by 0.05. The velocity profiles as a function of the ash fraction appear similar to that of the previously examined experiments (see figure 16), except an increase in the ash fraction tends to decelerate the plume more efficiently. The radial profiles tend to be grouped more closely together than those of the other experiments figure 17). Here again the increase in the ash fraction tends to cause a smaller VCP. The changes in the initial ash fraction have no effect on the profile of differential temperature with height; the entire differential temperature spectrum was plotted as a single line in figure 18. An interesting result shown in figure 19 is that the ash fraction decreases more rapidly (by dilution) in the cases where it had the greatest initial value. The ash fraction increases the density of the VCP fluid and thereby reduces its buoyancy as a result of increased body forces. Therefore an increased initial ash fraction should reduce the maximum height of the VCP as is shown in figure 20.

e. Summary of the Effects of the Characteristic VCP Variables

Another method of reviewing the data from these experiments is to group sets of a specific characteristic variable profile, for example, placing all of the velocity profiles together. Thus one could more easily resolve which parameters appeared to have the most (or least) significant effect upon a specific characteristic field.

The sets showing the vertical profile of the mean upward velocity (figures 1, 6, 11, and 16) exhibited the following: 1) Changes in the starting radius value bring about the least change in the spectrum of vertical profiles of the VCP mean velocity. 2) The initial value of the differential temperature can alter the vertical deceleration of the VCP flow as shown in the wide spectrum of vertical velocity profiles generated for the cases tested. 3) The initial value for the ash fraction (Chi) can also alter the acceleration by rapidly decreasing the velocity with height as initial values of chi are increased. This effect is not as pronounced as that due to the

differential temperature. 4) Increasing the initial value of the flow velocity causes a more rapid deceleration of the VCP in its early stages.

The vertical profiles of the characteristic radius (figures 2, 7, 12, and 17) show that the initial temperature difference and the initial ash fraction most greatly alter the VCP radius. Increasing Chi decreases the overall resulting size of the VCP and hence its radial profile is constricted. Increasing the differential temperature causes taller VCPs with expanded radial profiles.

The profiles of differential temperature (figures 3, 8, 13, and 18) show a moderate response to the initial differential temperature and to a lesser extent the initial radius. Increases in the differential temperature increase the rate of which the differential temperature decreases with height (figure 13). Increases in the starting radius have the slight effect of reducing the differential temperature lapse rate in the early ascent of the plume (figure 8).

The vertical profiles of the ash fraction slightly respond to changes in the characteristic variables (figures 4, 9, 14, and 19). A larger initial source

radius decreases the vertical rate of dilution of the ash fraction. Increasing the initial value of chi itself tends to increase the vertical rate of dilution of the ash fraction in the lower regions of the ascending VCP.

Effects of changing initial values of the characteristic variables upon the maximum height are shown in figures 5, 10, 15, and 20. Increases in initial velocity and initial starting radius produce VCPs of greater maximum heights; this phenomenon occurs at apparently equivalent rates. Similarly, increases in the intial differential temperature show increases in the maximum height of the VCP; this effect seems to be more pronounced than that resulting from the values of initial velocity or the intial radius. As expected, increasing the ash fraction decreases the maximum height of the VCP.

iii. Experiments With The Ambient Environment

Since the model was intended simulate a variety of volcanic events, it had to be capable of modeling various environmental conditions. Two experiments were performed to test the effects of the ambient environment upon the standard VCP model. By altering the height of the tropopause (experiment 6) and the environmental temperature profile (experiment 7), observations could be made upon the model's sensitivity to its surrounding environment. Once the response to the ambient environment is understood, the environmental parameters could be set to simulate specific geographical and/or seasonal conditions; the model could then be executed to produce a VCP event under those conditions.

a. Experiment 6: the effect of the tropopause height

The height of the tropopause as well as the ambient temperature profile may be selected as model input parameters. In the standard case the tropospheric temperature lapse was constant, although

the model can accommodate variable lapse rates. For all heights below the tropopause the ambient temperatures and densities are calculated from the initial values input for the lapse rate and source-level pressure above the tropopause the standard case uses an isothermal region up to an altitude of 20.0 kilometers. The tropopause represents a discontinuity in the vertical temperature gradient. Placement of the tropopause at various altitudes will allow one to observe possible changes in the VCP behavior in response to the altitude of this discontinuity. The model can accommodate discontinuities in both temperature and pressure fields. Specifically we have emplaced discontinuities at the stratopause and mesopause.

Values for the tropopause altitude were tested in a range from 6.0 to 20.0 kilometers in intervals of the 0.5 kilometers (figures 21 to 25). As expected, the vertical velocity profiles show no change from standard conditions. The vertical radial profiles also show no change (figure 22) from those of standard case. The differential temperature plots (figure 23) show no changes at heights below the tropopause. In each individual case the differential temperature branches from the curve at the height of the tropopause to

follow its nearly linear decrease to the maximum height. Changing the height of the tropopause has no effect upon the vertical profile of the ash fraction of the VCP (see figure 24). Changes in the vertical position of the tropopause have the effect of increasing the maximum height obtained by the VCP with increasing values of the tropopause height. This effect occurs in the range of values from 6.0 to 12.0 kilometers for the height of the tropopause. At values of tropopause height above 12.0 kilometers the standard VCP will not achieve any greater altitude. This leveling-off occurs at the altitude where the path of the decrease in the VCP differential temperature intercepts the path of the ambient temperature decrease with height; above this height further decreases in the tropopause elevation can not contribute to buoyant driving of the VCP.

b. Experiment 7: the effect of the ambient vertical temperature gradient

Seasonal and geographical considerations play an important part in the actual determination of a local vertical temperature gradient; therefore, experiments

with the ambient vertical temperature gradient can reflect the effects of location and season upon a given VCP event. The model uses an ambient vertical temperature gradient to calculate the environmental temperature at height. Values of the differential temperature are obtained as a result of the model solution; the ambient temperature at height is obtained and the actual VCP temperature at height is the sum of the ambient temperature and the differential temperature (at each height). The vertical temperature gradient is a model parameter which is set constant for all altitudes below the tropopause height. Gradients from 4.0 to 20.0 Kelvin per kilometer were tested in intervals of 0.5 Kelvin per kilometer. The standard case model was run for each value tested (see figures 26 to 30). For gradients less than approximately 7 Kelvin per kilometer the VCP decelerates with height along paths as previously described in other experiments - as the ambient vertical temperature gradient is increased (as an initial value) the deceleration is lessened as the VCP reaches greater heights. In cases it penetrates the tropopause, the VCP decelerates constantly above the tropopause. In the region of values from 7 to 15 Kelvin per kilometer, the vertical velocity profiles

show a continually diminishing deceleration with height as they approach the tropopause; above the tropopause an increase in the deceleration occurs until the maximum height is achieved. For gradient values greater then 15 Kelvin per kilometer the VCP decelerates most slowly prior to the tropopause and reaches a point of zero deeceleration. Prior to its passing through the tropopause barrier, the VCP undergoes a positive acceleration then reaches a point of zero acceleration before its final stage of deceleration into the maximum height obtained. This effect is more pronounced with increased values of the ambient vertical temperature gradient. Since the increased environmental temperature gradient would yield colder temperatures at a given altitude, the hot VCP would have a greater buoyant force potential than an identical VCP convecting in an atmosphere with a lower environmental thermal gradient. The increased buoyant force would effect both the thermal energy and momentum equations.

Setting the model for increasing environmental gradients increases the buoyant force terms causing the VCP to reach a greater maximum height. It is expected that the increased buoyancy and heights obtained by VCPs from increased environmental temperature gradients

will also result in VCPs of larger dimensions (i.e., their radii will be greater). So, larger values of the environmental temperature gradient will produce taller VCPs with an increased radius at the maximum height. Figure 27 shows the result of all cases tested where the sixth line from the bottom is the standard case).

Vertical profiles of the differential temperature all show a steady non-linear decrease in the early stages of the VCP. As the VCP approaches the tropopause this decrease diminishes, and in most cases the differential temperature reaches a constant value. After the VCP reaches the tropopause the differential temperature decreases almost linearly to its maximum height. For increasing values of the environmental vertical temperature gradient, the differential temperature decrease with height stops at a lower VCP altitude. After the differential temperature lapse rate goes to zero, the differential temperature will then increase with height up to the tropopause. At the tropopause boundary, the differential temperature will once again decrease with height in an almost linear fashion until the maximum height is obtained by the VCP. The region showing an increase in the differential temperature with height should be the

result of lower ambient temperatures experienced at a given height caused by values calculated from increased environmental gradients.

Increases in the environmental vertical temperature gradient tend to produce a taller, wider VCP in the upper stages of the flow (see figure 27). The increased radius in the upper regionof the VCP implies an increase in entrainment of the ambient environment, hence a slightly greater dilution of the gaseous and ash fractions within the VCP. Figure 29 shows the decrease of the ash fraction, Chi, in the upper regions of the VCP as the environmental vertical gradient is increased.

Increased values of the environmental vertical temperature gradient produce an increase in the buoyant force terms of both momentum and heat conservation equations. The increased initial buoyant force and the greater buoyant production at altitudes in the upper region of the VCP due to colder ambient temperature causes the standard case VCP to achieve greater maximum heights. A smooth continuous non-linear increase in the maximum height of the VCP was accomplished by increasing the environmental vertical temperature gradient through a range of values (figure 30).

By comparison of the results from the two experiments on the effects of the ambient environment (figure 30 with figure 25), it appears that the vertical temperature gradient has more influence on the maximum height obtained by the VCP than does the height of the tropopause.

iv. Experiments With The Pyroclastic Particulate Parameters

Four experiments tested the effects of the tuneable parameters of the pyroclastic contribution to the VCP model: These parameters are the Number Density of the Particulate Distribution in particles per cubic meter - ZNO, the Mode Radius of the Particulate Distribution function (the size in microns of the particle at the distribution function's maximum) - Rg, the Standard Deviation of the distribution function (as measured in the units of the particles' radial dimension) - Sigma, and the Mass Density of the individual particulate material (in kilograms per cubic meter) - RXDENS. Experiments were made with the standard model varying each of these parameters through a range of values while keeping all other model conditions at those of the standard case. Such tests comprised experiments 8, 9, 10, and 11.

The model has separated the four major pyroclastic parameters into portions of an algorithm which are not dependent upon the presence or concentration fraction of ash (chi) in the model. As such, these pyroclastic parameters pertain only to the portion of the volcanic

ejecta where the individual particulates of characteristic dimension are greater than those of the ash-dust fraction. In reality, particles comprising the ash fraction chi are of sizes which would exist under the near tail (small range) of the distribution function. For model purposes the ash fraction and the pyroclastic rock parameters are non-interacting. The pyroclastic particulate parameters are used in the model in the following manner: 1) distribute the original number density of particulates into the number of particles with a specific radius between two discrete sizes, as per the parameters of the distribution function (see eq. 2.51); 2) calculate the mass of each individual particle and of all of the particles in all of the discrete size bins; 3) calculate the weight force of all of the particles in all of the discrete bins; 4) calculate the drag force of each individual particle in each discrete size-bin and sum all of the drag force over all particles in all bins; 5) and finally, the summed drag force and summed weight force are used in the simultaneous equations of the model. These parameters yield the value of the net drag force and the pyroclastic mass (and hence weight force) as functions of height. The resulting drag and weight forces enter the model via the momentum

conservation equation (equation 2.61) as they are factors in the net force and the buoyancy terms.

a. Experiment 8: the effect of the particulate number density

This experiment seven cases were tested with the initial particle concentration ranging from 1.25E4 to 1.25E10 particles per cubic meter by each order of magnitude. The standard case (1.25E8 particles per cubic meter) was bracketed within this range by several orders of magnitude in either direction.

Previous experiments demonstrated that the characteristic velocity field decelerates with height through an inflection point into another region of greater vertical deceleration just prior to the maximun height achieved by the VCP (where the velocity is negative). This shape is also reflected in the Particulate Number Density experiment (see figure 31). For the first four cases (ZNO=1.25E4, 5, 6, and 7 particles per cubic meter) the VCP velocity profile was identical and the data were plotted as a single path. The fifth case was the standard case model and followed the general profile but slightly diverged from the

cases of lower order magnitudes. It can be shown that increased initial particle concentration causes the inflection point of the velocity profile to migrate toward a position corresponding to a distance closer to the VCP's starting point. This causes the VCP to retain a greater velocity at a given height for an increase in the particulate number density; this result was not expected. Conversely, the altitude at which the VCP has a specific value of the mean velocity (for example, one-half the starting velocity) is greater for cases with greater particulate number concentrations. This effect was noticed for all cases up to the concentration value of 1.25E10 particles per cubic meter. Attempts to run the model for cases with the pyroclastic particulate concentration greater than 1.0E11 per cubic meter resulted in a total collapse of the VCP, and forced the model to stop. In such cases it is believed that the drag force terms exceed the buoyant force terms by sufficient amount to consider the upward motion as impulsive in nature and hence without buoyancy; such conditions leave the model devoid of convection and stops the model.

Radial profiles of the VCP as a function of the initial pyroclastic particulate concentration show a constriction of the characteristic radial dimension at

all heights for increased number concentrations (figure 32). This is due to the retention of greater velocities at height for the increasing number concentration. Once again the cases in the range from 1.25E4 to 1.25E7 particles per cubic meter showed no variation.

Increasing the initial pyroclastic particulate concentration has little effect on the profile of the VCP differential temperature with height (figure 33). The cases tested seemed to form identical profiles in two regions - Cases for 1.25E4 to 1.25E7 particles per cubic meter and those of 1.25E8 to 1.25E10 particles per cubic meter. The profiles show all cases originally identical, diverging during the middle altitudes of the VCP and converging to identical values again near the upper regions of the VCP. In the region of divergent differential temperature profiles, the cases for an increased number concentration showed a very slight increase in the differential temperature lapse rate.

the vertical profiles of the ash fraction field also showed two distinct regimes with an increased dilution of the ash concentration with height for the cases with initial pyroclastic particulate

concentrations at or above those of the standard model (figure 34).

The cases tested for values of the initial pyroclastic particulate number concentration below that of the standard case (1.25E8 particles per cubic meter) show no variation in the maximum height reached by the VCP except that all values produced a slightly lower maximum height. Of the cases tested where the particulate number concentration exceeded that of the standard case, a slight increase in the maximun height occurred with an increase in the number density. Tests with concentrations in the vicinity of 1E11 particles per cubic meter resulted in a collapsed VCP and no reliable maximum height calculation.

b. Experiment 9: the effect of the mode radius of the distribution function

In this experiment the model was run varying the mode radius of the particulate distribution function from 25 microns to 500 microns by increments of 25 microns. By increasing the mode radius, the distribution function would generate a proportionately greater number of particles at larger radii; these

larger particles have greater drag forces exerted upon them, and their velocities may decrease more rapidly. As a result, larger particles fall out of the plume earlier than the smaller particles, and the net drag force exerted upon the VCP is diminished. If this hypothetical process is in effect, the larger the mode radius of the particulate distribution function, the greater the number of larger particles available to rain out of the plume, thereby leaving only those smaller particles to affect the net force and hence retard the momentum of the plume.

The velocity field profile for the smaller mode radius values resembles the characteristic profile for the standard case field. As the mode radius is increased, the inflection point of the deceleration change migrates toward a value at a greater velocity. This point of change in the vertical rate of deceleration occurs closer to the VCP starting coordinate for the increased values of the mode radius. In other words, the VCP retains a greater velocity at all altitudes and decreases its velocity with respect to vertical position more gradually for increased values of the mode radius (figure 36). This gradual, gentle decrease in the vertical velocity gradient seems to converge to a consistent form for the cases tested

where the mode radius exceeds the region of 300 microns up to the final case of 500 microns.

As the velocity appears to be greater at a given altitude for a VCP having its particles distributed about a larger mode radius, the resulting shape of the VCP is that with a taller, narrower profile (figure 37).

For shifting the mode radius to a larger value, the resulting VCP shows an extremely small decrease in the differential temperature field with height (figure 38). This miniscule change in Theta is probably due to a slightly higher velocity leading to proportionately greater entrainment and slightly greater cooling. A somewhat similar result is reflected in the profiles of the ash fraction field which show a more diminished fraction with height for cases where the pyroclastic particulate distribution (not directly proportional to the ash fraction) has a greater mode radius (figure 39). As seen in previous experiments, this suggests a greater dilution with height of the VCP fluid in such cases.

For all values tested within the stated range, a positive shift in the mode radius of the distribution function yielded a slight positive increase in the maximum height obtained by the VCP (figure 40). The

path of this height increase as a function of the mode radius of the distribution function is a flat low-trajectory curve of positive slope.

c. Experiment 10: the effect of the standard deviation of the particulate distribution function

In this experiment the standard model was used and all values of the rock (pyroclastic particulate) parameters were held at their standard values, while the standard deviation of the distribution function was varied. Twenty cases were evaluated in a range from 1.5 to 10.0 microns incremented by 0.5 microns and a lower limiting case of 1.25 microns was also included. These twenty cases were executed in an order of increasing sigma values (i.e. 1.25 to 10.0).

The characteristic velocity field plots appear to be of identical nature with those from the previous experiment - experiment number nine (see figure 41 and compare with figure 36). The two distinctly shaped regimes are for cases of sigma less than 3.5 which show the same vertical velocity profile as the standard case model (see figure 1), and the cases for sigma greater

than 6.0 which show a smooth gradual velocity decrease with increased VCP height.

Increasing the standard deviation of the distribution function has the effect of generating VCP's with a smaller characteristic radius (see figure 42). Virtually no effect is seen upon the vertical profile of differential temperature for the range of cases tested, which is verified in figure 43. For increasing values of the standard deviation, the curve of the ash fraction with height becomes widened (figure 44). Due to the shape of this curve in the standard case, this widening actually makes the profile appear to be a flatter, parabolic-like curve representing a greater dilution of the ash fraction as the VCP ascends. Upon examination of the maximum height data an interesting result was discovered. At values of sigma less than 2.0, the maximum height obtained by the VCP appears to be in the vicinity of that from the standard case (approximately 10.1 km); in the cases of larger standard deviations (2.0 to 10.0), a very low-trajectory, positive-curved relationship occurs between the increase of the deviation and a resulting increase in the maximum height of the modeled VCP (see figure 45). One could expect that the concentration of particulates, and to a lesser extent

their size distribution would affect the maximum height reached, but that the nature of the distribution would have no percievable contribution to this effect.

d. Experiment 11: effect of the mass density of the pyroclastic particulate material

The density of the pyroclastic material is a contributor to a few properties of the VCP. Each individual particle (of known dimension) adds mass to the VCP. By knowing the dimensions of each particle, its material density can be used to obtain its mass; the distribution function can then be employed to sum all of the particles and their total mass to the mass of the VCP fluid. The effect of altering the VCP fluid mass is a change in the fluid density itself. It is the fluid density of the VCP which enters the momentum and heat conservation equations as a part of the hydrodynamic model. The density of each individual particulate is also used in the calculation of the drag force due to that particle and hence becomes a part of the summed drag force term in the momentum conservation equation. Without considering the magnitude of the contribution due the "rock density," it was thought that an experiment should be performed to determine the

significance of this factor as it enters the model in two equations. The standard case model was run with values of the pyroclastic material density from 1000 to 2500 kilograms per cubic meter by increments of 250.

The shape of the VCP mean velocity vertical profile resembled that of the standard case model for all values of the rock density tested. Not only was the velcity profile of similar shape, but all values showed the seven cases plotted on top of each other as a single line (see figure 46). Examination of the radial profiles of the modeled VCP from this experiment showed that in the lower and middle regions of the VCP, the rock density plays no part in effecting changes in the VCP radius. In the upper regions of the VCP, just below the maximum height obtained, the cases with density values below the standard value (<2500 kg/m^3) show a very slight decrease in the VCP radius from that of the standard case (see figure 47). Both the vertical profiles of differential temperature and ash fraction show no response to changes in the rock density (figures 48 and 49 respectively); the profiles show the standard shape and have identical values for all seven cases tested. For all cases tested in the range from 1000 to 2500 kilograms per cubic meter, the increase in the maximum height obtained by the model

VCP was so minutely positive as to be plotted as a straight line of nearly zero slope (figure 50). It can be said that the density of the pyroclastic material has such a negligible effect upon the maximum height obtained by the model VCP as to be considered ineffective.

e. Analysis of the Particulate Velocities

At each step, the model calculates the upward velocities of the particles in each of the distributed size bins. This information is used by the model to calculate the drag force parameters, but is also writen into a separate output file for future analysis. In consideration of the results of the four experiments with the pyroclastic particulate parameters (experiments 8, 9, 10, and 11) some of the resulting output of the rock particulate velocities was thought appropriate for presentation. Data from the standard case model and the experiments with the Particulate Number Density, the Mode Radius of the Particulate Distribution, and the Standard Deviation of the Particulate Distribution are presented herein. Since the experiment with the mass density of the pyroclastic

particulate material revealed only subtle, inconsequential results, its data will not be included in this presentation of the analysis. As mentioned, the data on the rock particulate velocities are a by-product of each case executed upon the model, hence the data herein presented represent a subset of the total resulting data from the experiments 8, 9, 10, and 11.

Two distinct types of information will be presented here, both making use of the particulate velocity data: In the first, the vertical velocity profile for each of the characteristic size particles will be displayed; each plot will have fifty lines representing a distinct velocity-height path within the established VCP. The second type of information makes use of the velocity of a specific particle size from a discrete bin and the particle's radius; a contour of the velocity for each rock particle radius is fitted for each 500 meter step upward in the VCP. Examples of each of these types of plots are presented for the standard case model as figures 51 and 52 respectively.

The standard case

Concerning the standard case, each of the figures is explained in the following manner: Figure 51 has 50 lines emanating from the starting point of 400 m/s where all of the particles have the same velocity as the starting VCP velocity at the starting position. [It may be noted that the model can accommodate alterations to the initial velocities of the particles so as to reflect distributed velocities according to size and number as well. However, this was not performed for this study.] Each line represents the velocity path for all particles of the radius corresponding to an individual bin size. As the particles of each size move upward with the VCP fluid motion they are subject to drag forces retarding their velocities. At vertical positions where a particle's velocity becomes of magnitude zero, its path would be plotted as a flat line parallel to the velocity axis approaching its intercept with the height axis. For example, the bottom line parallel to the velocity axis of figure 51 represents the velocity-height path of the particles in the size range of the first nine bins which reach a zero magnitude velocity at a height

within 500 meters from the source. The next parallel line emanating from the velocity field represents particles with dimensions corresponding to the tenth size bin reaching a zero magnitude velocity within 2000 meters from the source. The third line parallel to the velocity axis has a zero value velocity magnitude at the height intercept within 3500 meters above the source representing particles of dimensions within the eleventh size bin.

However, not all particles that reach a zero velocity exhibit a flat line approaching the height axis; some particles have such a smooth gradual deceleration that their velocity paths approach zero just prior to the maximum height achieved by the VCP. The second type of diagram is presented in figures 52 and 53. Biaxial plots of the velocity and particle radius are presented for the range of particle radii as per the standard case model. The top line (at velocity=400 m/s) represents the starting velocity of the rock particles at the start of the VCP model execution; notice that the flat line represents all particles having the same initial value of velocity for initialization of the model. This velocity is also the starting velocity for the gaseous portion of the VCP. At the next 500 meter contour we observe that the

particles of radii within the first nine size bins have a zero magnitude velocity (parallel to the velocity axis intercepting the particle radius axis) and have actually been extracted from the model; particles of sizes larger than those of the newly excluded range tend to show a greater velocity for particles of greater radii. Figure 53 shows the same information only for a larger range of particle radii; thus the figures for each case have two plots of the particle velocity as a function of the particle radius-showing identical information over two size scales, and a third plot with the logarithm of the entire range of radii.

Some interesting information may be gathered from the data presented in the "velocity as a function of particle radius" plots. Within the first 1500 meters of the flow above the source, the slowest particles appear to be those of bin ten (radius of approximately 80 microns) which is also the smallest size remaining in the distribution. When the VCP has reached a position 2000 meters above the source, the slowest moving particles are still those of the smallest size remaining in the number distribution, but now corresponding to those of the eleventh size bin. After the flow of the VCP has reached 2500 meters upward from the source, the slowest particles no longer correspond

to the smallest size particles, but to those of the twenty-first bin (radius=101.6 microns). At greater distances above the source the size of the slowest moving particles shifts positively from the 128 micron range to the 512 micron size range. Near the top of the VCP along the contours of greater altitude one notices that particles of the size range from approximately 400 microns to 825 microns (corresponding to particles in the sizes between the twenty-sixth and thiry-first bins) start to reach zero magnitude velocities and are withdrawn from the number distribution. At all altitudes examined, in the standard case model the particles of larger radii (radius greater than approximately 750 micron) are moving with greater velocities than the smaller particles and the largest particles retain the greatest velocity at all distances from the source.

Experimental examples

Particulate velocity data from the experiments upon the pyroclastic particulate parameters was analyzed in similar fashion to that from the standard case. The following cases are presented herein to demonstrate the effect(s) of the pyroclastic parameters

upon the velocity behavior of the rock particles: Three cases from the Particulate Number Density experiment - ZNO = 1.25E4, 1.25E6, and 1.25E10 particles per cubic meter; three cases from the Mode Radius of the Distribution experiment - a_g = 25, 125, and 250 microns; and, three cases of the Standard Deviation of the Distribution Function experiment - sigma = 1.25, 3.00, and 5.00. For completeness and continuity, a set of four figures is presented with each case-the particulate velocity spectrum in the height field, and three exhibiting the ranges of the particulate velocity plotted as a function of the particle radius,each contoured at 500 meter height intervals from the source.

Particulate number density - ZNO

Upon examination of the cases where the Particulate Number Density was varied, one sees changes of two orders of magnitude (1.25E4 to 1.25E6 particles per cubic meter) showing no effect upon the velocities of the pyroclasts. The cases presented in the four orders of magnitude below the density of the standard case model show such minute deviations from the standard result as to be inconsequential to the

particle velocities (compare figures 55 and 59 with the standard case figure 51). One must be aware that such changes in the input parameters have an effect upon the characteristic variable fields for the ranges tested, but they are effective in changing the velocity field of the individual particles. The one case presented here for a Particulate Number Density being of greater value than the standard case is that of ZNO=1.25E10. Figures 63 to 66 show that for increased particle concentrations in the region of two orders of magnitude above that of the standard case, the velocities of the characteristic particulate sizes tend to exhibit a narrower spectrum. Of interest is the range of velocities between the slowest size range and the fastest; it is very small, with velocity magnitudes being equivalent with the fastest of those from cases previously presented and with those from the standard case. At altitudes shown, the velocities of all but the slowest sizes tend to be almost equivalent; this effect is most easily recognized in figure 66, which shows that the larger particles have only slightly higher velocity magnitudes than the smaller particles remaining at any height.

Mode radius of the distribution function - a_g

Analysis of the experimental results of the Mode Radius data showed the following: When the mode radius of the distribution function is small (25 micron case) the velocities are grouped over a smaller spectrum than the standard case, and tend to have a lower magnitude velocity for each particle size than the standard case. For the case of a_g=25 microns (figure 67), at all heights the larger particles are moving faster than the remaining smaller particles in the distribution (figures 68-70). The case presented for the mode radius at 125 microns (figures 71-74) shows little variation from the standard case, with the exception of marginally greater particle velocities for the slowest ranges of particles. For the case of the mode radius equal to 250 microns (figures 75-78) the velocity field once again is a narrow group with very little difference between the velocity magnitudes of the slowest and the fastest particles at any position along the VCP flow.

Standard deviation of the number distribution - σ

Three cases are presented for the review of the effect of the standard deviation of the particle distribution (see figures 79-70). The case of sigma=1.25 most closely resembles the standard case result with the particulate velocity field so minutely different as to be indistinguishable (compare figure 79 to figure 51). Shifting the standard deviation from 1.25 to 5.00 has the effect of narrowing the velocity field spectrum. Results of this experiment show all of the pyroclastic particles of each characteristic bin, moving with velocity magnitudes of a more restricted range between the slowest and the fastest particles. The narrowing of the velocity spectrum is toward the greater velocities such that at each height all of the particles are moving with greater velocity magnitudes than in the standard case. Velocity magnitudes appear to be increasing for increased values of the standard deviation. In the upper regions of the VCP as it approaches its maximum height, the larger particles remaining in distribution tend to have a steady velocity greater than those of the smaller particles; the smaller particles tend to be more rapidly

decelerating prior to their reaching a zero velocity magnitude.

v. Experiments with the Thermal properties of the VCP

Two experiments were performed to test the effects of the thermal properties of the VCP. The model is general enough to be usable for a wide range of values for the specific heat capacity of the VCP fluid. Appropriate selection of values used as a parameter which may be input into the model can simulate various compositional changes in the ash and gases of the VCP. The first of these two experiments involved testing the standard case model for values of the specific heat capacity of the VCP ranging from 500 to 3100 Joules per kilogram per Kelvin in increments of 50 J/Kg K. These thirty-one cases formed the data set of experiment 12. The second experiment in this group was to test the effect of the parameter Delta (Δ) as found in equations 2.35ii and 2.66. As previously mentioned, the Delta parameter is a measure of the buoyant restoration of a parcel of the VCP fluid as it undergoes convection. This buoyant restoration is related to the stability of the VCP as it passes through a stratified environment. By definition, Delta

has a maximum value of unity - corresponding to the case of a dry adiabatic atmosphere. A value of unity would imply an atmosphere with a constant lapse rate of temperature equaling the ratio of the local gravitational acceleration to the specific heat capacity at constant pressure. This maximum value of Delta, and the definition of Delta itself, can also be applied to a case where the vertical temperature gradient within the VCP is equal to the ratio of the local gravitational acceleration to the specific heat at constant pressure of the VCP fluid. The standard case model was run with values of Delta from 0.10 to 0.95 by increments of 0.05. The data set of experiment 13 consisted of those eighteen cases. One should note that Delta is not intended to be a tuneable parameter in this model, but is functionally dependent upon the VCP's temperature and gaseous composition at height. As such, it is not apropriate to set Delta at a predetermined constant value for actual modelling situations such as the simulation of a specific single VCP producing event. The purpose of the experiment with the Delta parameter is to reveal the relative significance of the combination of vertical temperature gradient and specific heat capacity (as they relate to

buoyancy and stratification) with respect to the general behavior of a modeled VCP.

a. Experiment 12: the effect of the specific heat of the VCP fluid

Thirty-one cases were tested upon the standard model by varying the specific heat of the VCP gases. To accomplish this, the mixing and composition of the VCP gases were switched-off in the model, and the specific heat was set as an initialized constant for use in the Heat Conservation equation. Each case resulted in data which was plotted in the usual manner (bivariate plots of the characteristic variable field with the VCP height).

As modeled, the gaseous effluent was a mixture of steam, carbon dioxide, and entrained moist air. The mixture ratio of these gases will account for the calculated value of the specific heat of the VCP gases as it affects the thermal energy conservation relationships. Specific heat values ranging from 500 to 3100 J/Kg K in increments of 100 J/Kg K were used to bracket the equivalent cases of 100% steam to 100% CO_2 at the specified pressures.

The results of the experiment upon the specific heat of the VCP fluid are as follows: The field lines of velocity-height paths as a function of the specific heat of the VCP appear non-linear (see figure 91). As the value of the specific heat was increased, the rate of VCP velocity decrease with altitude was lessened. As in the experiments with the differential temperature and the ambient vertical temperature gradient (experiments 4 and 7 respectively), each case showed 1) the velocity decrease to be initially rapid (greater deceleration), 2) a period of less rapid velocity decrease with height (less deceleration), 3) and finally a phase of more rapid velocity decrease (increased deceleration) as the VCP approached its maximum altitude. As the initial value of the VCP specific heat is increased, there is a greater amount of thermal energy as a starting condition; hence, the VCP will achieve a greater altitude and a greater radius. Larger values of the specific heat will produce taller VCPs each with an increased radius at the maximum altitude; a similar effect was achieved by increasing the environmental temperature gradient (experiment 7). Figure 92 appears to reflect similar results to those from the differential temperature and ambient temperature gradient experiments, except that

the VCP radii produced by higher specific heat values (i.e. differing mixture ratios of H_2O to CO_2) appear to be marginally greater at all heights (compare figure 92 with figures 12 and 27).

Vertical profiles of the differential temperature (figure 93) all show a steady non-linear decrease in the earlier stages of the VCP. As the height of the VCP approaches the tropopause height this decrease in differential temperature diminishes. In cases where the specific heat of the VCP is of sufficient value to drive the model beyond the tropopause boundary-as in values which result in VCPs at least as productive as the standard case model, the decrease in differential temperature actually diminishes to some value constant in height until the tropopause is reached. After the rate of differential temperature change with height goes to zero and the VCP penetrates the tropopause, the differential temperature will once again decrease with height in almost linear fashion until the maximum altitude is achieved by the individual VCP. Once again, a somewhat similar effect was produced by the changes made in experimenting with input values for the ambient vertical temperature gradient (experiment 7-see figure 28).

Altering the initial value of the specific heat of the VCP, equivalently reflecting alterations in the initial ratios of the constituents of the VCP fluid, has no apparent effect upon the profile of the ash fraction (chi) with height (figure 94).

For combinations of the constituent components of the VCP effluent which may yield specific heat capacities significantly higher than that of pure dry air, an increase in the adiabatic lifting potential of such a fluid is expected. As such, the lifting term in the equation expressing the conservation of thermal energy is increased, thereby increasing the overall thermal energy available to drive the VCP upward. It is then expected that a VCP with an effluent composition of relatively high specific heat capacity would result in an event which achieves a greater maximum altitude than a VCP with a lesser specific heat in similar environmental surroundings. By appearance, figure 95 displays this expected result. A smooth, continous, non-linear, positive increase in the maximum altitude of a VCP event was obtained from increased values of the specific heat capacity of the VCP fluid. Similar maximum altitude effects were brought about as a result of experimenting with the initial values of the differential temperature Theta, the ambient

vertical temperature gradient $(dT/dz)_{env}$, and to a lesser degree, the initial upward velocity U_{start} (compare figure 95 with figures 15, 30, and 5 respectively).

From this experiment one could assert that the maximum altitude achieved by any single VCP event is rather strongly dependent upon the gaseous composition and the gas-ash combination (which determines the specific heat capacity) of the volcanic effluent.

b. Experiment 13: the effect of the (stratification) parameter Delta

The standard model was run with values of Delta set at 0.10 to 0.95 in increments of 0.05. From the eighteen cases which were run, the resulting figures 96 to 99 were plotted for every other case for visual simplicity; figure 100 incorporates the data from all of the cases executed.

For increasing values of the Delta parameter, the velocity-height path of the VCP shows lessened deceleration with height in the early stages of the advancing VCP passing into a region of greater deceleration with height as the VCP approaches its maximum altitude. Figure 96 shows the lower lines

corresponding to lower values of Delta, with the upper lines being increased values of Delta. One notices that lesser values of Delta produce VCPs which have a velocity-height path with greater deceleration with height than that of the standard case (which lies almost along the second line from the top). Consider the definition of Delta (equation 2.35iii and 2.66); greater values of Delta can be expected for conditions which would exist in an event where the vertical gradient of the VCP temperature is lessened given the VCP specific heat is a constant, or for a given vertical temperature gradient, the VCP specific heat is decreased. As previously discussed, there are many interplaying conditions which could combine to produce such results. However, we are only concerned here with the explanation of such possible results as they may reveal something about the nature of the VCP behavior. Lower values of Delta would be indicative of stable stratification within the VCP, and convection based purely upon thermal considerations would be restricted; all thing being constant, the VCP would achieve a lesser maximum altitude. Greater values of Delta indicate unstable stratification, thereby enhancing the thermal convection - producing a taller VCP.

Conditions existing in a VCP event which would have a large Delta value would likewise aid in producing a taller VCP. For individual cases where conditions would yield increasing values of a calculated Delta, the resulting VCP events would not only be successively taller, but would be of narrower radial profile at heights less than the maximum (figure 97). The general observation that a taller VCP will have a final radius at its maximum altitude greater than those VCPs of a lesser maximum altitude was not contradicted by this experiment.

For cases where conditions would result in a low Delta value, the decrease in the differential temperature with height was a smooth, upwardly parabolic-type curve (figure 98). The differential temperature-height path was continuous from the starting altitude to the maximum altitude achieved. Successively increasing values of the Delta parameter resulted in the same general shape of the differential temperature-height path, where the rate of decrease in differential temperature with height was reduced. Conditions which would render combinations of the VCP model parameters such that the stable stratification was decreased (increased Delta) would apparently allow a VCP to retain a higher internal temperature (assuming

a higher differential temperature for any given ambient temperature profile). Said VCP temperature would also be less diminished with height than in an event sustaining more stable conditions.

This experiment showed that the vertical profile of the ash fraction-height path remained unchanged under conditions which could produce individual VCP events having different values of the stratification parameter (figure 99).

Making use of the result of the standard case model VCP, which achieved a maximum altitude of 10.12 kilometers, and the intercept of that value upon the Delta Parameter axis of figure 100, information about the standard case model may be obtained. From figure 100, an estimate of the initial value that the model calculates for the stratification parameter (as functionally determined by equation 2.66) was found to be aproximately 0.7. Since an ideal dry incompressible fluid behaving perfectly adiabatically in a constant lapse of temperature has a Delta value of unity, it appears that the standard model behaves as a "non-dry", almost adiabatic phenomenon. It is therefore believed that assumptions applied during the modeling of the thermodynamics involved in a VCP event seem adequately justified.

IV

A SIMULATION STUDY

IV. A SIMULATION STUDY: THE 22 APRIL 1979 ERUPTIVE EVENT OF LA SOUFRIERE

This section discusses the model simulation of the documented eruption of La Soufriere, St. Vincent, West Indies on April 22, 1979. The La Soufriere event has been described elsewhere (Shepherd et al., 1979, Shephard adn Sigurdsen, 1982). The model input inclued the values of the pyroclastic particulate material, the ambient environmental conditions, and the main flow field characteristics of the VCP.

The method was as follows: first, set any input parameters for which exact values can be obtained to their initial conditions. Next, determine reasonable ranges of values for any and/or all of the remaining required parameters. The model was run for a series of cases using all possible permutations of the parameters. The resulting VCPs were then compared to the descriptions of the historic La Soufriere event.

A set of reasonable initial values for all of the model input parameters were established. We then verified that using of these values in the model resulted in VCPs which closely resembled La Soufriere. Finally, a statistical analysis determined the most probable modes of the initial input parameter values.

Analysis of these resulting mode values related the simulated VCPs to conditions which might have represented the La Soufriere event. The model was then executed using the mode values of each initial input parameter to yield a modeled La Soufriere VCP based upon mode values of those which produced cases of La Soufriere similar events. The mode-simulated La Soufriere VCP was then again compared to the historic La Soufriere VCP. Comparisons of the La Soufriere similar modeled VCPs, the most probable parameter values, and the resulting mode case modeled VCP, with the actual La Soufriere event would indicate whether the model herein developed is functionally valid for simulation purposes. Favorable comparisons would suggest that the model behaves reasonably as a predictive tool.

Before running the simulation test, values for all variables had to be determined which would resemble those of La Soufriere. Since satellite data revealed that the maximum altitude of the La Soufriere VCP was between 18 and 21 kilometers (Krueger, 1982; McCormick et al., 1982), initial values for the significant VCP parameters should result in modeled VCPs with maximum altitudes in that range. Validation studies revealed that nine parameters were most important determining

the maximum altitude achieved by a single VCP. These nine parameters were then to be used as input for the model in ranges of values which would be reasonable for a La Soufriere event. Each of these nine parameters was tested for three selected values over a range appropriate for La Soufriere conditions. All possible combinations of these tri-valued parameters were then tested. All other parameters were either set at standard values, or set at values indicative of conditions during the La Soufriere event.

The model requires some starting points from which to begin calculating solutions. The hydrodynamic equations of the model must have specified initial conditions for the characteristic main flow variables of radial length scale, velocity, differential temperature, and ash fraction. Sparks and Wilson (1982) show a profile of the La Soufriere VCP development over time; this figure, based upon a motion picture film, provided values of the VCP visible radius at calculated altitudes. Interpolation of this figure for the fully established VCP yielded an estimate for the radius of the VCP of approximately 1500 meters at an altitude of 3 kilometers. Values of the starting radius and the starting altitude for this simulation were selected in a range centered around this value.

The remaining VCP characteristic main flow variables were subjected to preliminary model testing to insure that selected values would produce model VCPs with resulting maximum altitudes within the 18 to 21 kilometer range while making use of the "known" radial profile constraint. The remaining characteristic main flow variables were likewise initialized for values within reasonable ranges.

Values for the ambient environmental parameters were selected as deemed reasonable for a tropical, springtime day. Initial values for the pyroclastic particulate parameters were determined by centering the ranges of each variable on values found in the published literature.

The initial particulate number density was varied through a range of 1.25E8 to 1.25E9 particles per cubic meter, the mode radius of the number distribution function was in the range from 125 to 250 microns, and the standard deviation of the number distribution remained at the standard value, σ=1.60 (Sigurdsson, 1982; Sparks and Wilson, 1982).

Table 8 summarizes the initial values of the nine input parameters. This nine-by-three matrix of input parameter values was used as input to the model for 3^9 = 19,683 individual cases which represent all possible

combinations of these specific simulated La Soufriere event conditions. The model was then allowed to continually execute and produce results for each case being initialized with a unique combination of these nine variable parameters. All of the resulting output data were saved for further analysis.

As previously mentioned, some of the physical attributes of the La Soufriere VCP were known and used to provide initial values for the model. Control points on the radial profile at specific height intercepts were provided from the work of Sparks and Wilson (1982). It is known that the event was considered to be phreatomagmatic (Shepherd et al., 1979; Shepherd and Sigurdsson, 1982; Sigurdsson, 1982); therefore, the steam fraction values should be relatively high. Ground sampling of air-fall pyroclasts provided the necessary ranges for values of the pyroclastic particulates (Sigurdsson, 1982). Another extremely important piece of information was that the La Soufriere event VCP achieved a maximum altitude somewhere between 18 and 21 kilometers (Shepherd et al., 1979; Krueger, 1982). By using the maximum altitude as a limiting condition, the model was restricted to retain only information for the cases

which produced a VCP event within the 18 to 21 kilometer maximum altitude range.

From the possible combinations of values for the significant input parameters only 449 unique cases produced a VCP with maximum altitude within the 18 to 21 kilometer range. Each case was equally likely to produce a La Soufriere VCP. Data from these 449 cases were the basis for the simulation study of the La Soufriere event.

The frequency distribution of the values of each input parameter were produced. A summary of the modal or most frequent values of the input parameters is presented in Table 9. Using the modal values as input results in the maximum altitudes achieved of 20.8 ± .100 kilometers. This maximum altitude of the modeled La Soufriere VCP represents the most probable result given the specific input parameters within the ranges as simulated. Similarly, the modal values of the input parameters represent the most probable values for each parameter which when input into the model would result in a VCP within the 18 to 21 kilometer maximum altitude range.

A comparison of the model simulation resulting in a most probable maximum altitude for the La Soufriere event of 20.8 ± .100 kilometers with a satellite data

value greater than 18 kilometers (Krueger, 1982) and that of the Sparks and Wilson model at 19.8 kilometers, shows this model to be reasonably well validated. This leads to the following statements concerning the model and the simulation of the La Soufriere event: 1) the values for the input parameters used in the simulation were reasonable; 2) the ranges of values were not excessive, but bracketed well the conditions which were necessary to produce a VCP similar to La Soufriere; 3) closer examination of the data from these specific individual cases which did show similarity to La Soufriere may be used to further reveal the nature of the actual behavior and conditions of La Soufriere; 4) the La Soufriere event most probably reached into the stratosphere since the most probable maximum altitude exceeds the most probable tropopause height of 16 km, and the higher reported values of 17 and 18 km (Barr and Heffter, 1982; and, Krueger, 1982 respectively); 5) the derivations, assumptions, and implementation techniques employed in the model seem justified in as much as they can be used to simulate an historic, documented VCP producing event.

TABLE 8

SOUFRIERE SIMULATION: INPUT PARAMETER VALUES

Input parameters were adjusted from those of the previously tested Standard Case Model to values deemed reasonable for a tropical, spring event in accordance with published values (see Sparks & Wilson 1982, Sigurdsson 1982, Krueger 1982, etc.).

THE FOLLOWING WERE TESTED IN ALL POSSIBLE COMBINATIONS AT THESE INITIAL VALUES:

ZTROP	16	18	20	Km
RSTART	1250	1500	1750	m
USTART	275	300	325	m/s
THETA	200	250	300	K
CHI	0.25	0.35	0.45	
HUMIDITY	0.30	0.50	0.70	
ZNO	1.25E8	5.0E8	1.25E9	m^{-3}
MODE RADIUS	125	200	250	μm
STEAM FRACTION	0.60	0.70	0.80	

TABLE 9

SOUFRIERE SIMULATION: MODE VALUES OF PARAMETERS

From the many generated cases simulating La Soufriere, only 449 unique cases could be generated which yielded VCPs which attained a maximum altitude within the range from 18.0 to 21.0 kilometers.

FROM THESE 449 CASES THE FOLLOWING "MOST PROBABLE" VALUES WERE OBTAINED (AS THE MODES):

ZTROP	16	Km
RSTART	1250	m
USTART	300	m/s
THETA	200	K
CHI	0.45	
HUMIDITY	0.30	
ZNO	1.25E9	m^{-3}
MODE RADIUS	200	μm
STEAM FRACTION	0.80	

MODE CASE MAXIMUM ALTITUDE WAS AT 20.8 Km ± 100 m

Analysis of Simulation Results

Figures 101 to 110 show the results from the simulation of La Soufriere based upon the statistical analysis of the 449 cases which yielded a VCP considered to be a La Soufriere like candidate. Histograms show the number of occurrences of each specific value of an input parameter by plotting the number of occurrences against the individual parameter value. Figure 101 verifies that the mode of the maximum altitude achieved from the set of model input parameters was 20.8 kilometers. As mentioned, this value was considered as evidence of the model's accuracy.

The effect of the tropopause height upon the maximum altitude of the model VCP was shown to be significant in the case of La Soufriere. Clearly the most probable value for the height of the tropopause was near the 16 kilometer (figure 102). Statistical analysis of the 449 Soufriere similar cases showed lesser occurrences of the 18 and 20 kilometer conditions were involved in resulting VCPs within our limits of interest. These conditions indicate that for such cases the model produced resulting VCPs (predicts) which are of maximum altitude beyond the 21 kilometer

limit imposed on this simulation. Therefore it appears unlikely that the La Soufriere VCP had achieved its actual height based upon the input as herein modeled had the tropopause actually been much above 16 kilometers. It has been mentioned that reported values of the tropopause at the local time of the La Soufriere event were a bit higher than 16 kilometers (17 km in Barr and Heffter, 1982; and 18 km in Krueger, 1982). However, the important information on the geophysical scale is that the model predicted stratospheric penetration regardless of which height of the tropopause was used. Many researchers are in agreement that the event of 22 April 1979 did indeed inject material into the stratosphere (Shepherd et al., 1979; Krueger, 1982; McCormick et al., 1982; Sparks and Wilson, 1982). As often occurs in published accounts of historic events, a contrary opinion may be found; there are references which do not place the event of 22 April 1979 as one which reached into the stratosphere (Barr and Heffter, 1982).

According to the most probable case, the model predicted that the VCP radius at 3 kilometers altitude was in the range of 1250 to 1500 meters (figure 103). One must remember that for this simulation the model used a value of the initial characteristic radius (not

visibly defined) in the neighborhood of values taken from visual sightings of the actual plume edge. Not much significance can be placed upon the initial value of the La Soufriere simulated VCP based upon a radial value of 1250 meters at 3 kilometers altitude, except that if the radius was to be in the 1750 to 2000 meter range the VCP would most probably achieve an altitude beyond the imposed 21 kilometer limit.

Values of the centerline mean flow velocity at the 3 kilometer altitude point appear almost equally probable within the tested range of 275 to 325 meters per second (figure 104). This result indicates that the actual La Soufriere VCP velocity at the 3 kilometer altitude was probably somewhere within this rather wide range. Values below that of 275 meters per second would result in VCPs of lesser altitude, and values greater than 325 meters per second would probably produce VCPs of maximum altitude in excess of 21 kilometers. It should be considered that mean flow velocity was not a strong indicator of whether the given specified ranges of initial conditions would produce a La Soufriere similar event.

From the validation and sensitivity studies, the effect of the initial differential temperature upon the maximum altitude seems significant. Given a set of

conditions, increasing the initial differential temperature will result in VCPs achieving greater maximum altitudes. The differential temperature was a strong factor in the simulation of La Soufriere cases (figure 105). Cases which had differential temperatures in excess of 200 K at the 3 kilometer altitude resulted in modeled VCPs achieving maximum altitudes beyond the 21 kilometer limiting condition.

Increasing the initial ash fraction in the VCP model demonstrated a reduction in the maximum altitude achieved. For the La Soufriere simulation, increased values of the initial ash fraction increased the number of occurrences of cases where the simulated VCP was within the 18 to 21 kilometer altitude range (figure 106). Such a result indicates that the actual La Soufriere VCP was indeed ash-rich.

Results from the distribution of model occurrences of La Soufriere similar VCPs based upon individual values of the VCP's initial steam fraction are not easily interpreted (figure 107). Although a simple statistical analysis located the mode to be at 0.80, the visual representation shows a hint at bi-modality. From the mode result, one concludes that the initial steam fraction must be approximately 0.80. This implies that the initial H_2O/CO_2 ratio be around

four-to-one (4:1). Such a result readily supports a phreatomagmatic eruption as the source of the VCP. However, a reduction of the initial steam fraction to 0.70 reduces by half the number of modeled VCPs which occurred as La Soufriere similar; yet, initial steam fraction values of 0.60 showed a greater probability of producing a similar La Soufriere VCP than those cases where 0.70 was used. It is not yet known whether the model produced a set of VCPs all of which achieved maximum altitudes greater than 21 kilometers for the cases of the steam fraction at 0.70, or if there are mixed effects in the simulation due to the ranges of all of the variables input to the model. Atmospheric sampling of gases from the 17 April 1979 La Soufriere event showed that the CO_2 mixing ratio was increased only slightly (10%) above the normal local background level immediately following the eruptive event (Cronn and Nutmagul, 1982). Such experimental results also reflect that the eruptive events of La Soufriere April 1979, though not specifically the event of 22 April, may not have been extremely Carbon Dioxide rich. Since this model makes use of only H_2O and CO_2 mixed with the entrained ambient fluid, one may therefore suspect that the mode value of the initial steam fraction equal to

0.80 is in agreement with experimental evidence of the actual historic conditions.

Analysis of the effect of the relative humidity of the ambient environment reflected the mode value of 0.30 to be a condition twice as probable for the simulation of a La Soufriere VCP than cases for increased values of the relative humidity (figure 108). On the outset, a relative humidity equal to 0.30 is a rather low value for a tropical spring day in the Caribbean. This result may be explained as follows: as the VCP entrains its ambient fluid, the composition of gaseous portion of the VCP effluent is altered. If the alterations decrease the specific heat capacity of the VCP fluid then the thermal driving forces are reduced as buoyancy is diminished. If, on the other hand, the specific heat capacity of the VCP fluid is decreased to a lesser extent (or increased) due to entrainment of an ambient fluid with a greater specific heat than dry air, the buoyancy is diminished to a lesser extent and the dampening of the thermal driving mechanism is reduced. This allows the VCP to achieve a greater final altitude. Since increasing the liquid water content of air increases its specific heat capacity (at a constant pressure), the entrainment of ambient fluid of a high moisture content into the ascending VCP

increases its maximum altitude. Cases modeled using values of the relative humidity at 0.50 and above probably resulted in model VCPs maximizing above the 21 kilometer limiting condition. This resulting effect is apparently due to the sensitivity of the model to the specific heat capacity of the ambient fluid entrained.

In general, increasing the initial number concentration of the particulates, increases the drag forces retarding the VCP's upward motion, which tends to reduce the maximum altitude achieved. For the cases simulating the La Soufriere conditions one observes that increasing the particulate number density increases the probability of simulating the La Soufriere VCP result (figure 109). The cases where the concentrations were lower had decreased probabilities of resulting in a VCP within the 18 to 21 kilometer maximum altitude range. It is expected that for such cases the model produced VCP's that reached altitudes above the 21 kilometer limiting condition. This would seem to indicate that the La Soufriere VCP was highly particulate laden. Studies on the air-fall tephra deposits, and accounts from ground bases observers seemed to indicate that the eruptive sequence was increasing in particulate ejecta over time as the VCP became established (Shepherd et al., 1979; Sparks and

Wilson, 1982). This would suggest some correlation between the simulation result and actual field observations.

Based upon the initial input values, which were somewhat guided by the known results of ground sampling studies, the simulated cases did indicate that the mode radius of the particle distribution function was most probably in the range between 200 to 250 microns (figure 110). Cases which simulated La Soufriere with a lesser value for the particulate distribution function mode radius had greatly reduced probabilities of being similar to the actual La Soufriere VCP; it is believed that in such cases the model produced VCPs which had increased probabilities of reaching maximum altitudes above the 21 kilometer upper limit.

Looking at the simulated results of the initial particulate number concentration parameter and the mode radius of the distribution function together reveals some specifics about the La Soufriere VCP's particulates. The particulate parameters as used in this model simulation are those which most likely would describe particulates the majority of which would be considered to be those resulting in the formation of the air-fall tephra deposits. The largest particles would be considered pyroclastic bombs, and the smallest

would be considered ash (both classifications existing in the tails of the particle number distribution and hence comprising relatively few actual particles). If a connection can be made between what is modeled as existing within the VCP and what is later to be found upon the ground, then the near-vent air-fall tephra deposits should closely resemble the particles in the VCP and hence share the attributes of the pyroclastic particulate parameters as modeled. It would then be expected that the near-vent air-fall tephra deposits would be fine-grained with a mode radius somewhere between 200 to 250 microns. This is exactly what was reported in studies on the ground samples (Shepherd et al., 1979; Sigurdsson, 1982).

A final experiment in simulating the VCP from the La Soufriere eruptive event was devised making use of the "most probable" (mode) values of the input parameters which yielded a La Soufriere similar event. The model was executed using the most probable (mode value) of each initial input parameter which was previously determined from the statistical analyses upon the four hundred forty-nine cases showing conditions similar to La Soufriere. This test was then a single model run resulting in a single VCP to yield a modeled La Soufriere VCP based upon mode values of

those which produced cases (449) similar to La Soufriere. The mode simulated La Soufriere VCP achieved a maximum altitude of 18.81 ± .100 kilometers and is summarized in Table 10. It is interesting to note that even the simulation run based upon the mode values of conditions which produced many unique cases resulting in La Soufriere similar VCPs shows the model predicts a stratospheric injection from the La Soufriere event. This author believes that the mode value of the many cases which produced La Soufriere similar VCPs based upon hundreds of unique but equally probable initial conditions yielding a most probable maximum altitude for La Soufriere of 20.8 kilometers to be an accurate reflection of the actual VCP. The slightly lower, but still in agreement with previously published accounts, value based upon executing the model in modal conditions probably indicates that the actual La Soufriere event was not behaving strictly in accordance with the established modes.

Not surprisingly then, one notices that for the case of a specific historic eruptive event, given either specific values for existing condition and/or a reasonable range of values for the model to initialize the significant parameters with, the model will produce simulated VCP cases ("predictions") which may reasonably resemble the actual VCP.

TABLE 10

SOUFRIERE SIMULATION: MODE VALUE EXPERIMENT

As an experiment, the model was executed using the most probable values as generated from the 449 cases which adhere to the condition that the maximum altitude be in the range from 18.0 to 21.0 kilometers.

INPUT VALUES:

ZTROP	16	Km
RSTART	1250	m
USTART	300	m/s
THETA	200	K
CHI	0.45	
HUMIDITY	0.30	
ZNO	1.25E9	m^{-3}
MODE RADIUS	200	μm
STEAM FRACTION	0.80	

RESULT: MAXIMUM ALTITUDE ACHIEVED WAS 18.81 Kilometers

V.

FIGURES

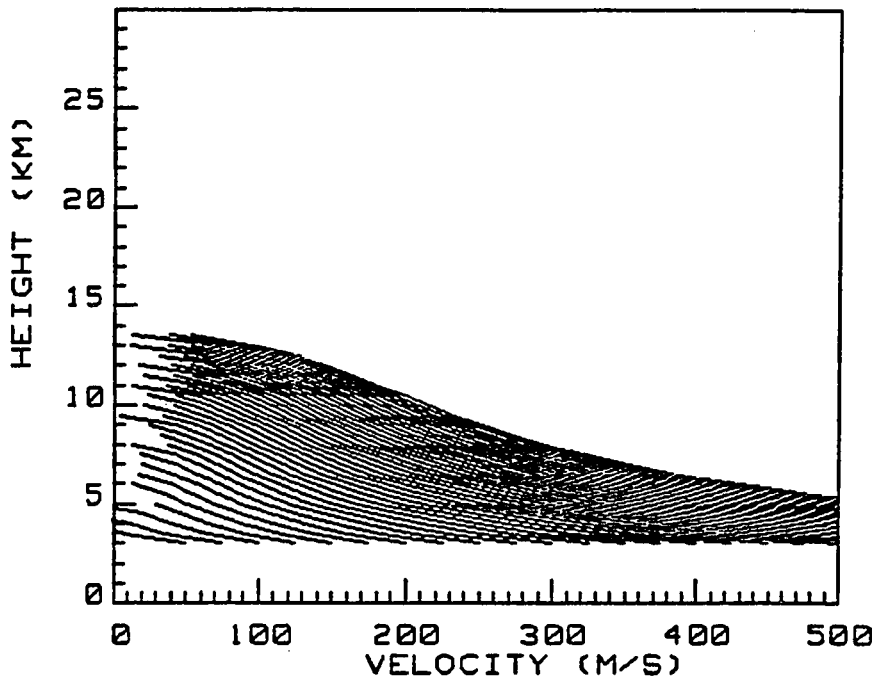

Figure 1. Effect of initial velocity upon the VCP velocity - height profile. Initial velocity in a range from 50 to 1000 m/s in 50 m/s increments.

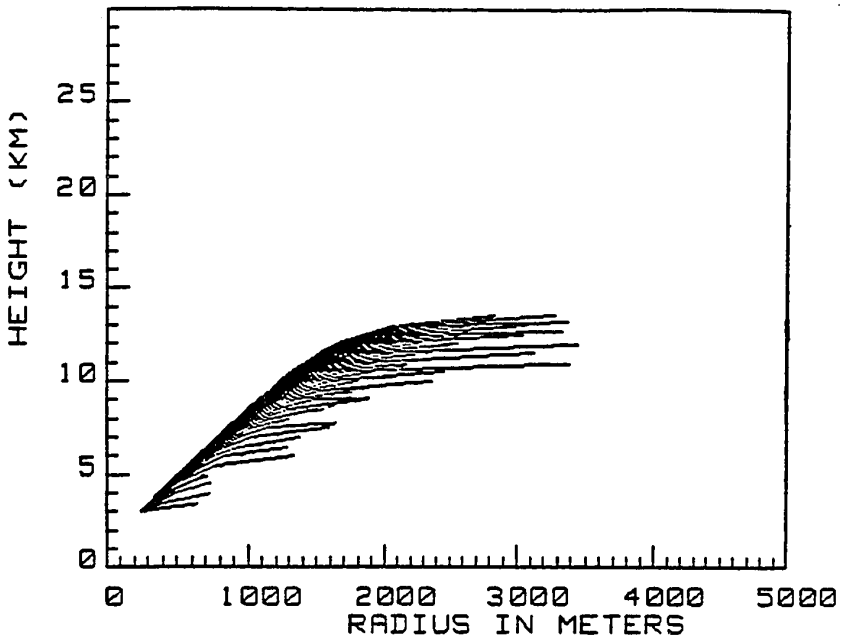

Figure 2. Effect of initial velocity upon the VCP radial profile. Initial velocity in a range from 50 to 1000 m/s in 50 m/s increments.

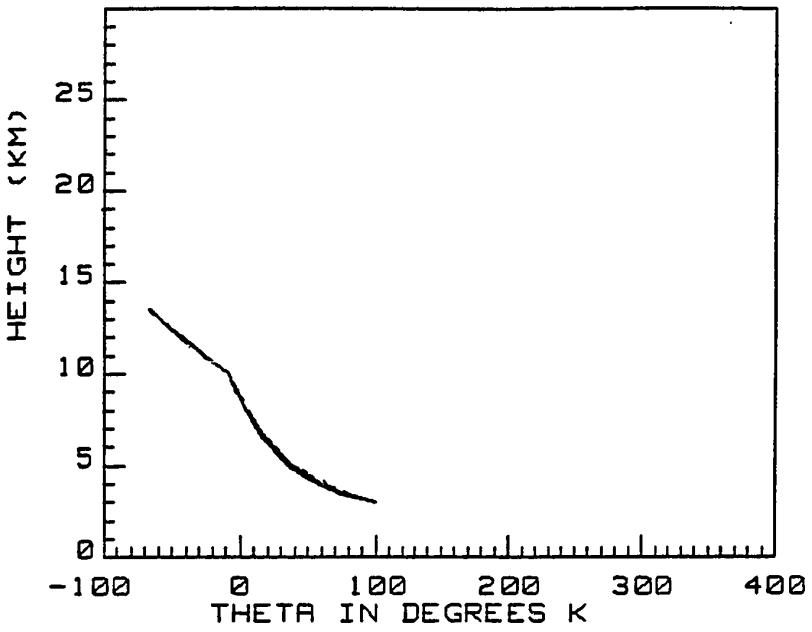

Figure 3. Effect of initial velocity upon the VCP differential temperature - height profile. Initial velocity in a range from 50 to 1000 m/s in 50 m/s increments.

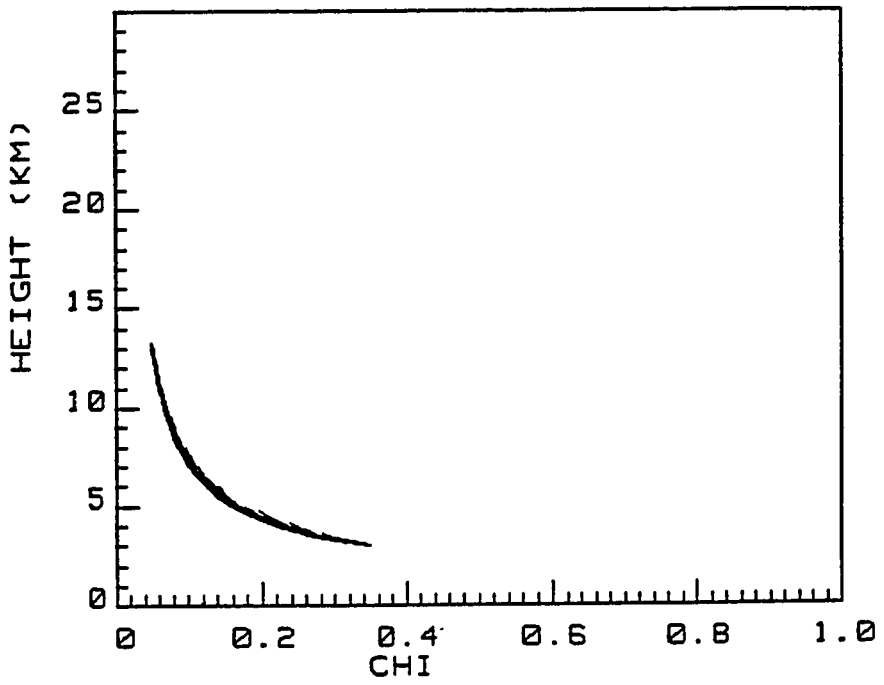

Figure 4. Effect of initial velocity upon the VCP ash fraction - height profile. Initial velocity in a range from 50 to 1000 m/s in 50 m/s increments.

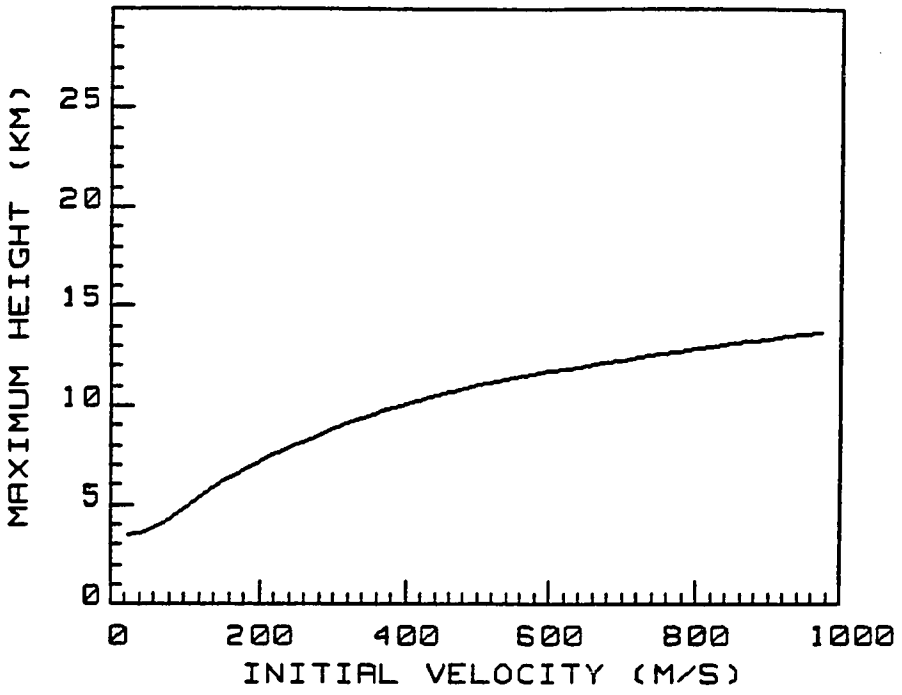

Figure 5. Effect of initial velocity upon the VCP maximum altitude. Initial velocity in a range from 50 to 1000 m/s in 50 m/s increments.

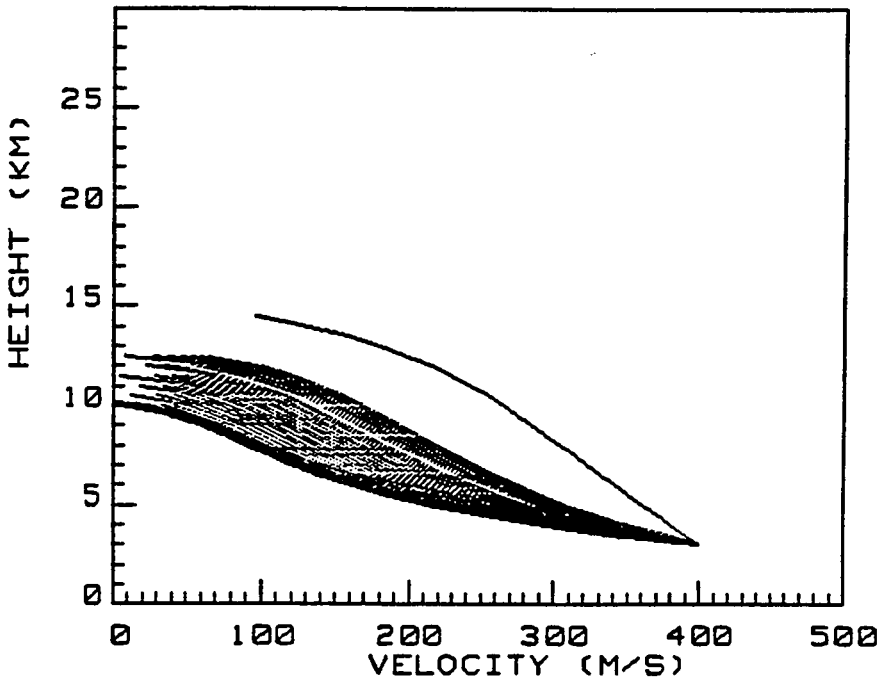

Figure 6. Effect of initial radius upon the VCP velocity - height profile. Initial radius in a range from 25 to 1000 m in 25 m increments.

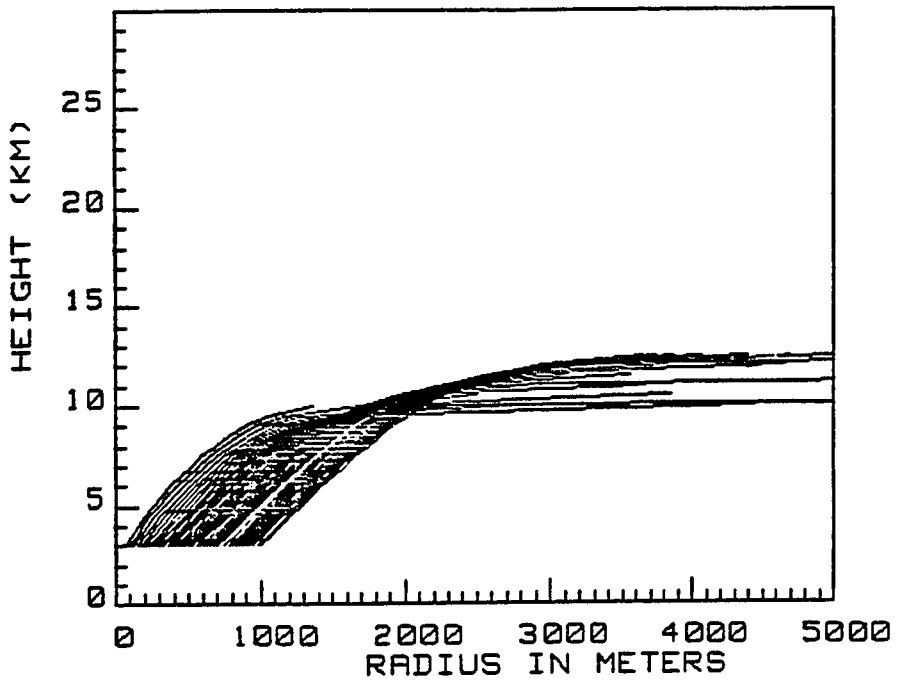

Figure 7. Effect of initial radius upon the VCP radial profile. Initial radius in a range from 25 to 1000 m in 25 m increments.

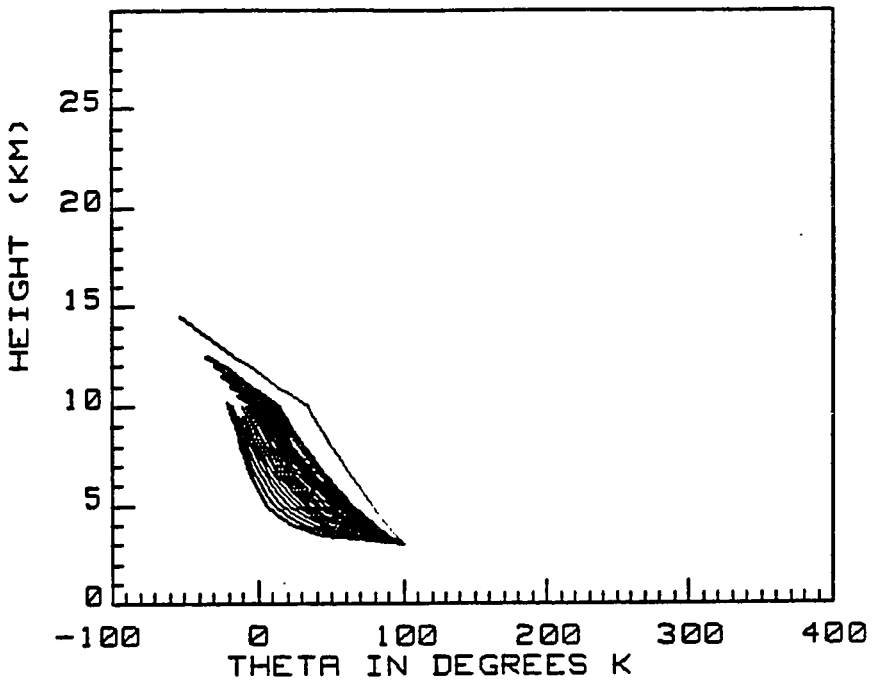

Figure 8. Effect of initial radius upon the VCP differential temperature - height profile. Initial radius in a range from 25 to 1000 m in 25 m increments.

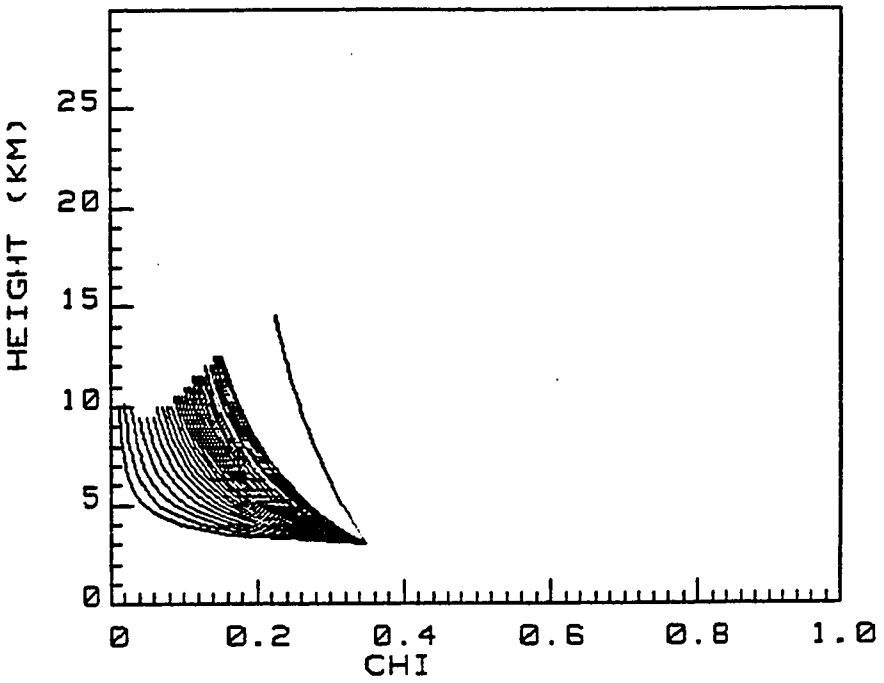

Figure 9. Effect of initial radius upon the VCP ash fraction - height profile. Initial radius in a range from 25 to 1000 m in 25 m increments.

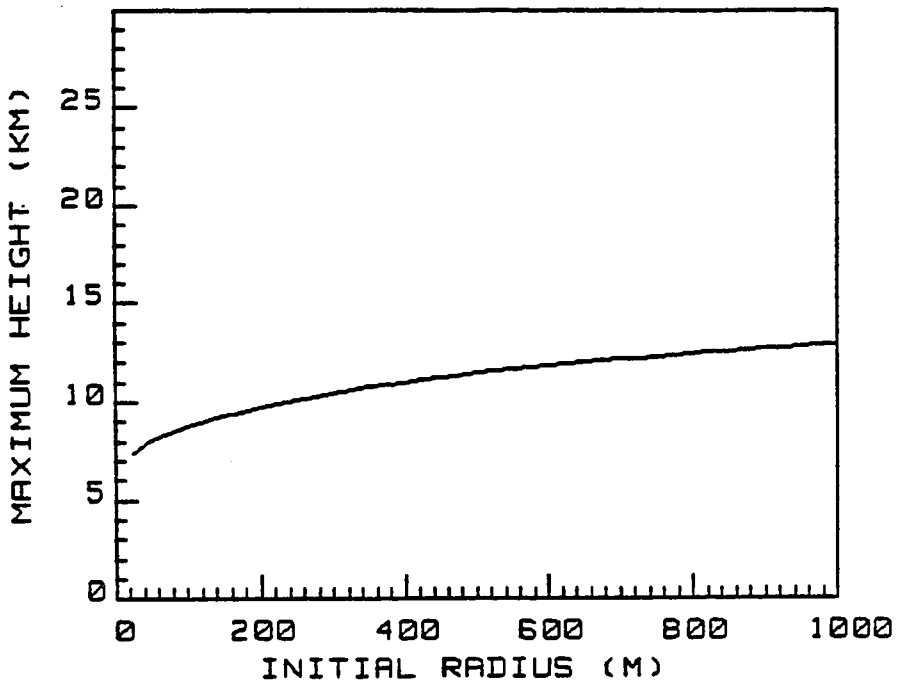

Figure 10. Effect of initial radius upon the VCP maximum height. Initial radius in a range from 25 to 1000 m in 25 m increments.

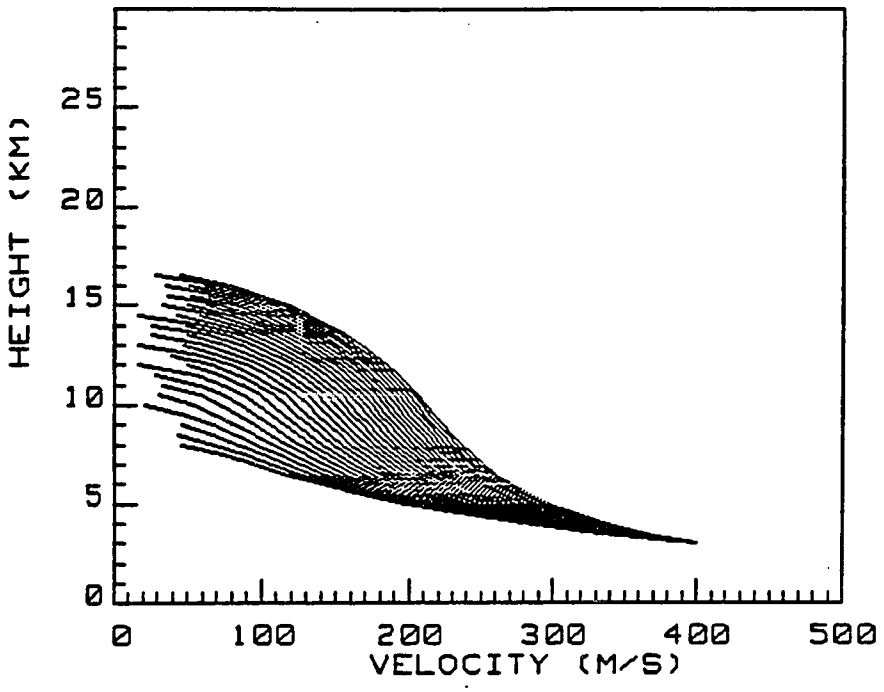

Figure 11. The effect of the initial differential temperature upon the VCP velocity - height profile. Initial differential temperature in a range from 25 to 1000 K in 25 K increments.

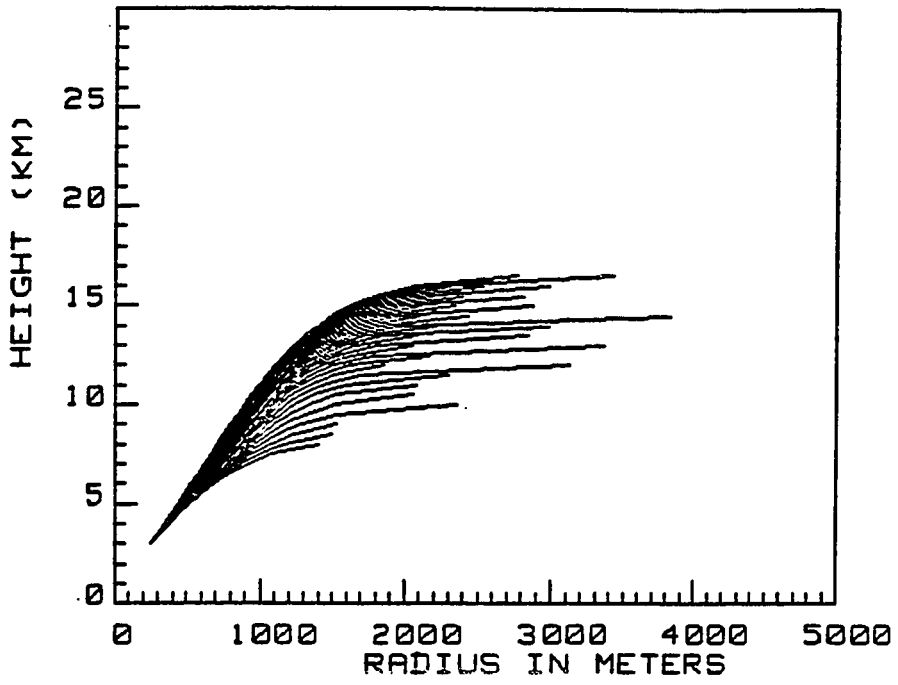

Figure 12. Effect of initial differential temperature upon the VCP radial profile. Initial differential temperature in a range from 25 to 1000 K in 25 K increments.

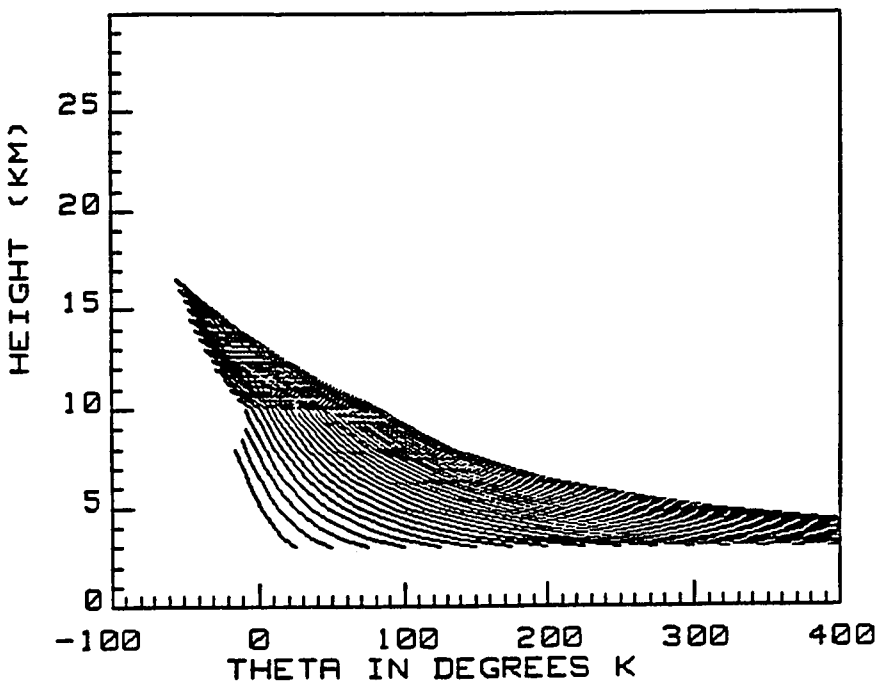

Figure 13. Effect of initial differential temperature upon the VCP differential temperature - height profile. Initial differential temperature in a range from 25 to 1000 K in 25 K increments.

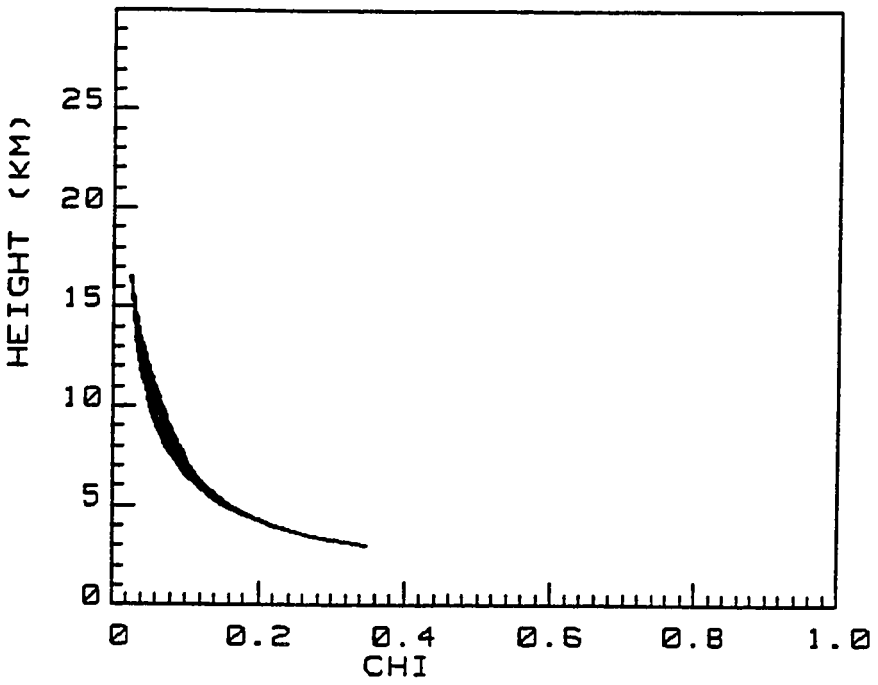

Figure 14. Effect of initial differential temperature upon the VCP ash fraction - height profile. Initial differential temperature in a range from 25 to 1000 K in 25 K increments.

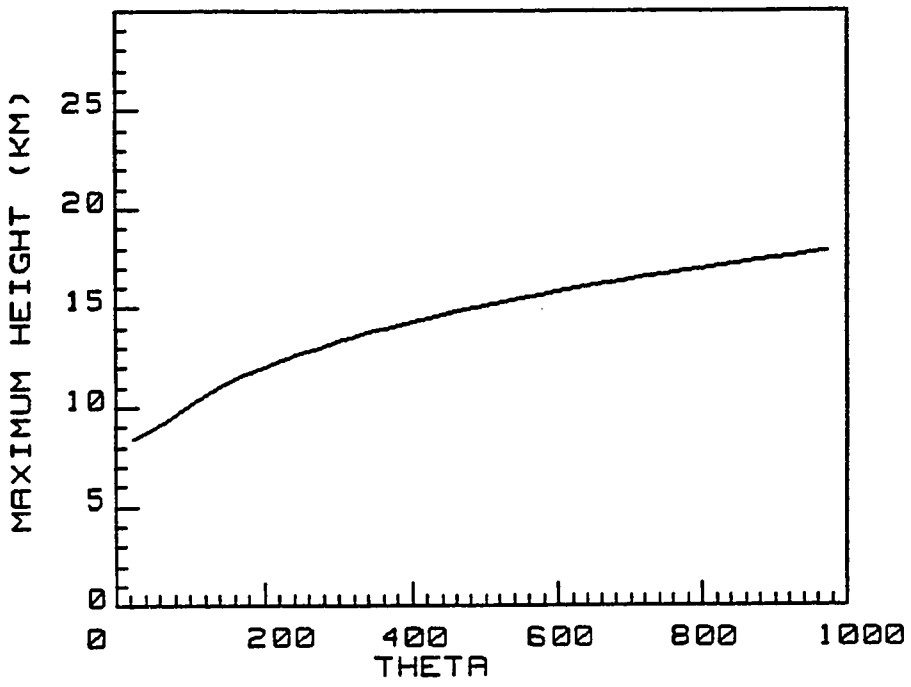

Figure 15. Effect of initial differential temperature upon the VCP maximum height. Initial differential temperature in a range from 25 to 1000 K in 25 K increments.

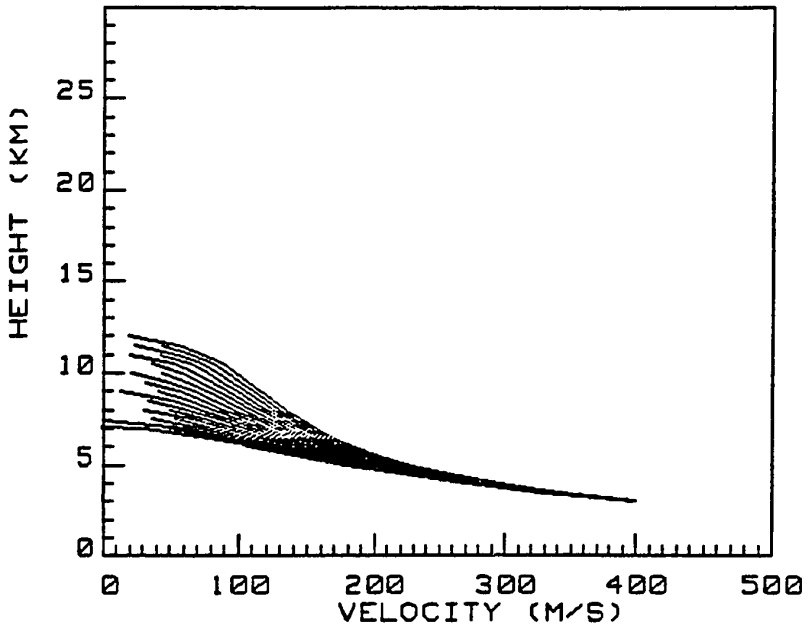

Figure 16. Effect of initial ash fraction (chi) upon the VCP velocity - height profile. Initial ash fraction (chi) in a range from 0.00 to 0.95 in 0.05 increments.

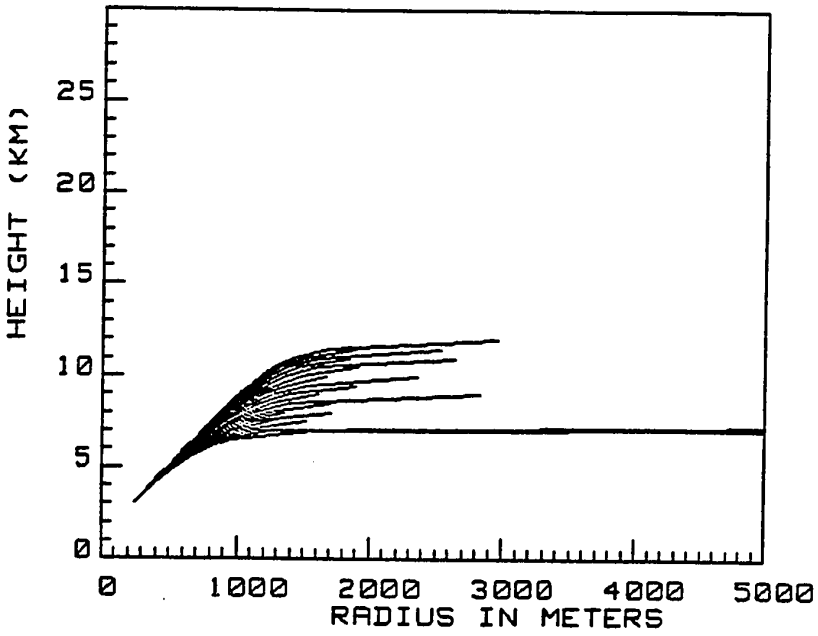

Figure 17. Effect of initial ash fraction (chi) upon the VCP radial profile. Initial ash fraction (chi) in a range from 0.00 to 0.95 in 0.05 increments.

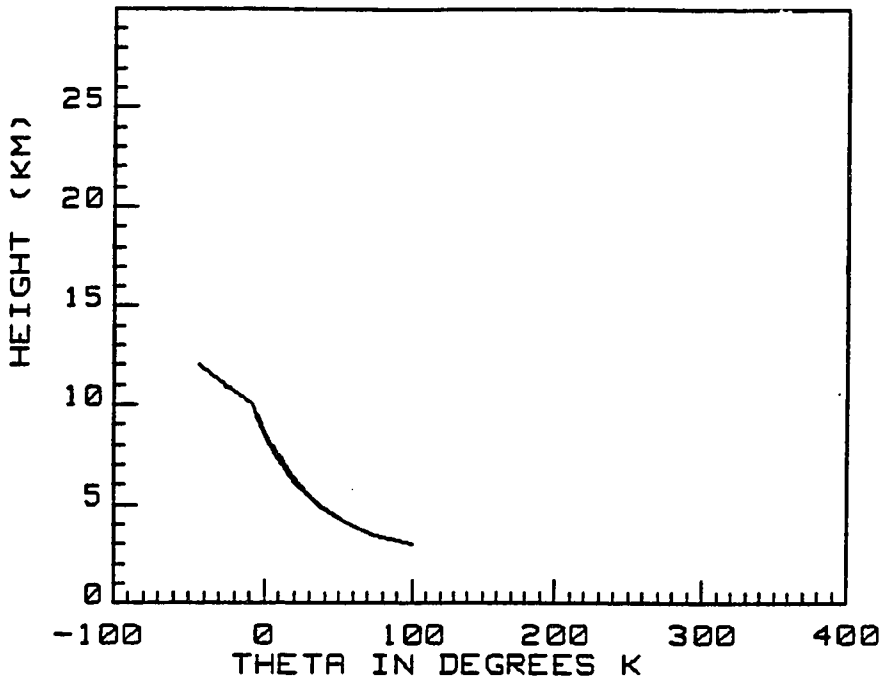

Figure 18. Effect of initial ash fraction (chi) upon the VCP differential temperature - height profile. Initial ash fraction (chi) in a range from 0.00 to 0.95 in 0.05 increments.

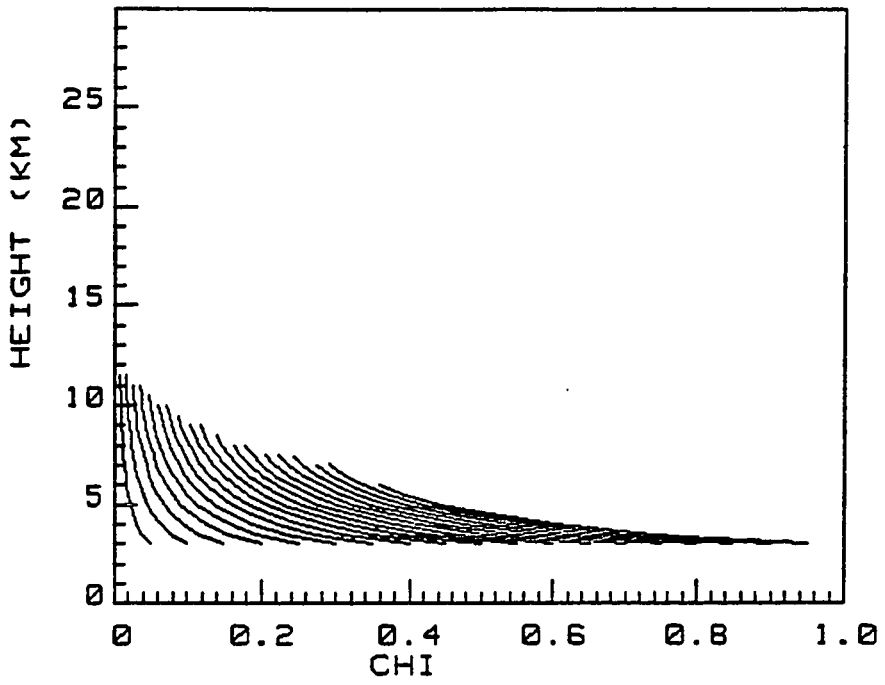

Figure 19. Effect of initial ash fraction (chi) upon the VCP ash fracion - height profile. Initial ash fraction (chi) in a range from 0.00 to 0.95 in 0.05 increments.

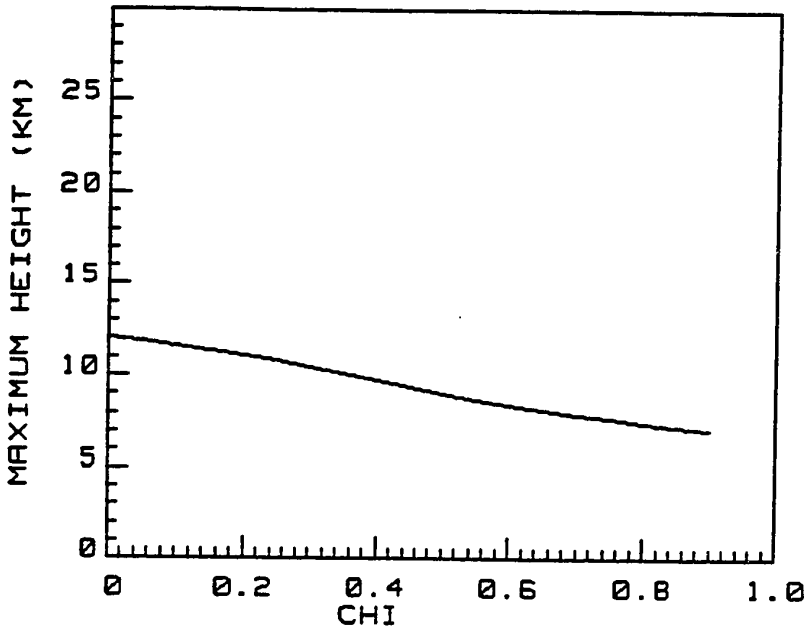

Figure 20. Effect of initial ash fraction (chi) upon the VCP maximum height. Initial ash fraction (chi) in a range from 0.00 to 0.95 in 0.05 increments.

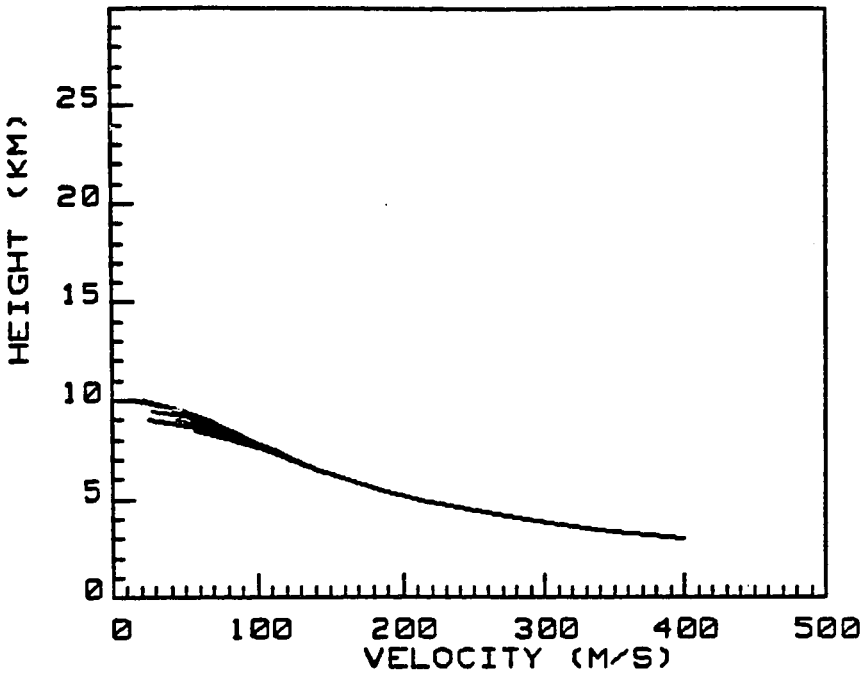

Figure 21. Effect of initial tropopause height (Ztrop) upon the VCP velocity - height profile. Tropopause heights in a range from 6.0 to 20.0 kilometers in 0.50 km increments.

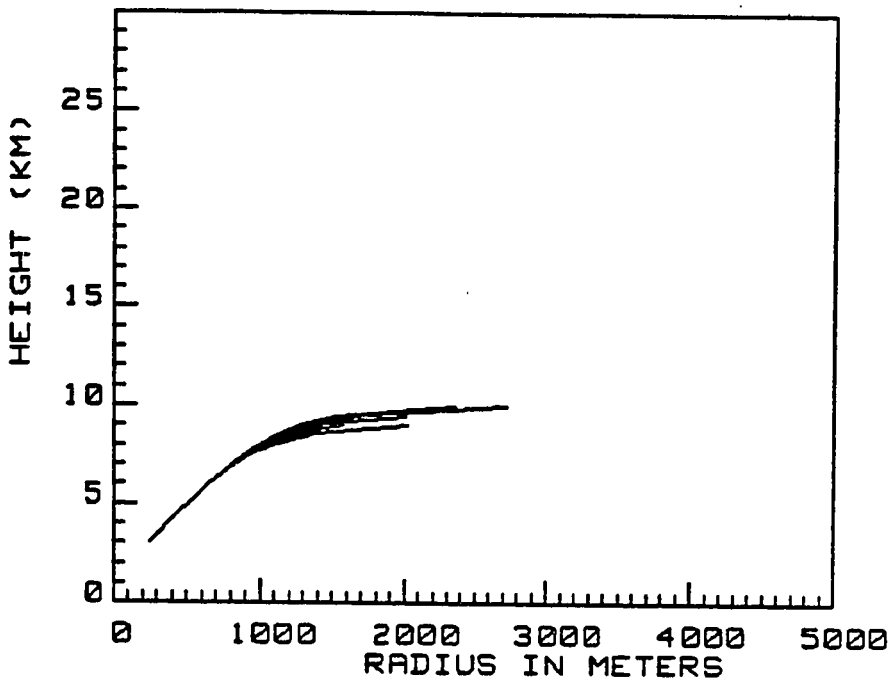

Figure 22. Effect of initial tropopause height (Ztrop) upon the VCP radial profile. Tropopause heights in a range from 6.0 to 20.0 kilometers in 0.50 km increments.

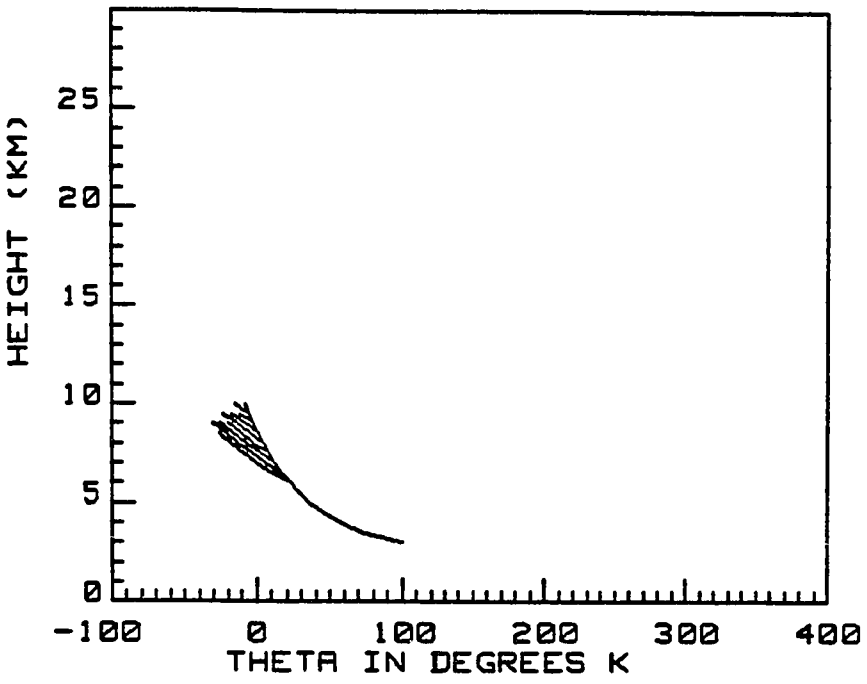

Figure 23. Effect of initial tropopause height (Ztrop) upon the VCP differential temperature - height profile. Tropopause heights in a range from 6.0 to 20.0 kilometers in 0.50 km increments.

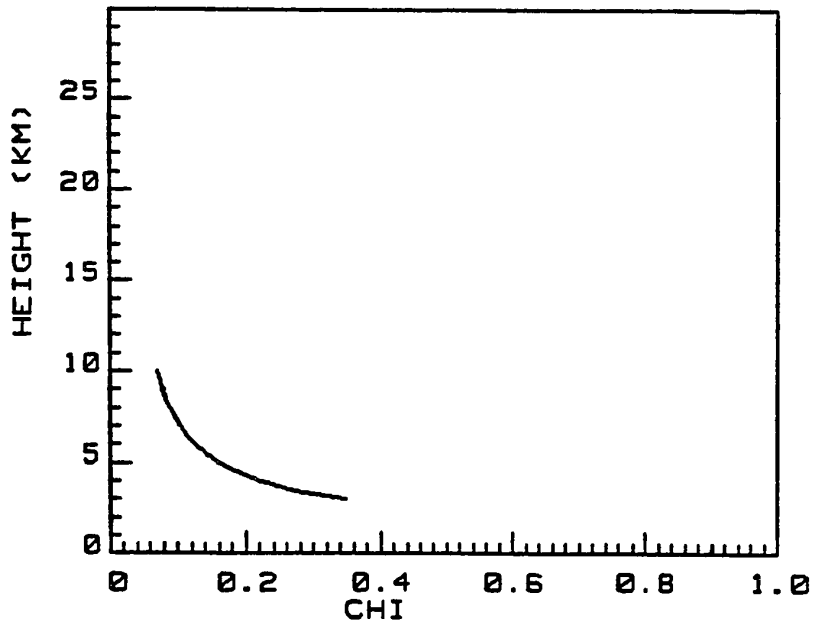

Figure 24. Effect of initial tropopause height (Ztrop) upon the VCP ash fraction - height profile. Tropopause heights in a range from 6.0 to 20.0 kilometers in 0.50 km increments.

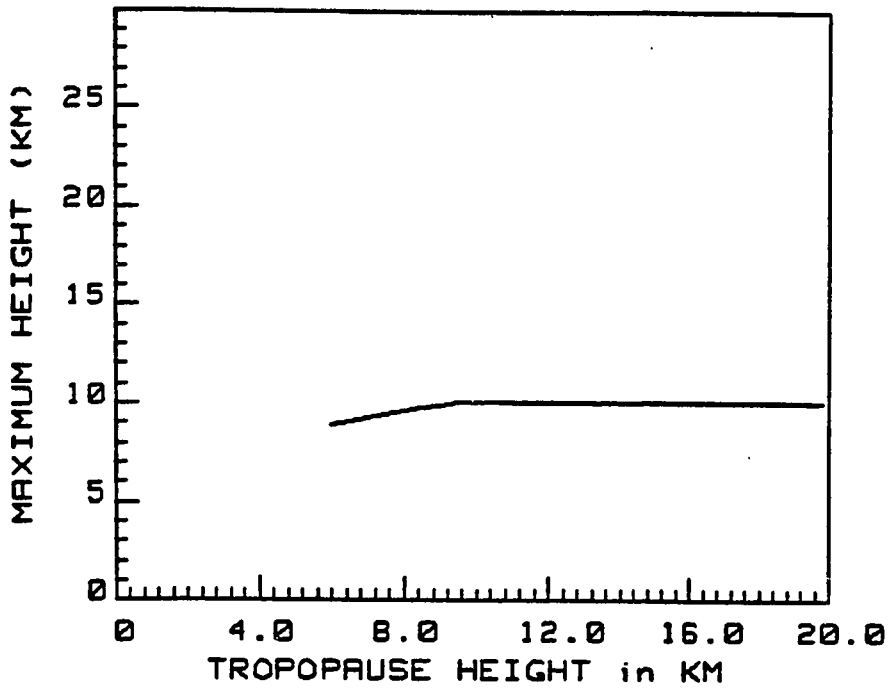

Figure 25. Effect of initial tropopause height (Ztrop) upon the VCP maximum height profile. Tropopause heights in a range from 6.0 to 20.0 kilometers in 0.50 km increments.

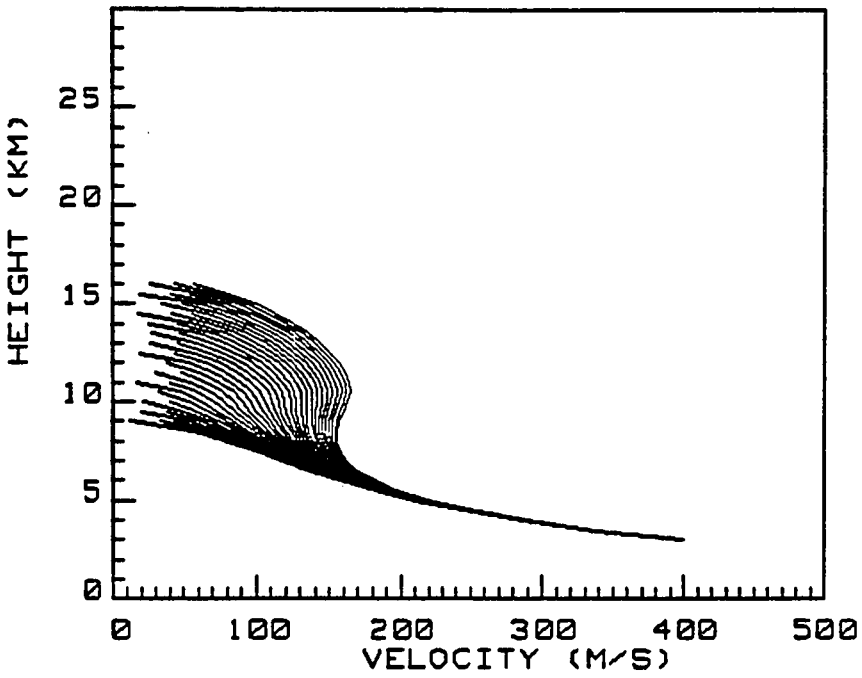

Figure 26. Effect of environmental temperature lapse rate (dT/dz)env upon the VCP velocity - height profile. Environmental lapse in a range from 4.0 to 20.0 K/km in 0.50 K/km increments.

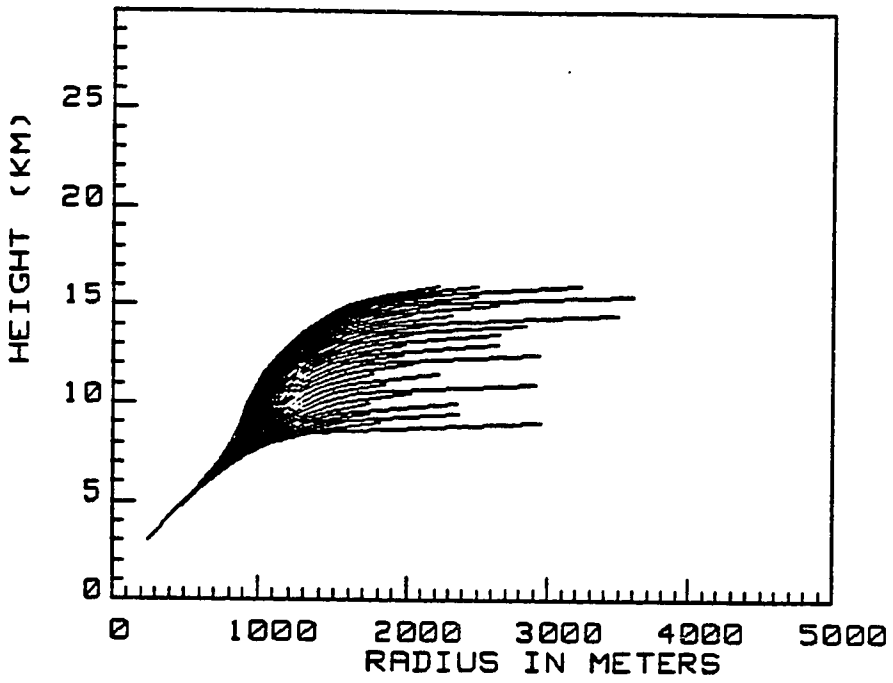

Figure 27. Effect of environmental temperature lapse rate (dT/dz)env upon the VCP radial profile. Environmental lapse in a range from 4.0 to 20.0 K/km in 0.50 K/km increments.

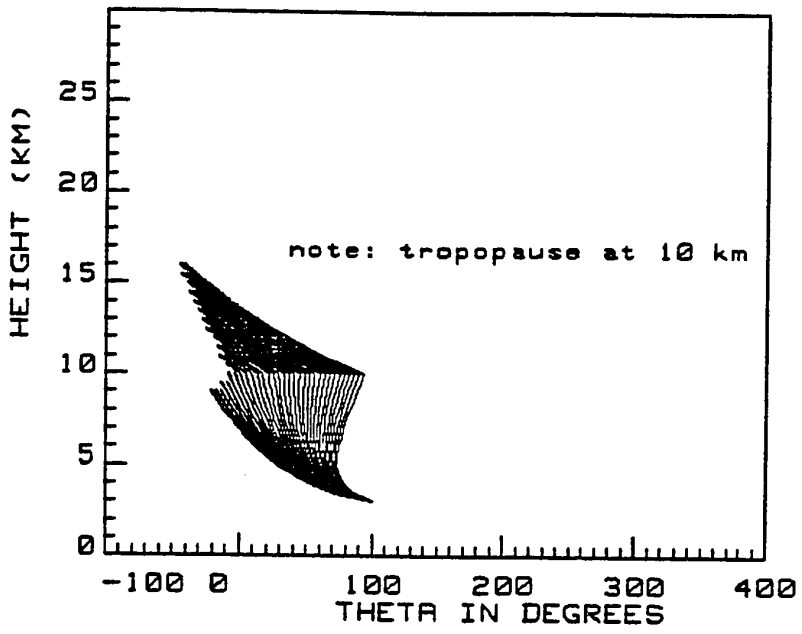

Figure 28. Effect of environmental temperature lapse rate (dT/dz)env upon the VCP differential temperature - height profile. Environmental lapse in a range from 4.0 to 20.0 K/km in 0.50 K/km increments.

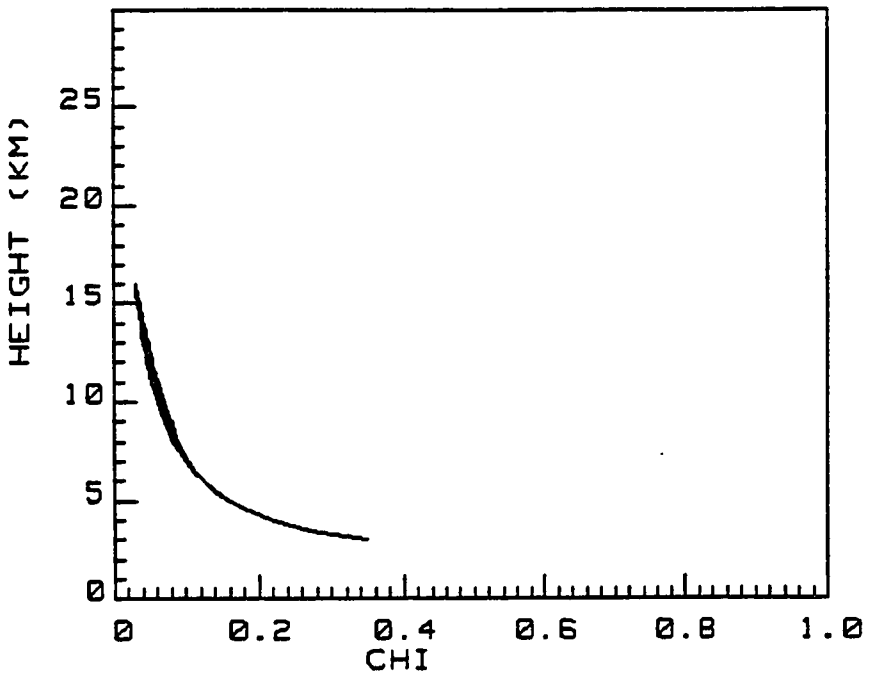

Figure 29. Effect of environmental temperature lapse rate (dT/dz)env upon the VCP ash fraction - height profile. Environmental lapse in a range from 4.0 to 20.0 K/km in 0.50 K/km increments.

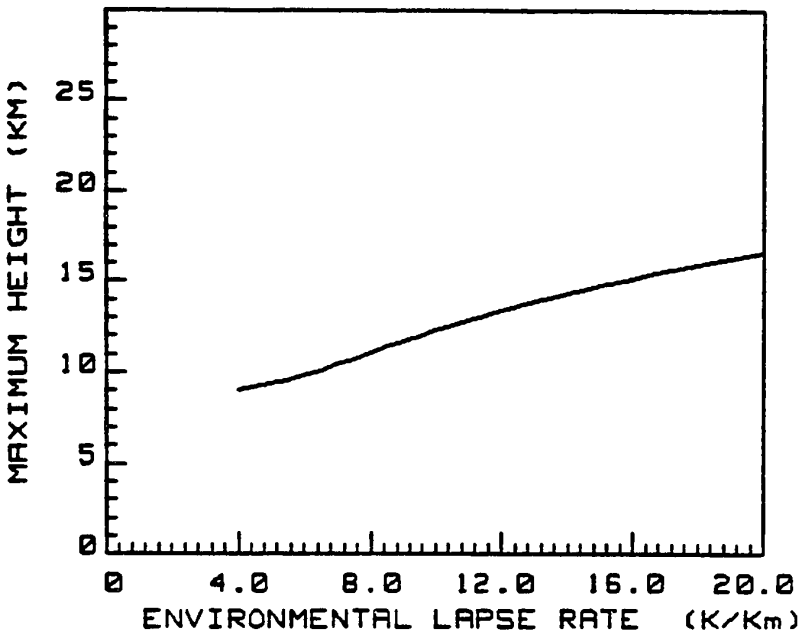

Figure 30. Effect of environmental temperature lapse rate (dT/dz)env upon the VCP maximum height profile. Environmental lapse in a range from 4.0 to 20.0 K/km in 0.50 K/km increments.

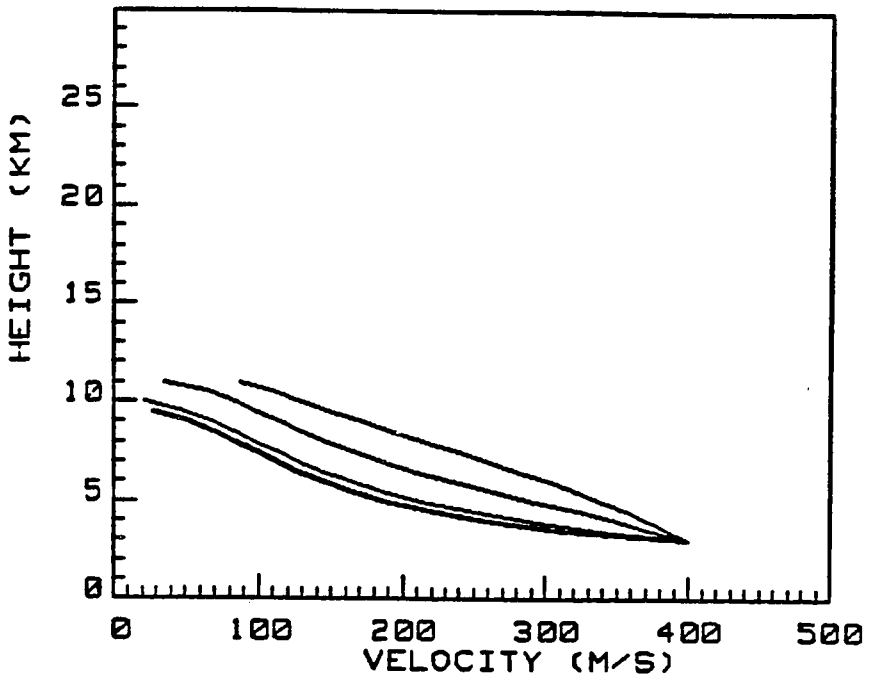

Figure 31. Effect of initial Particulate Number Density (ZNO) upon the VCP velocity - height profile. Particulate number densities in a range from 1.25 E+4 to 1.25 E+10 per cubic meter in increments of one order of magnitude.

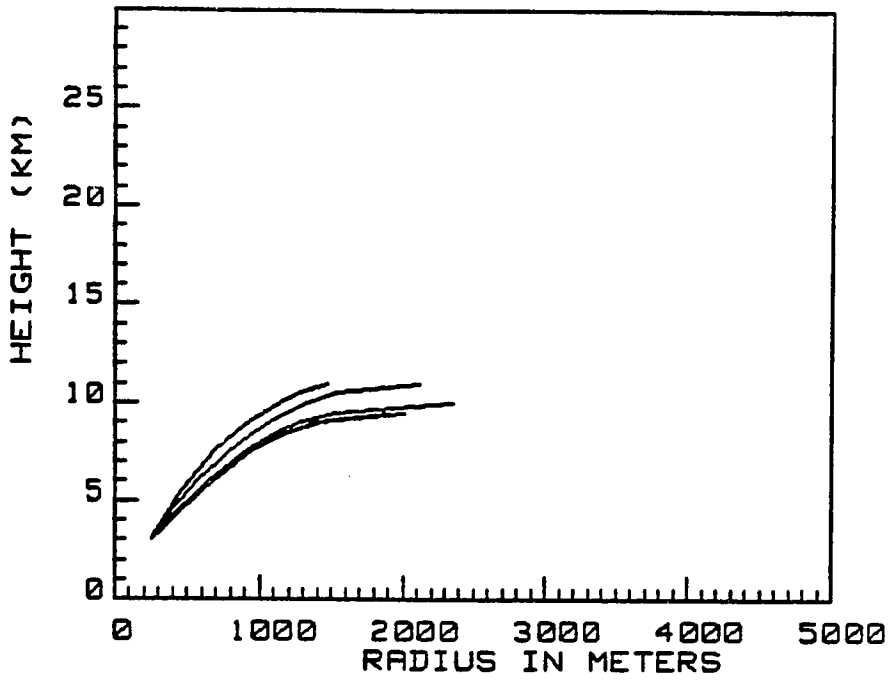

Figure 32. Effect of initial Particulate Number Density (ZNO) upon the VCP radial profile. Particulate number densities in a range from 1.25 E+4 to 1.25 E+10 per cubic meter in increments of one order of magnitude.

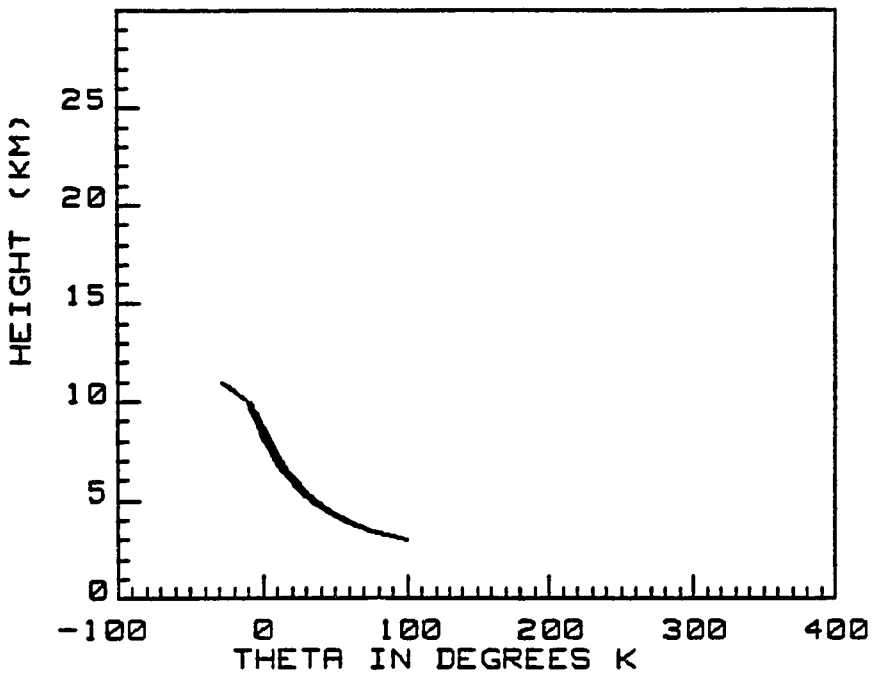

Figure 33. Effect of initial Particulate Number Density (ZNO) upon the VCP differential temperature - height profile. Particulate number densities in a range from 1.25 E+4 to 1.25 E+10 per cubic meter in increments of one order of magnitude.

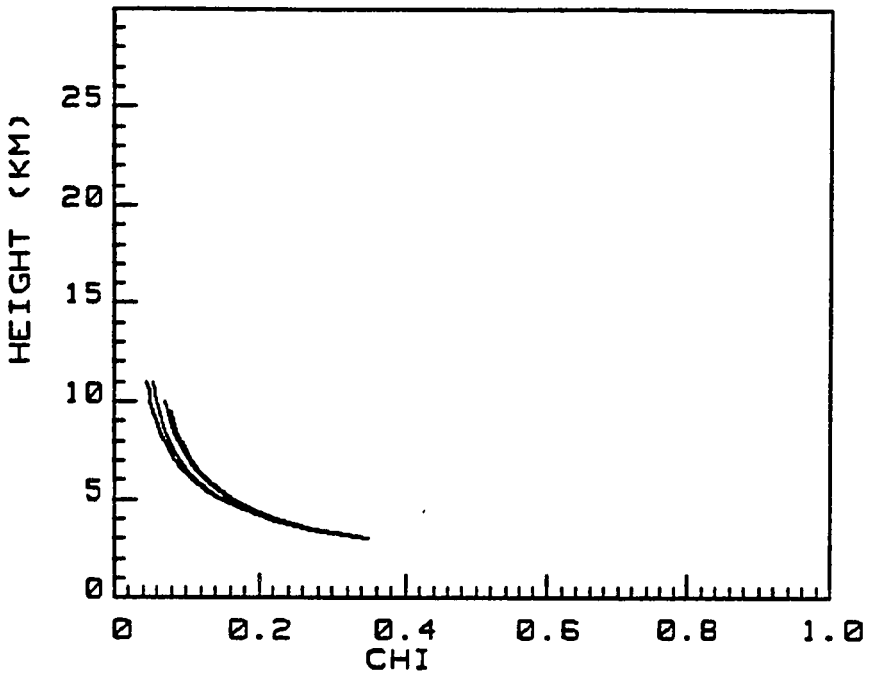

Figure 34. Effect of initial Particulate Number Density (ZNO) upon the VCP ash fraction - height profile. Particulate number densities in a range from 1.25 E+4 to 1.25 E+10 per cubic meter in increments of one order of magnitude.

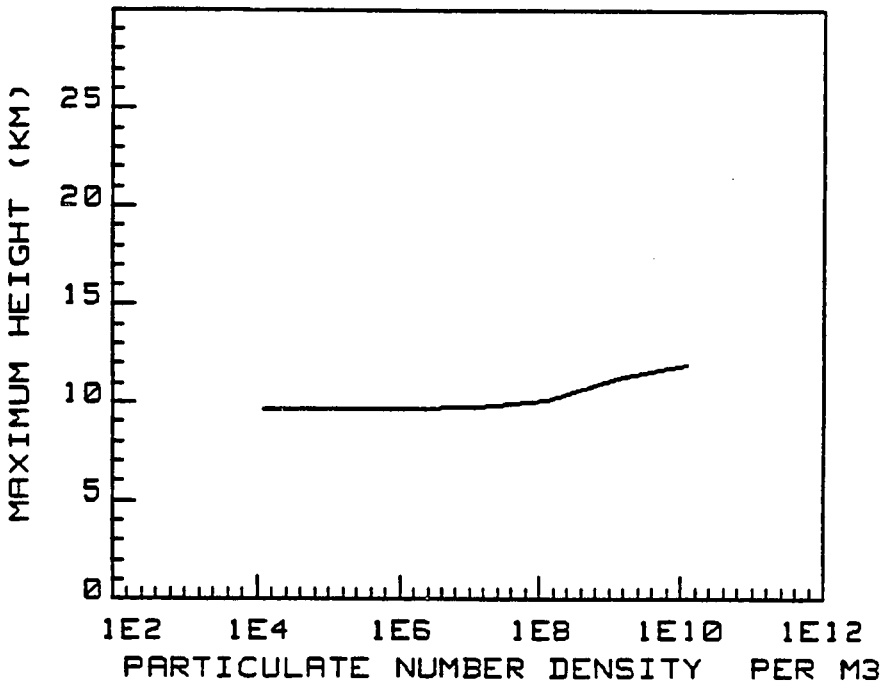

Figure 35. Effect of initial Particulate Number Density (ZNO) upon the VCP maximum height. Particulate number densities in a range from 1.25 E+4 to 1.25 E+10 per cubic meter in increments of one order of magnitude.

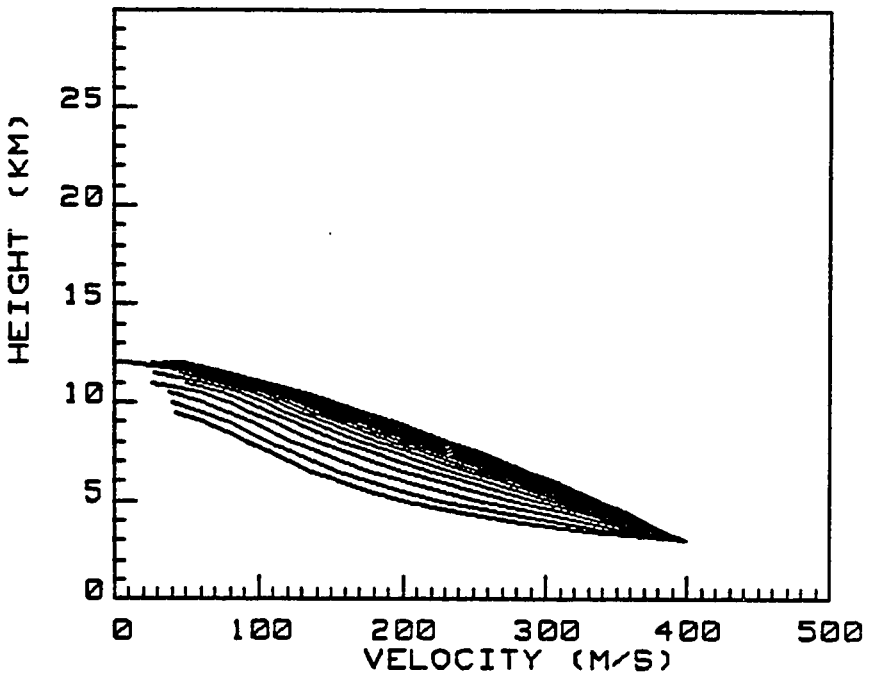

Figure 36. Effect of initial Mode Radius (a_g) of the particulate number distribution upon the VCP velocity - height profile. Mode Radius set in a range from 25 to 500 micron in increments of 25 microns.

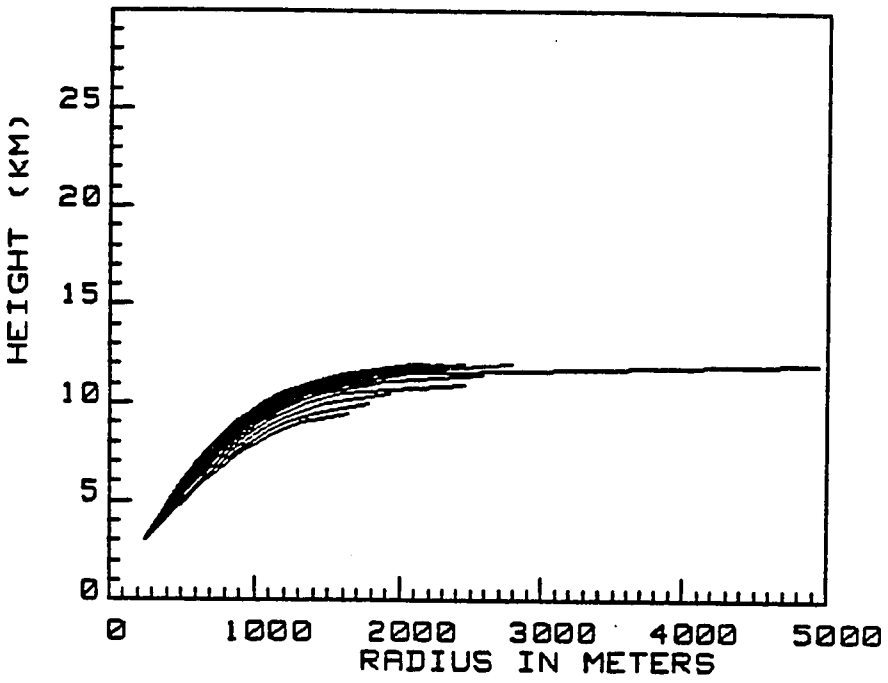

Figure 37. Effect of initial Mode Radius (a_g) of the particulate number distribution upon the VCP radial profile. Mode Radius set in a range from 25 to 500 micron in increments of 25 microns.

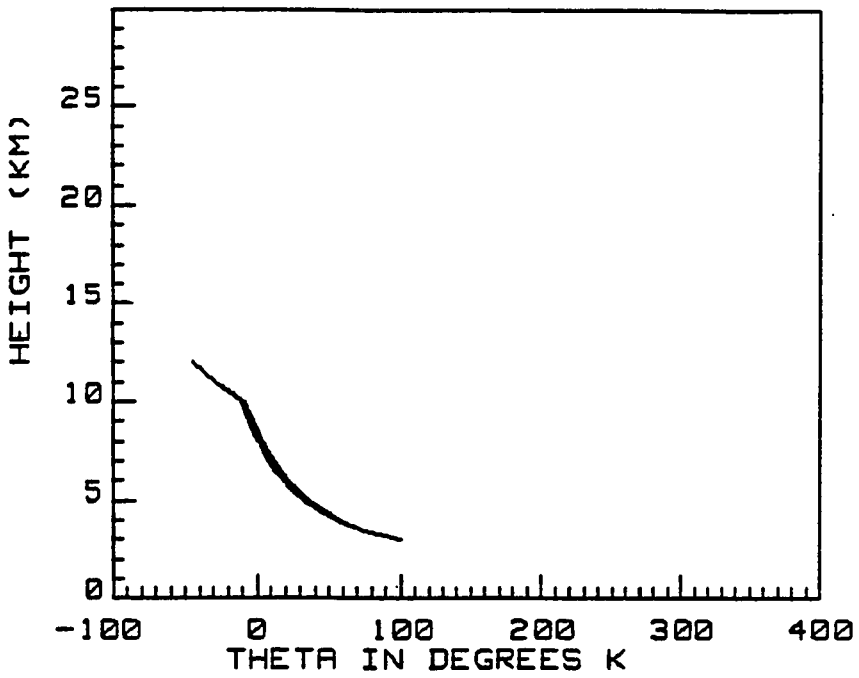

Figure 38. Effect of initial Mode Radius (a_g) of the particulate number distribution upon the VCP differential temperature - height profile. Mode Radius set in a range from 25 to 500 micron in increments of 25 microns.

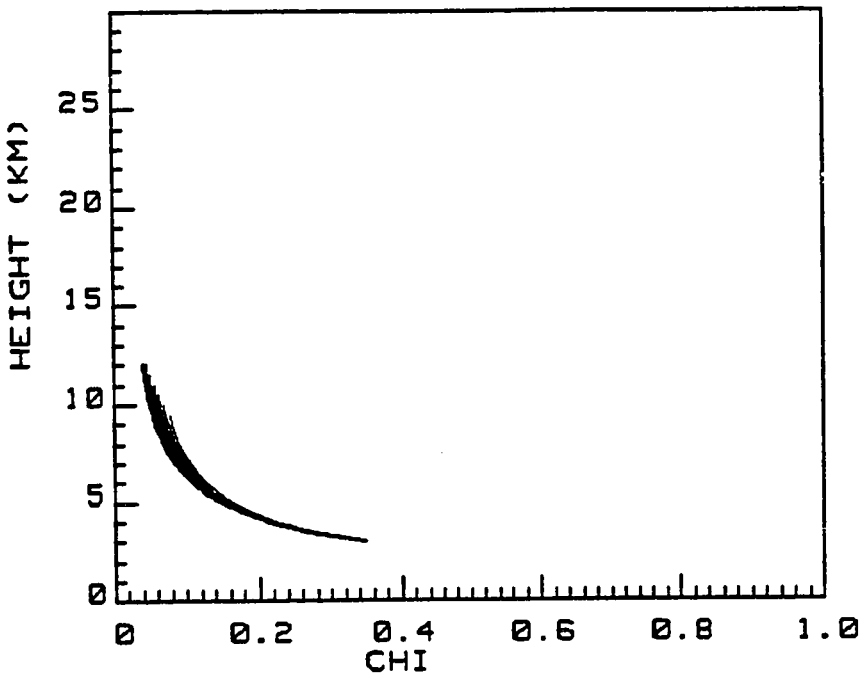

Figure 39. Effect of initial Mode Radius (a_g) of the particulate number distribution upon the VCP ash fraction - height profile. Mode Radius set in a range from 25 to 500 micron in increments of 25 microns.

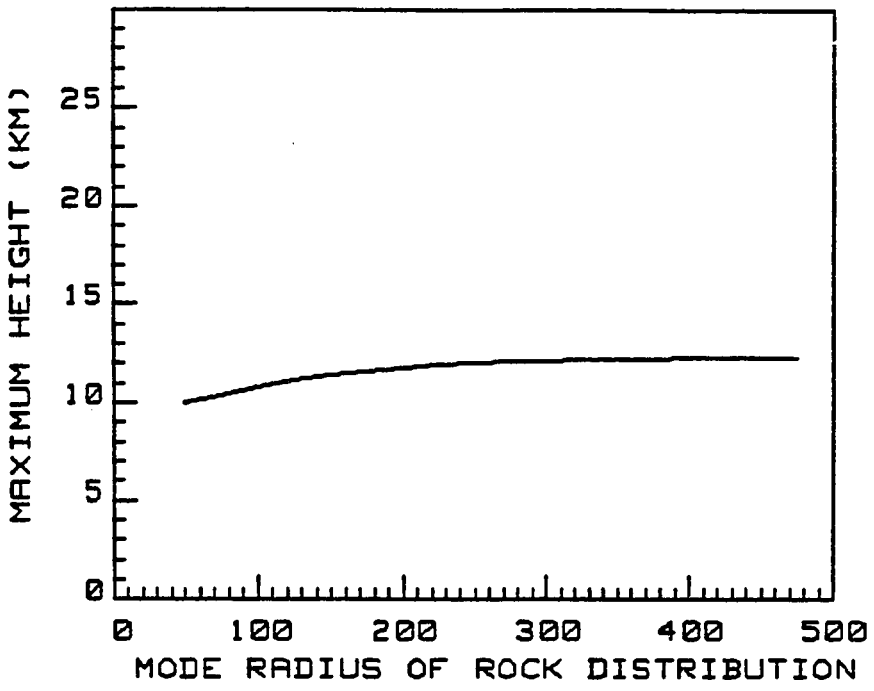

Figure 40. Effect of initial Mode Radius (a_g) of the particulate number distribution upon the VCP maximum height. Mode Radius set in a range from 25 to 500 micron in increments of 25 microns.

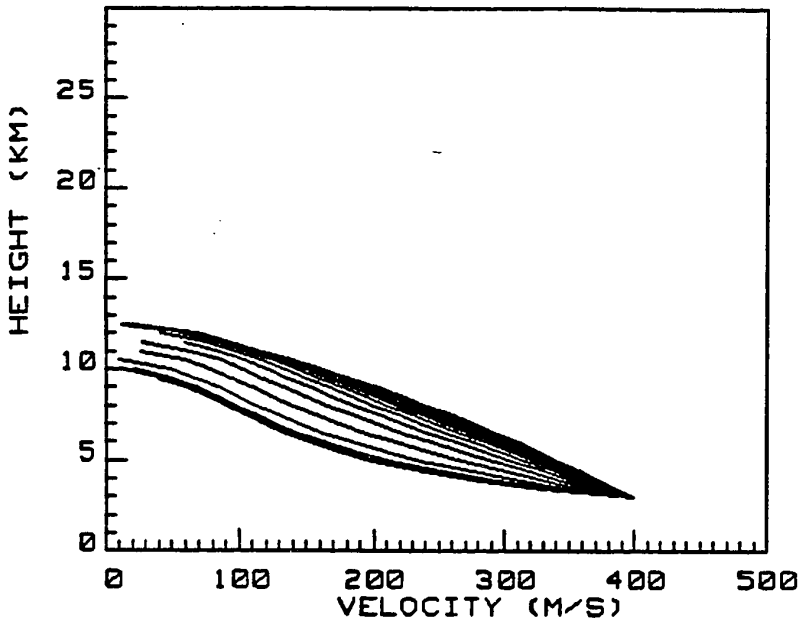

Figure 41. Effect of the standard deviation (σ) of the particulate number distribution upon the VCP velocity - height profile. Standard deviation set in a range from 1.25 to 10.0 in increments of 0.50.

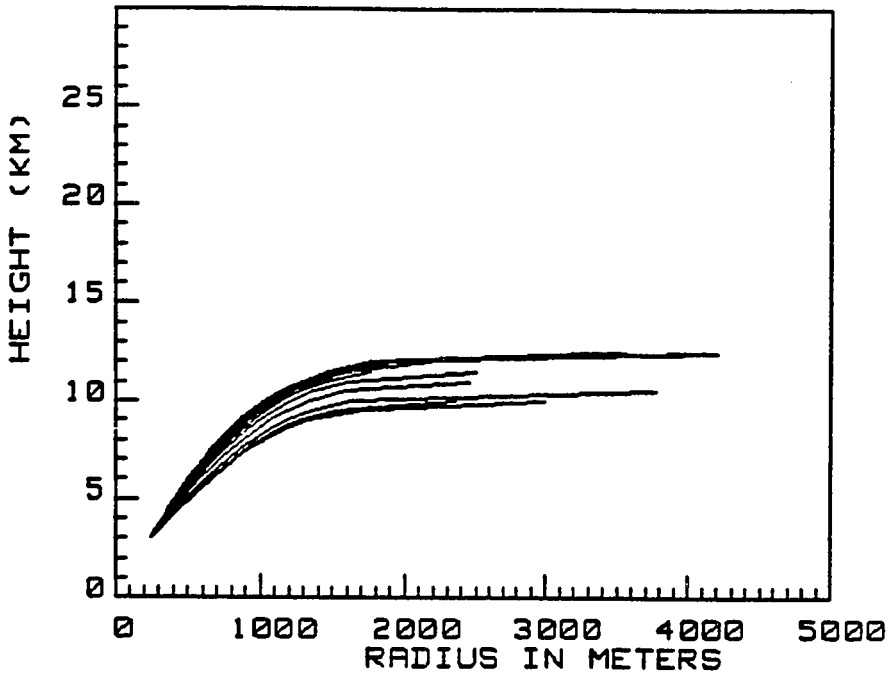

Figure 42. Effect of the standard deviation (σ) of the particulate number distribution upon the VCP radial profile. Standard deviation set in a range from 1.25 to 10.0 in increments of 0.50.

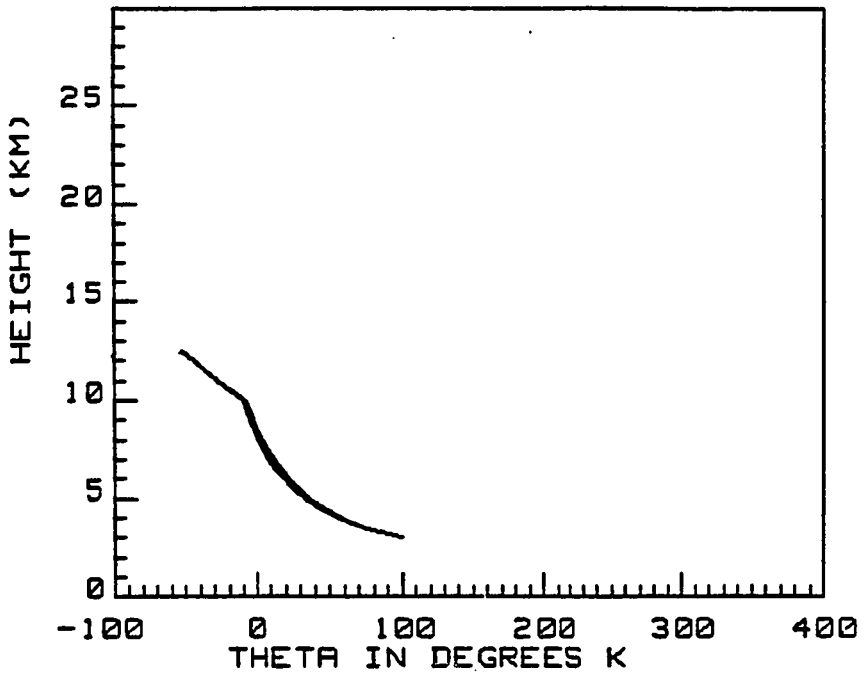

Figure 43. Effect of the standard deviation (σ) of the particulate number distribution upon the VCP differential temperature - height profile. Standard deviation set in a range from 1.25 to 10.0 in increments of 0.50.

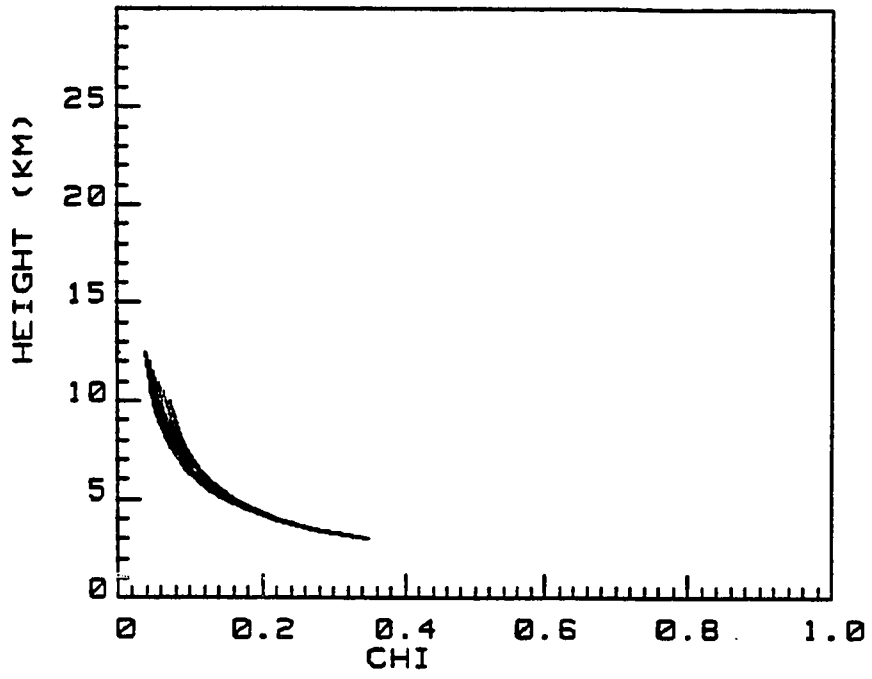

Figure 44. Effect of the standard deviation (σ) of the particulate number distribution upon the VCP ash fraction - height profile. Standard deviation set in a range from 1.25 to 10.0 in increments of 0.50.

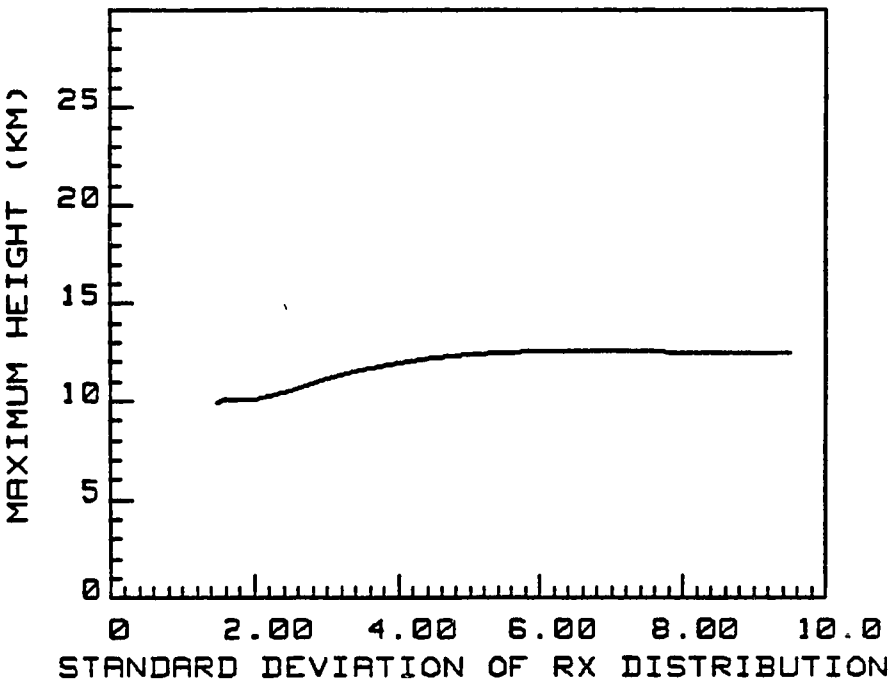

Figure 45. Effect of the standard deviation (σ) of the particulate number distribution upon the VCP maximum height. Standard deviation set in a range from 1.25 to 10.0 in increments of 0.50.

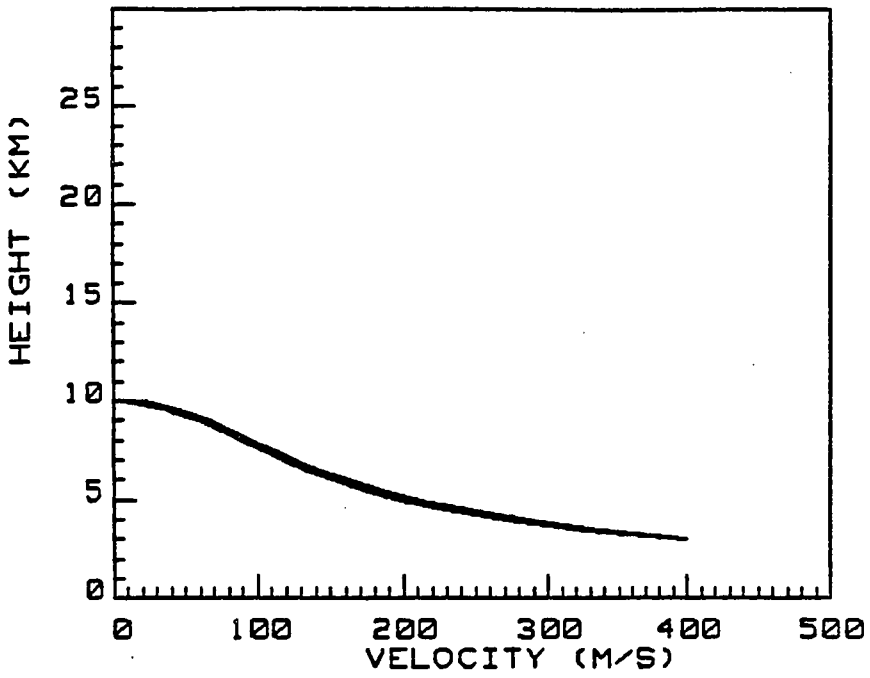

Figure 46. Effect of the mass density of the pyroclastic particulate material upon the VCP velocity - height profile. Pyroclastic particulate material density in the range from 1000 to 2500 Kg/m^3 in increments of 250 Kg/m^3.

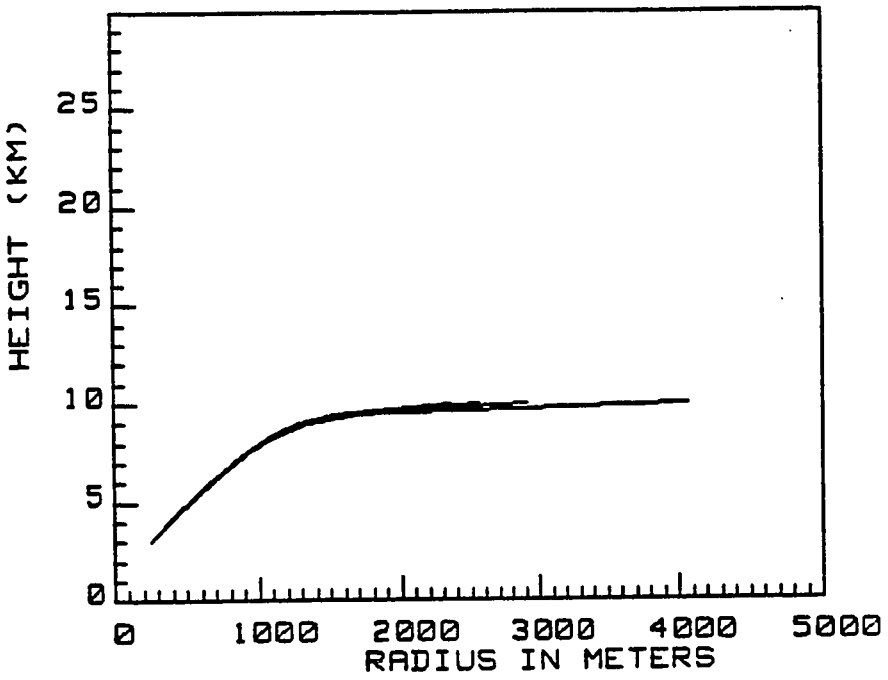

Figure 47. Effect of the mass density of the pyroclastic particulate material upon the VCP radial profile. Pyroclastic particulate material density in the range from 1000 to 2500 Kg/m^3 in increments of 250 Kg/m^3.

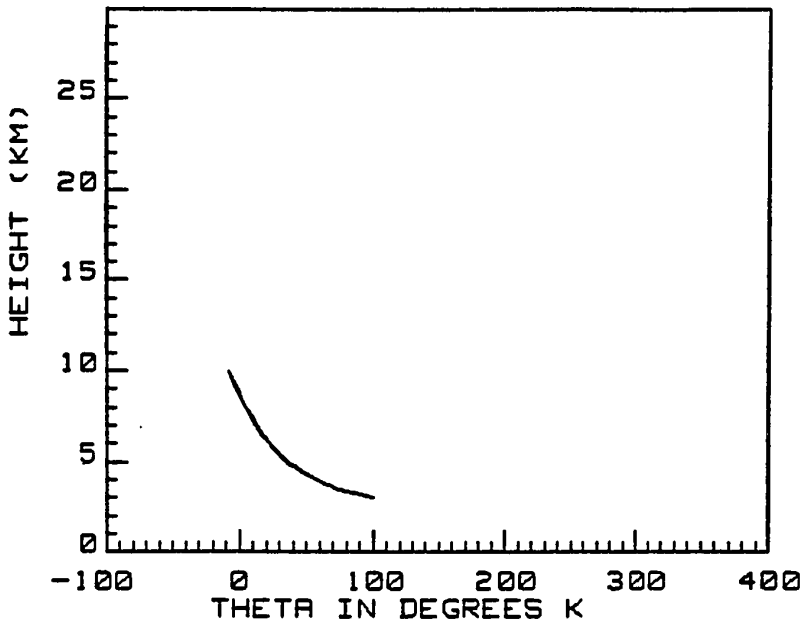

Figure 48. Effect of the mass density of the pyroclastic particulate material upon the VCP differential temperature - height profile. Pyroclastic particulate material density in the range from 1000 to 2500 Kg/m^3 in increments of 250 Kg/m^3.

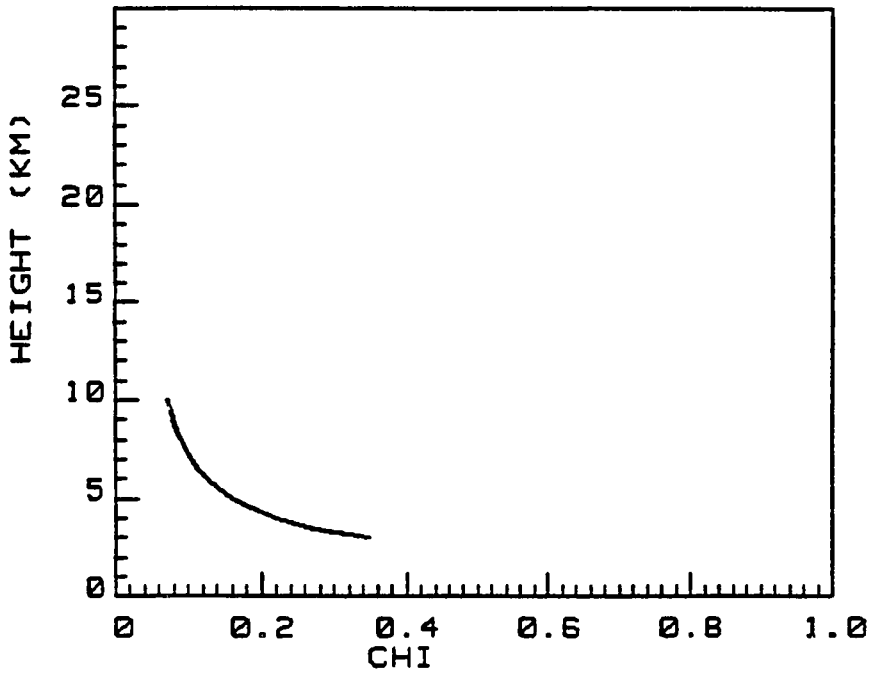

Figure 49. Effect of the mass density of the pyroclastic particulate material upon the VCP ash fraction - height profile. Pyroclastic particulate material density in the range from 1000 to 2500 Kg/m^3 in increments of 250 Kg/m^3.

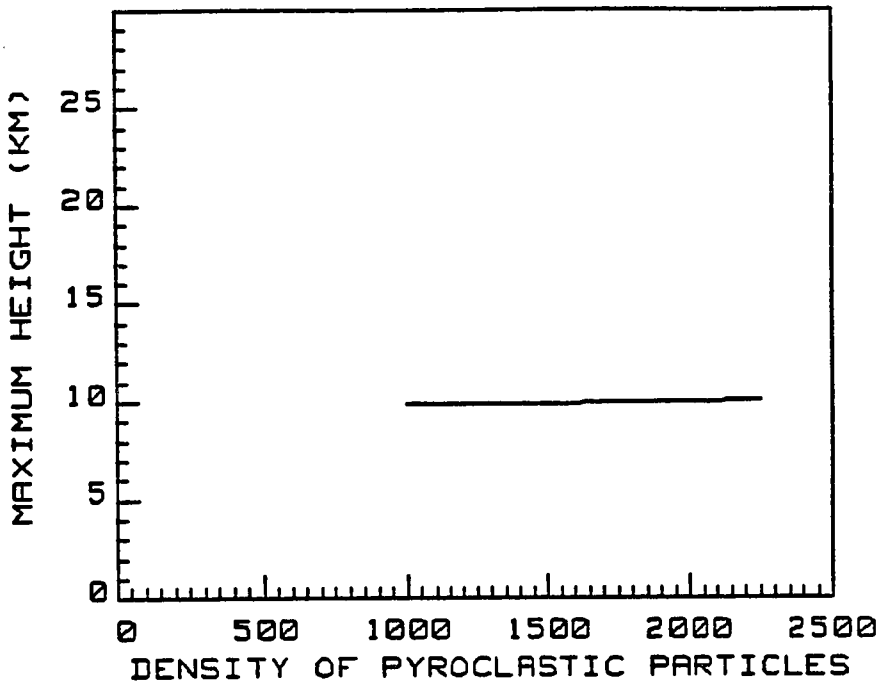

Figure 50. Effect of the mass density of the pyroclastic particulate material upon the VCP maximum height. Pyroclastic particulate material density in the range from 1000 to 2500 Kg/m^3 in increments of 250 Kg/m^3.

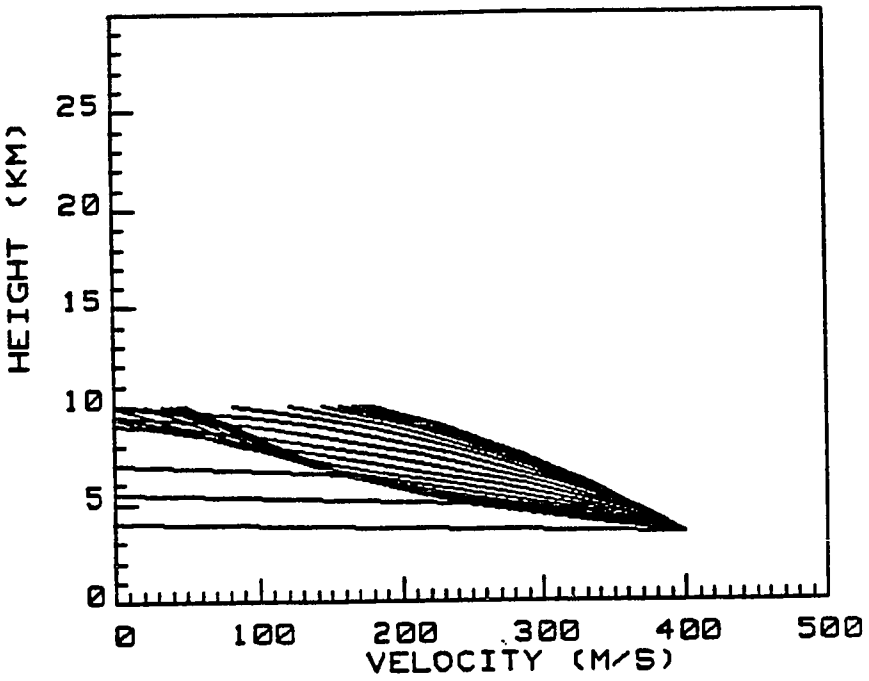

Figure 51. Standard Case Model: Velocity - height profiles of the pyroclastic particulates as shown for each individual bin size (all 50 bins).

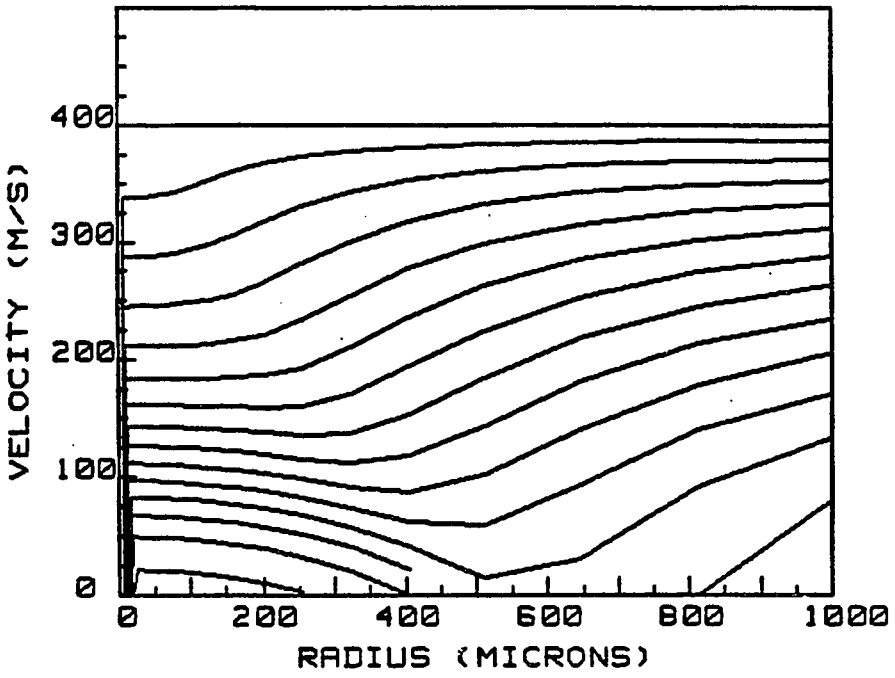

Figure 52. Standard Case Model: Velocity contours of the pyroclastic particulates within the sizes ranging below 1000 micron radius. Each line represents a contour of velocities at equal height intervals of 500 meters along the length of the established VCP.

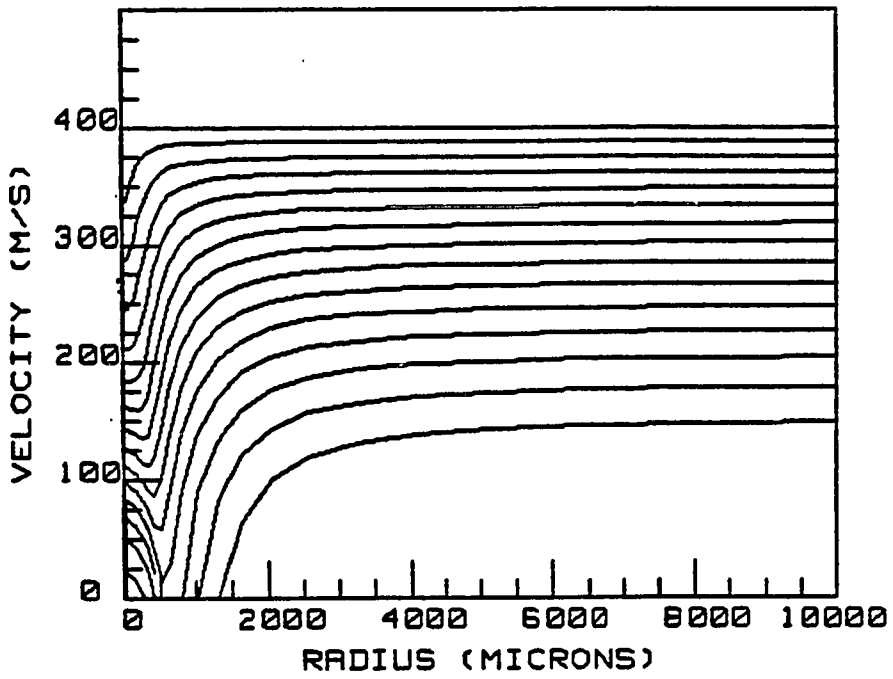

Figure 53. Standard Case Model: Velocity contours of the pyroclastic particulates within the sizes ranging below 10,000 micron radius. Each line represents a contour of velocities at equal height intervals of 500 meters along the length of the established VCP.

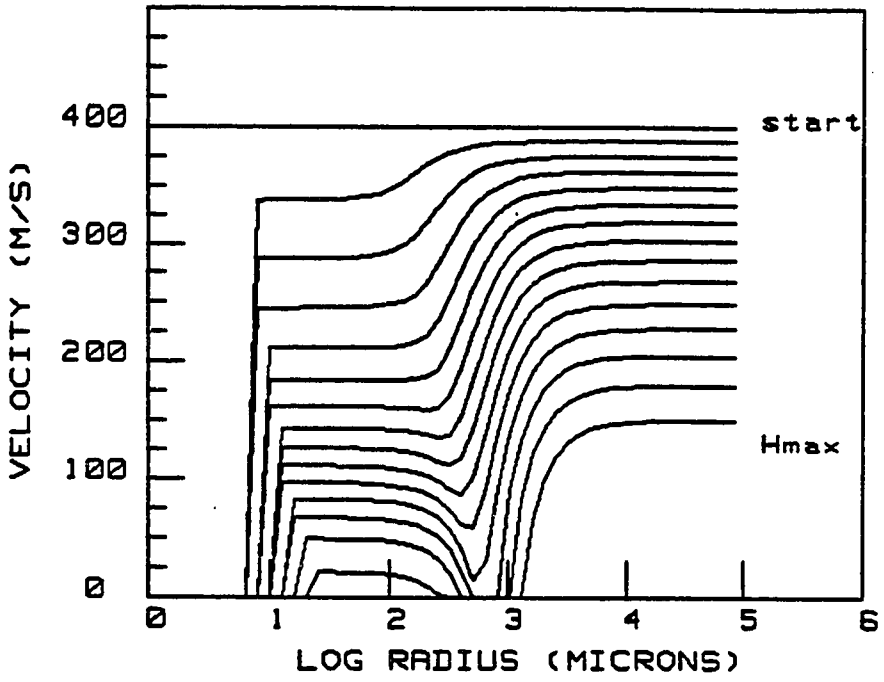

Figure 54. Standard Case Model: Velocity contours of the pyroclastic particulates of the entire size distribution. Each line represents a contour of velocities at equal height intervals of 500 meters along the length of the established VCP.

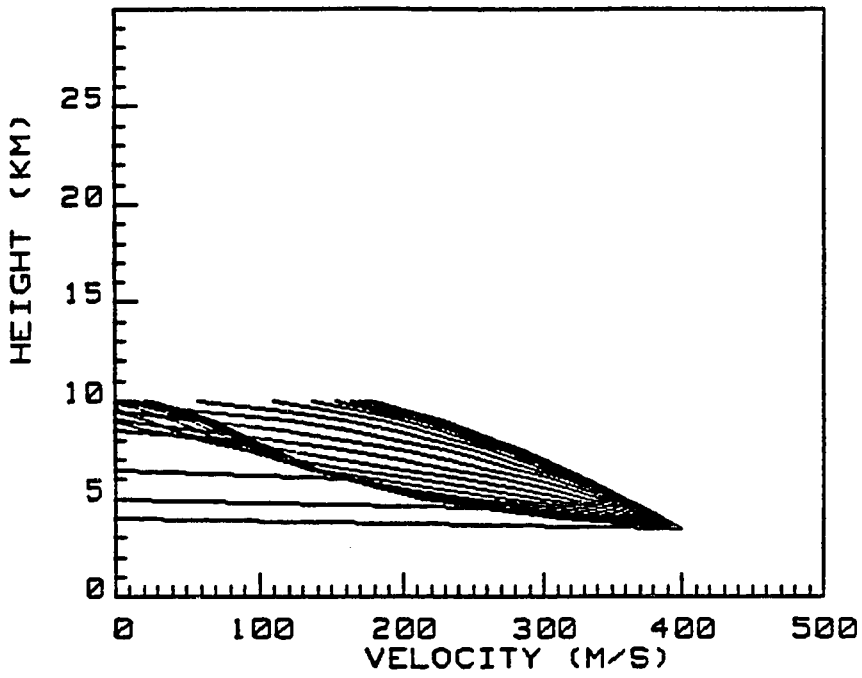

Figure 55. Effect of particulate number density with ZNO=1.25E4. Velocity - height profiles of the pyroclastic particulates (all 50 bins).

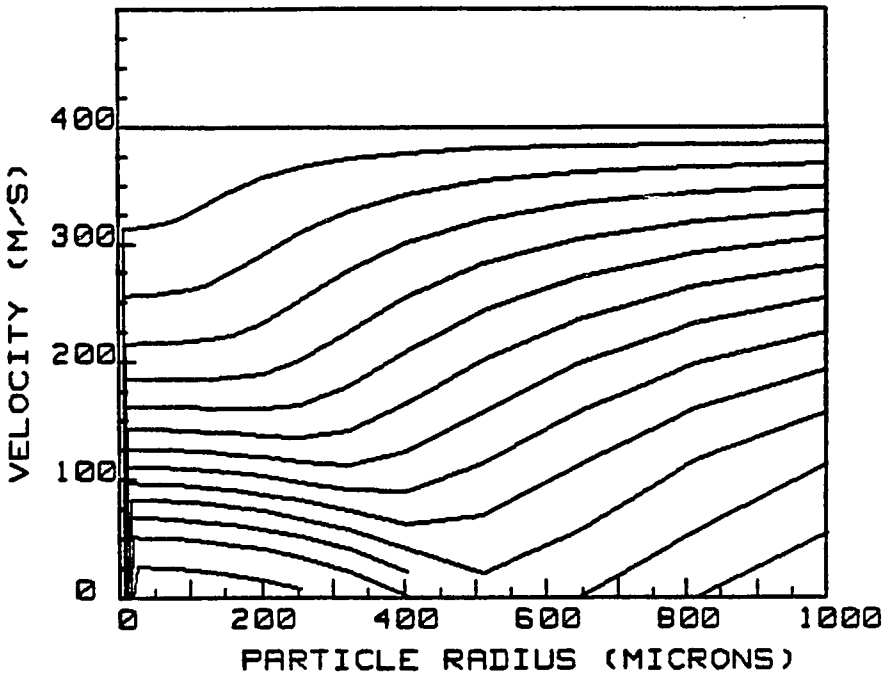

Figure 56. Effect of particulate number density with ZNO=1.25E4. Velocity contours of the pyroclastic particulates within the sizes ranging below 1000 micron radius. Each line represents a contour of velocities at equal height intervals of 500 meters along the length of the established VCP.

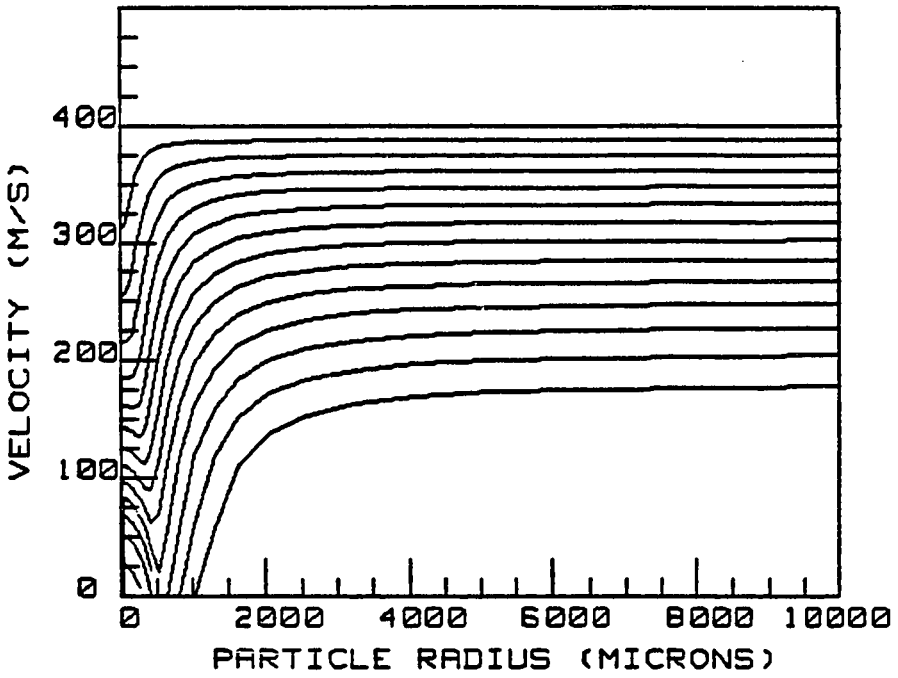

Figure 57. Effect of particulate number density with ZNO=1.25E4. Velocity contours of the pyroclastic particulates within the sizes ranging below 10,000 micron radius. Each line represents a contour of velocities at equal height intervals of 500 meters along the length of the established VCP.

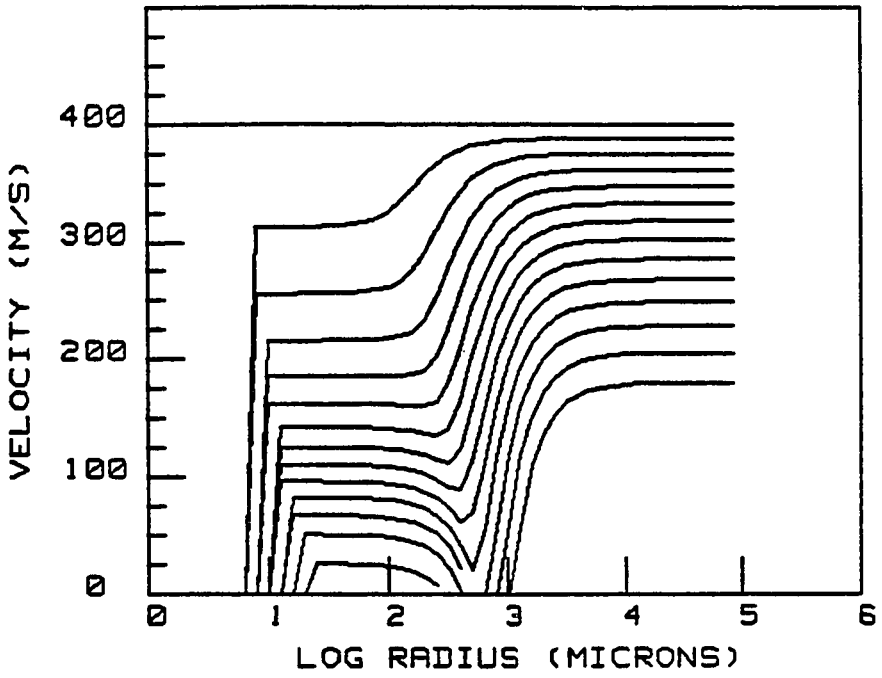

Figure 58 Effect of the particulate number density with ZNO=1.25E4. Velocity contours of the pyroclastic particulates of the entire size distribution. Each line represents a contour of velocities at equal height intervals of 500 meters along the length of the established VCP.

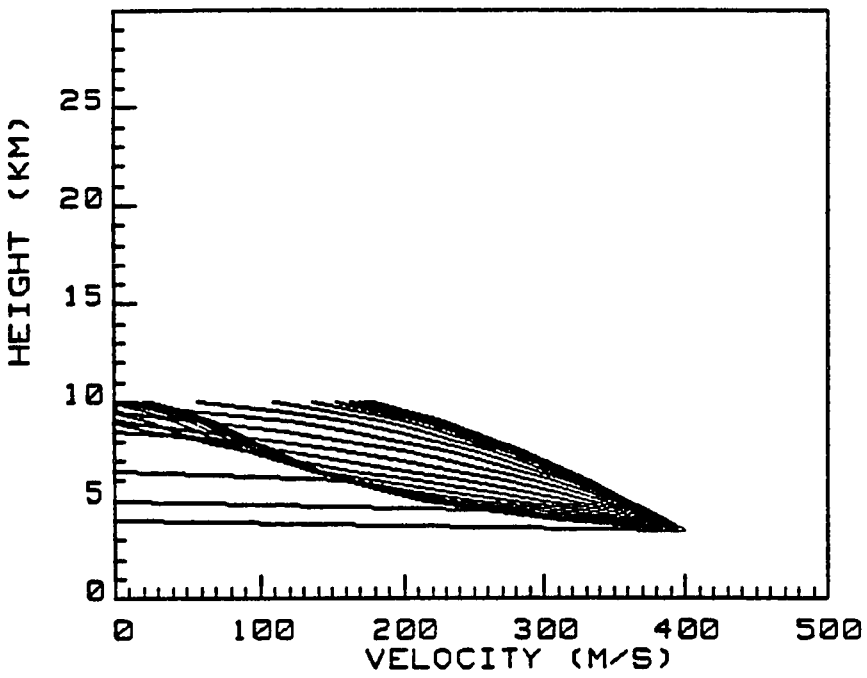

Figure 59. Effect of particulate number density with ZNO=1.25E6. Velocity - height profiles of the pyroclastic particulates (all 50 bins).

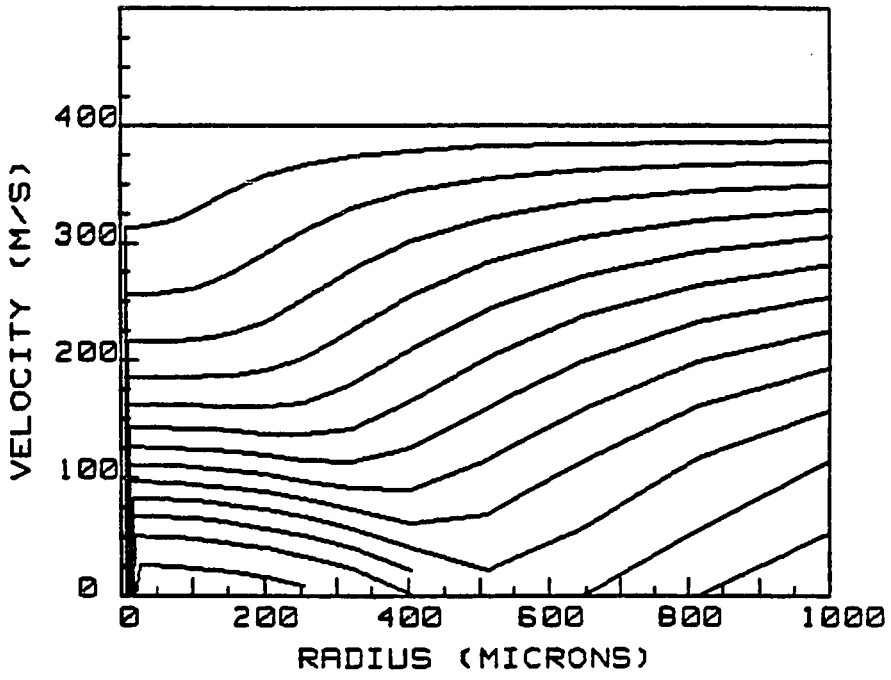

Figure 60. Effect of particulate number density with ZNO=1.25E6. Velocity contours of the pyroclastic particulates within the sizes ranging below 1000 micron radius. Each line represents a contour of velocities at equal height intervals of 500 meters along the length of the established VCP.

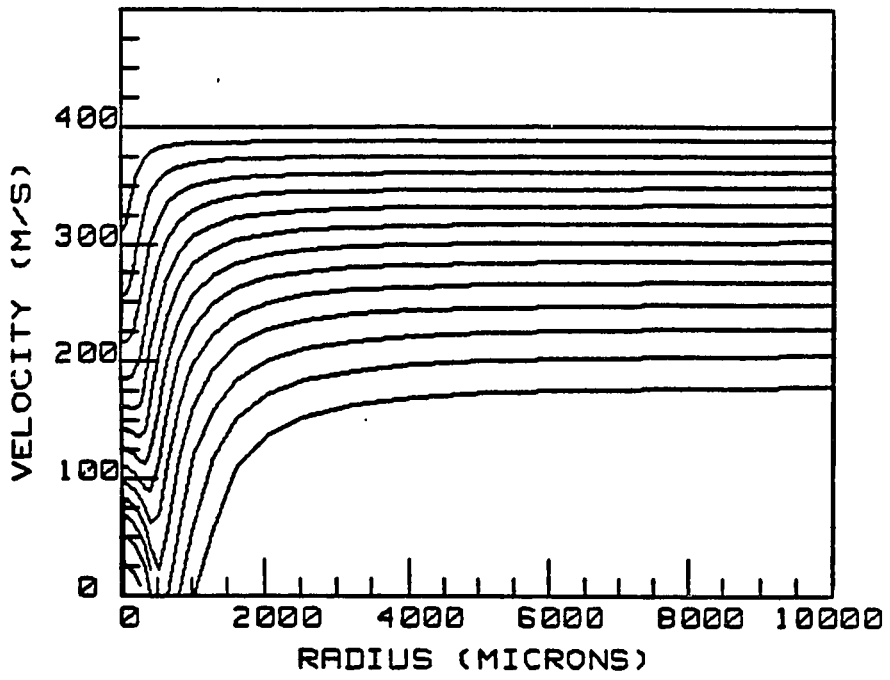

Figure 61. Effect of particulate number density with ZNO=1.25E6. Velocity contours of the pyroclastic particulates within the sizes ranging below 10,000 micron radius. Each line represents a contour of velocities at equal height intervals of 500 meters along the length of the established VCP.

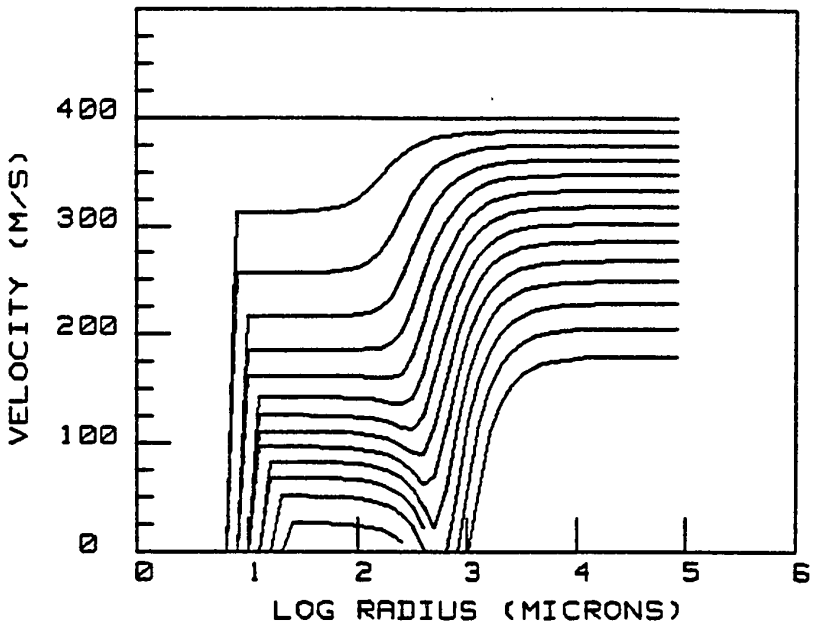

Figure 62 Effect of the particulate number density with ZNO=1.25E6. Velocity contours of the pyroclastic particulates of the entire size distribution. Each line represents a contour of velocities at equal height intervals of 500 meters along the length of the established VCP.

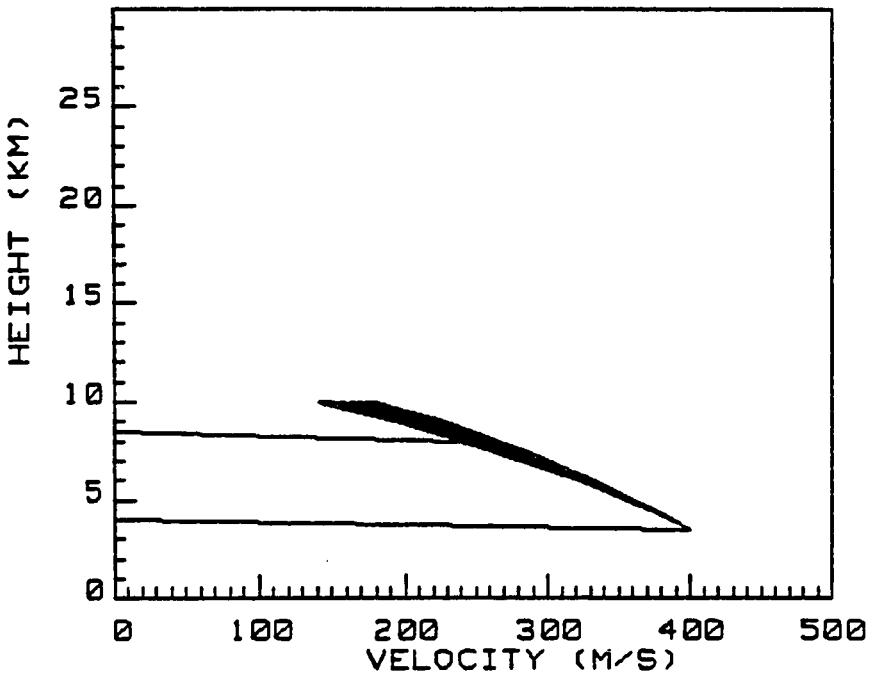

Figure 63. Effect of particulate number density with ZNO=1.25E10. Velocity - height profiles of the pyroclastic particulates (all 50 bins).

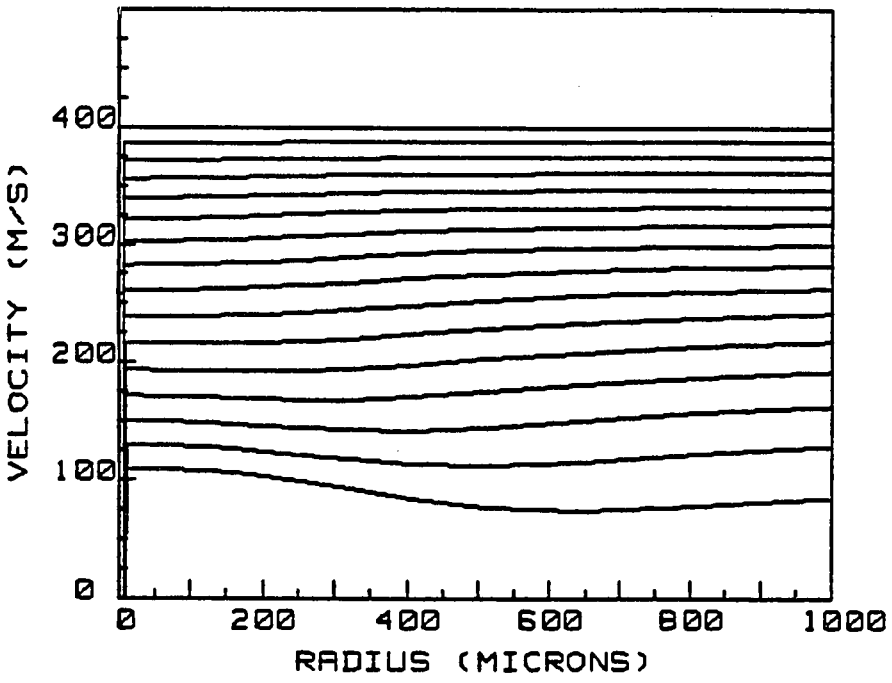

Figure 64. Effect of particulate number density with ZNO=1.25E10.Velocity contours of the pyroclastic particulates within the sizes ranging below 1000 micron radius. Each line represents a contour of velocities at equal height intervals of 500 meters along the length of the established VCP.

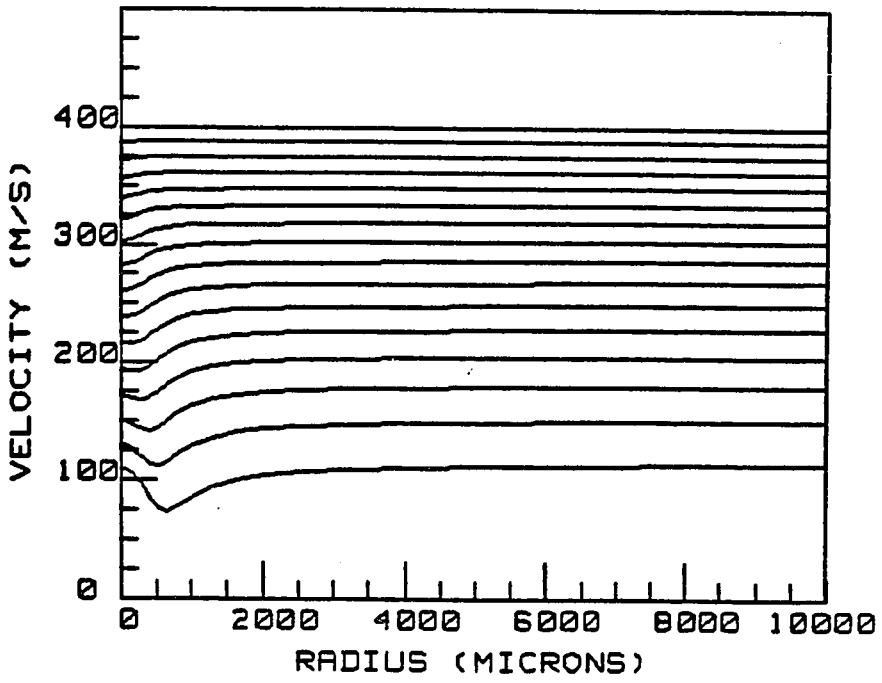

Figure 65. Effect of particulate number density with ZNO=1.25E10. Velocity contours of the pyroclastic particulates within the sizes ranging below 10,000 micron radius. Each line represents a contour of velocities at equal height intervals of 500 meters along the length of the established VCP.

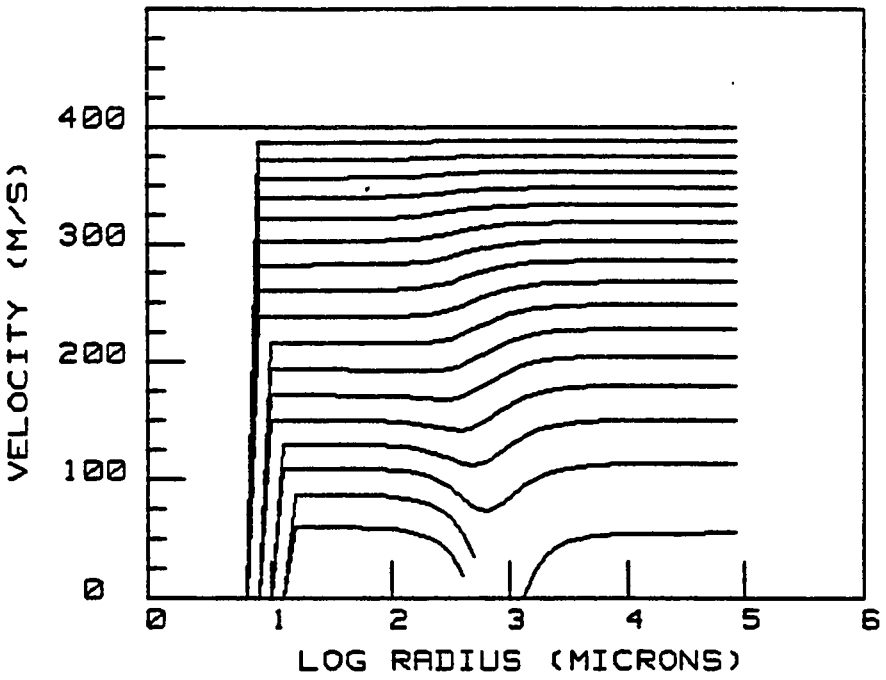

Figure 66. Effect of the particulate number density with ZNO=1.25E10. Velocity contours of the pyroclastic particulates of the entire size distribution. Each line represents a contour of velocities at equal height intervals of 500 meters along the length of the established VCP.

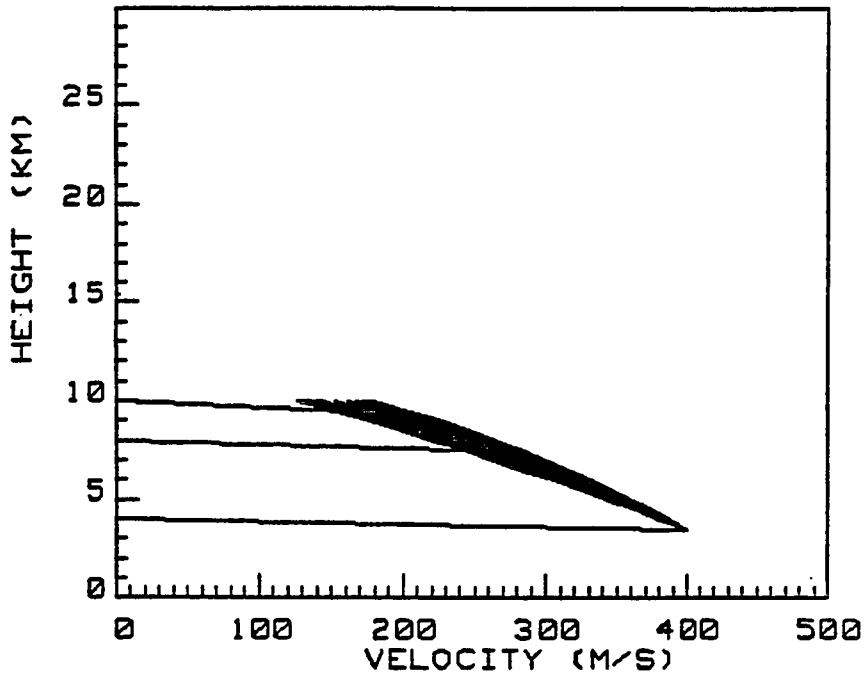

Figure 67. Effect of mode radius of the particulate distribution function with a_g=25 microns. Velocity - height profiles of the pyroclastic particulates (all 50 bins).

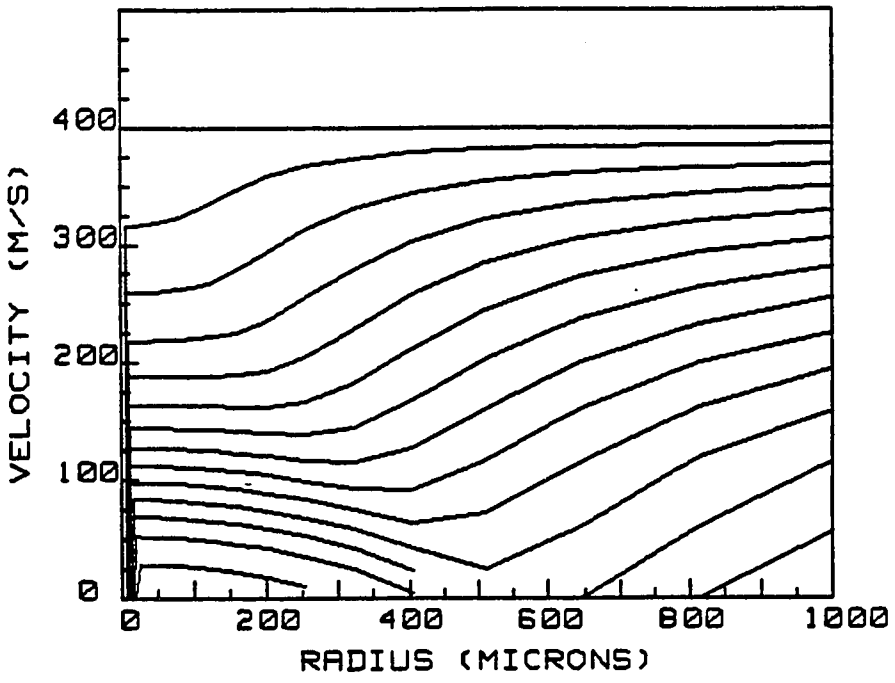

Figure 68. Effect of the mode radius of the particulate distribution function with a_g= 25 microns. Velocity contours of the pyroclastic particulates within the sizes ranging below 1000 micron radius. Each line represents a contour of velocities at equal height intervals of 500 meters along the length of the established VCP.

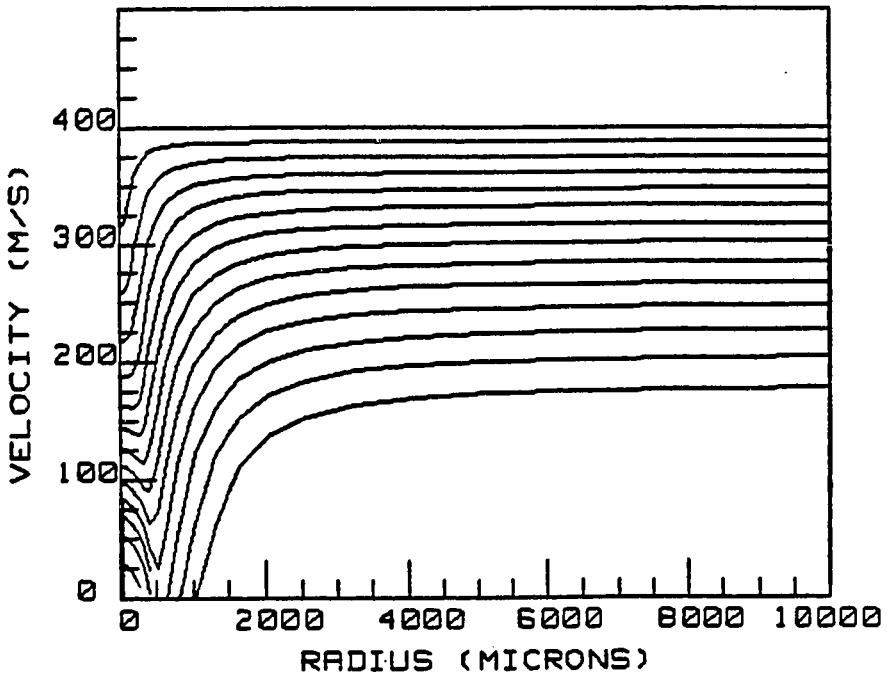

Figure 69. Effect of the mode radius of the particulate distribution function with a_g= 25 microns. Velocity contours of the pyroclastic particulates within the sizes ranging below 10,000 micron radius. Each line represents a contour of velocities at equal height intervals of 500 meters along the length of the established VCP.

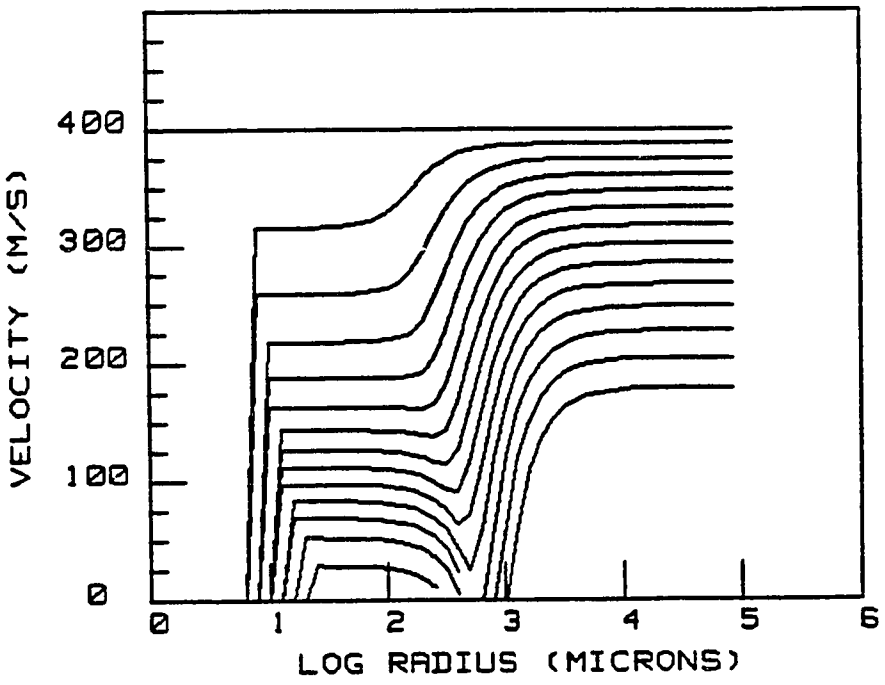

Figure 70. Effect of the mode radius of the particulate distribution function with a_g= 25 microns. Velocity contours of the pyroclastic particulates of the entire size distribution. Each line represents a contour of velocities at equal height intervals of 500 meters along the length of the established VCP.

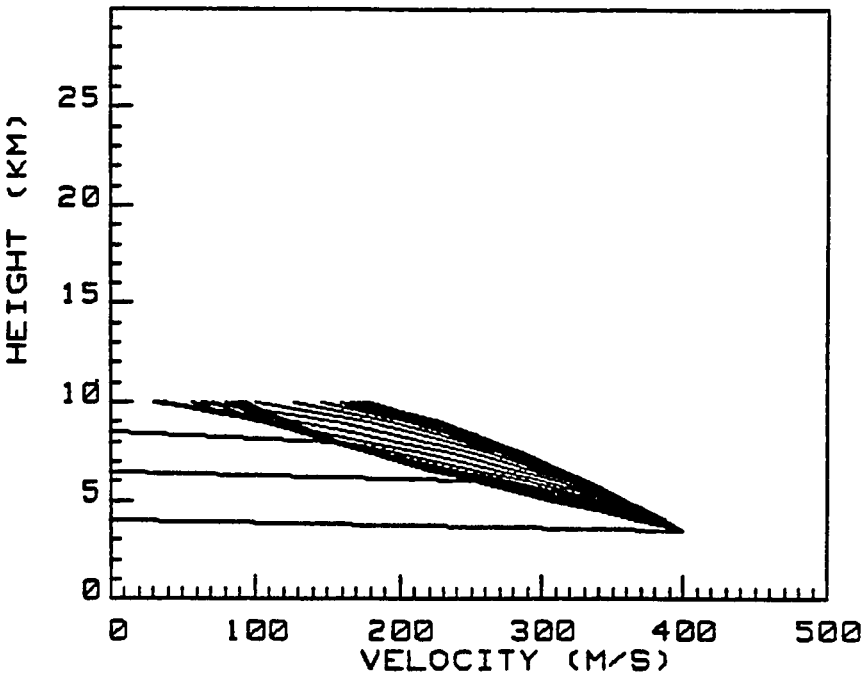

Figure 71. Effect of the mode radius of the particulate distribution function with a_g= 125 microns. Velocity - height profiles of the pyroclastic particulates (all 50 bins).

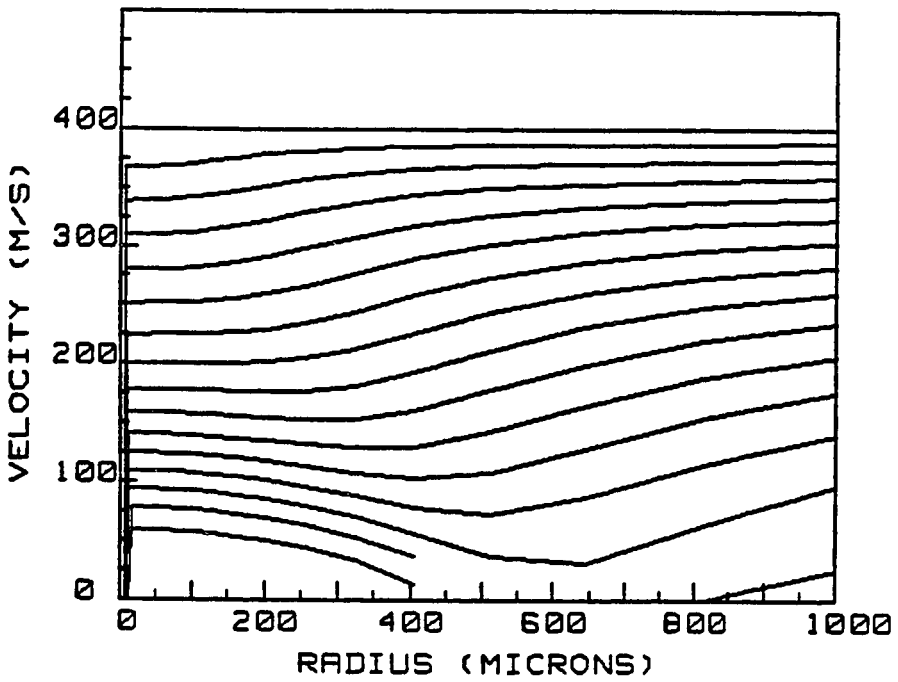

Figure 72. Effect of the mode radius of the particulate distribution function with a_g= 125 microns. Velocity contours of the pyroclastic particulates within the sizes ranging below 1000 micron radius. Each line represents a contour of velocities at equal height intervals of 500 meters along the length of the established VCP.

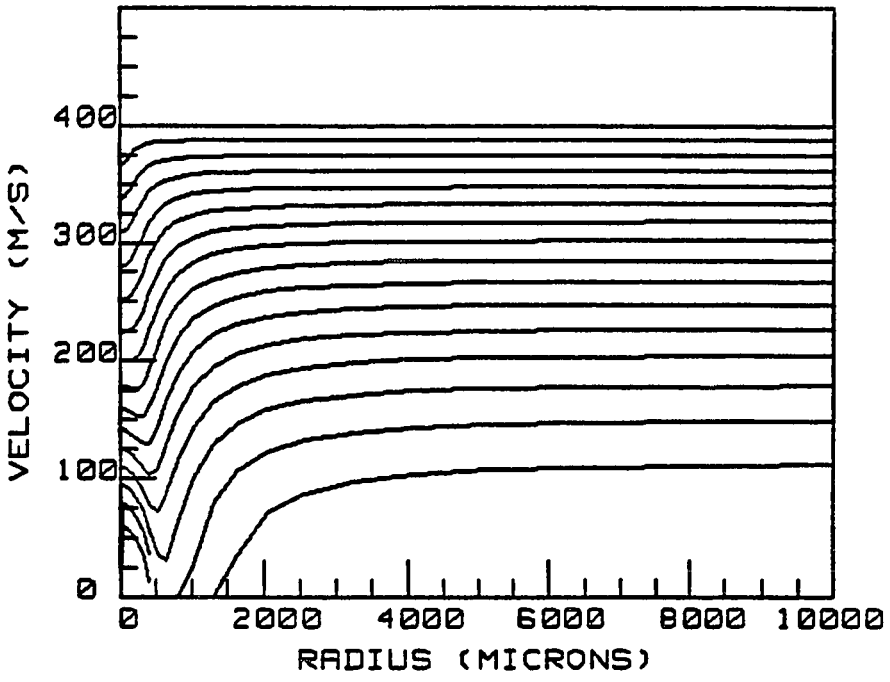

Figure 73. Effect of the mode radius of the particulate distribution function with a_g= 125 microns. Velocity contours of the pyroclastic particulates within the sizes ranging below 10,000 micron radius. Each line represents a contour of velocities at equal height intervals of 500 meters along the length of the established VCP.

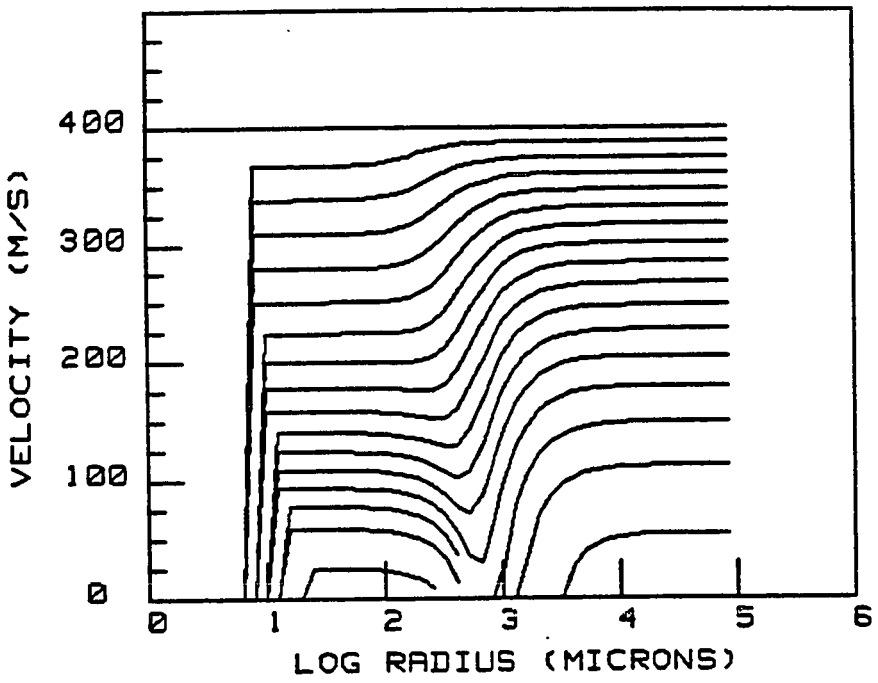

Figure 74. Effect of the mode radius of the particulate distribution function with a_g= 125 microns. Velocity contours of the pyroclastic particulates of the entire size distribution. Each line represents a contour of velocities at equal height intervals of 500 meters along the length of the established VCP.

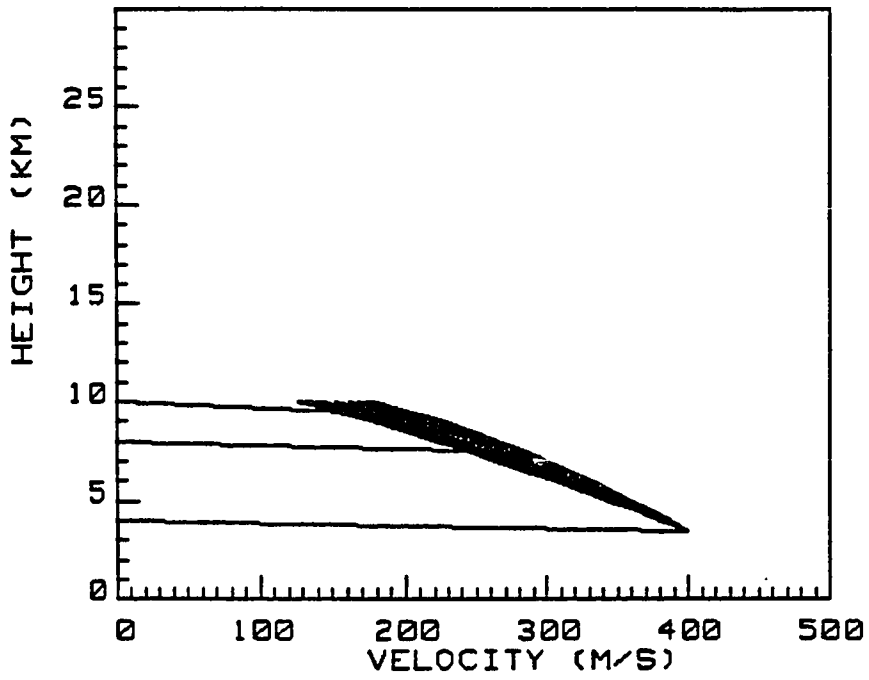

Figure 75. Effect of the mode radius of the particulate distribution function with a_g= 250 microns. Velocity - height profiles of the pyroclastic particulates (all 50 bins).

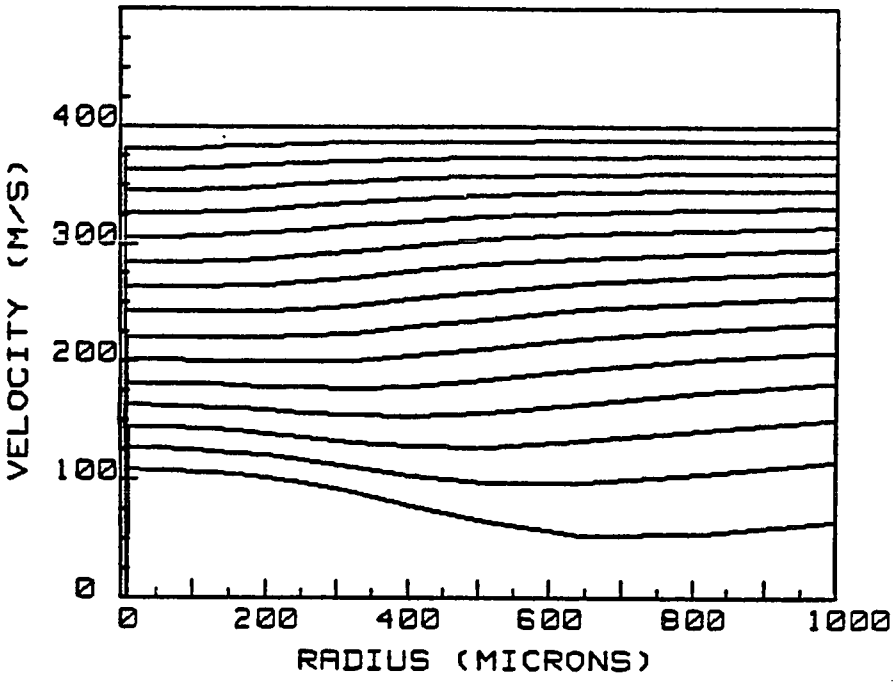

Figure 76. Effect of the mode radius of the particulate distribution function with a_g= 250 microns. Velocity contours of the pyroclastic particulates within the sizes ranging below 1000 micron radius. Each line represents a contour of velocities at equal height intervals of 500 meters along the length of the established VCP.

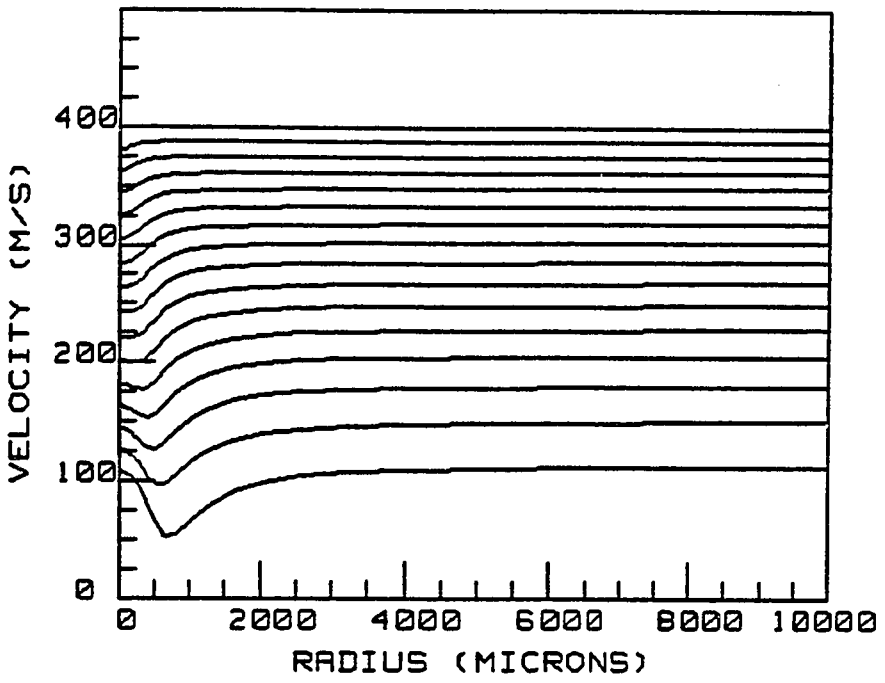

Figure 77. Effect of the mode radius of the particulate distribution function with a_g= 250 microns. Velocity contours of the pyroclastic particulates within the sizes ranging below 10,000 micron radius. Each line represents a contour of velocities at equal height intervals of 500 meters along the length of the established VCP.

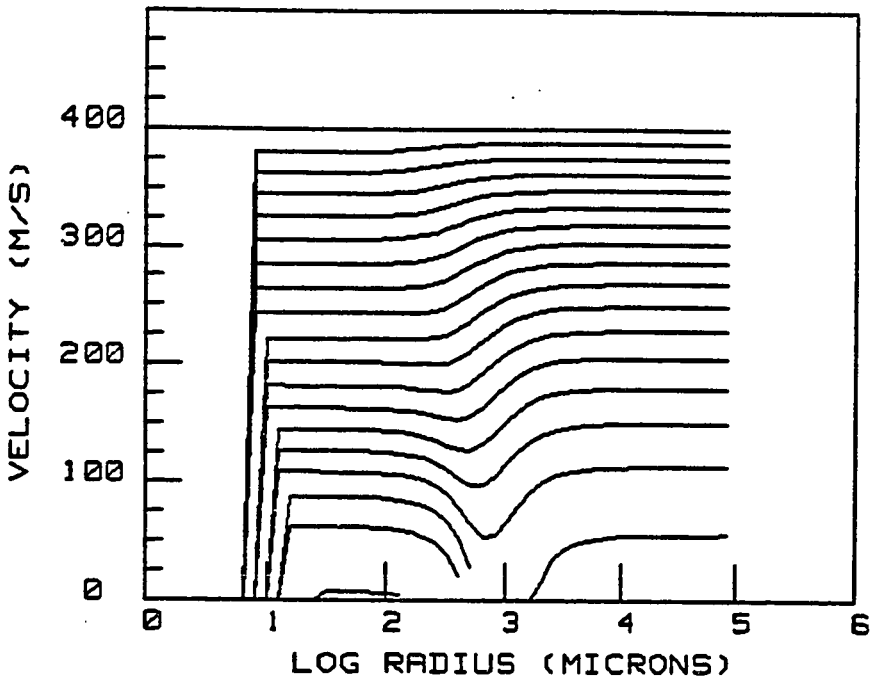

Figure 78. Effect of the mode radius of the particulate distribution function with a_g= 250 microns. Velocity contours of the pyroclastic particulates of the entire size distribution. Each line represents a contour of velocities at equal height intervals of 500 meters along the length of the established VCP.

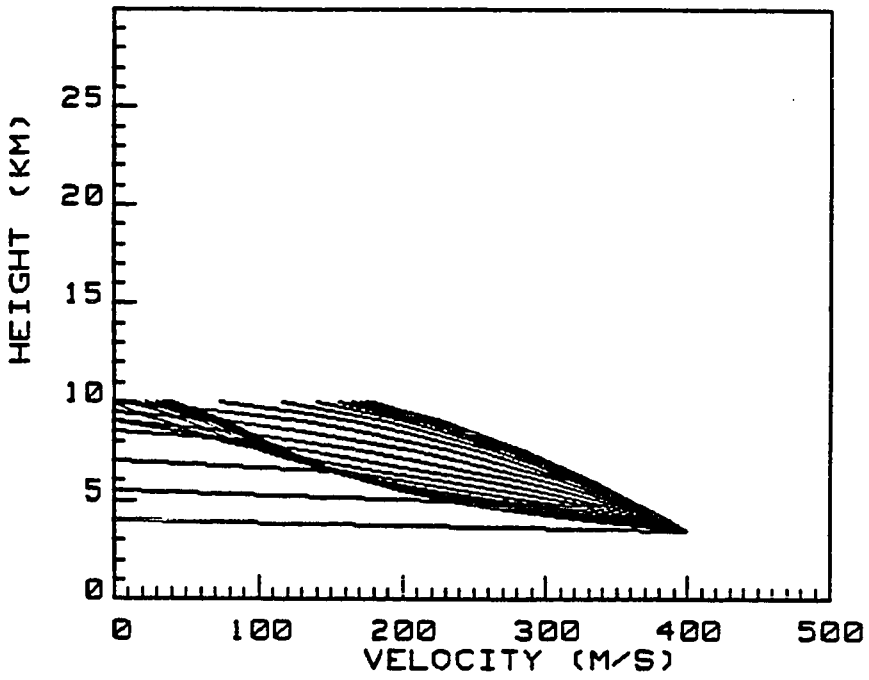

Figure 79. Effect of the standard deviation of the particulate distribution function with σ = 1.25 microns. Velocity - height profiles of the pyroclastic particulates (all 50 bins).

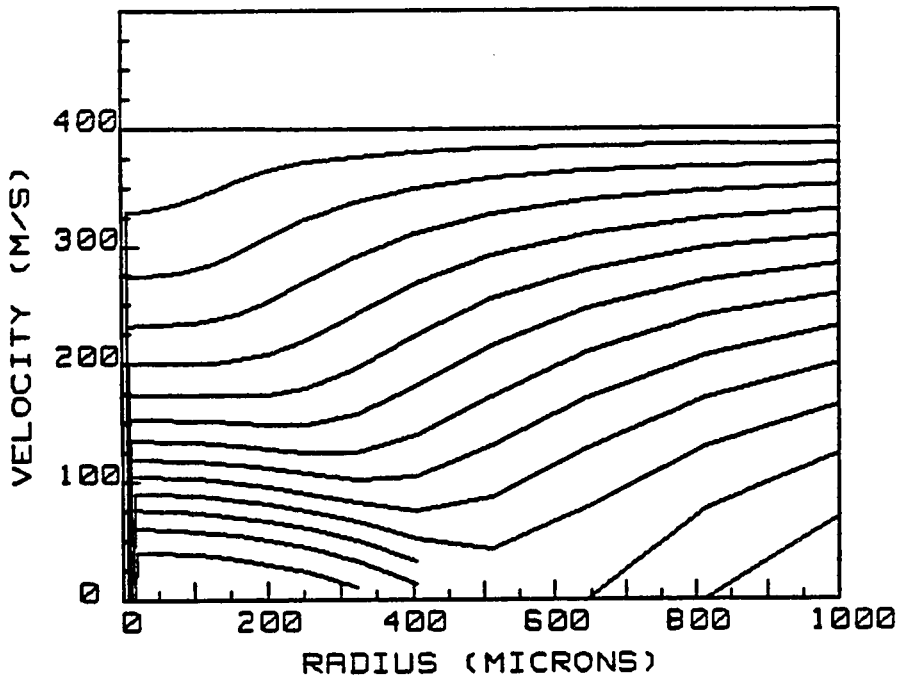

Figure 80. Effect of the standard deviation of the particulate distribution function with σ = 1.25 microns. Velocity contours of the pyroclastic particulates within the sizes ranging below 1000 micron radius. Each line represents a contour of velocities at equal height intervals of 500 meters along the length of the established VCP.

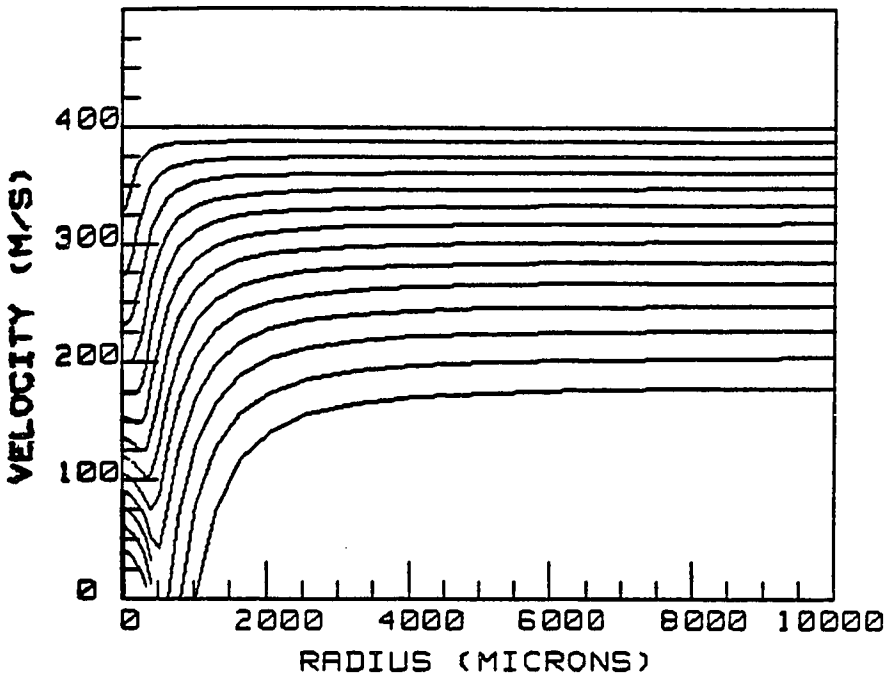

Figure 81. Effect of the standard deviation of the particulate distribution function with σ = 1.25 microns. Velocity contours of the pyroclastic particulates within the sizes ranging below 10,000 micron radius. Each line represents a contour of velocities at equal height intervals of 500 meters along the length of the established VCP.

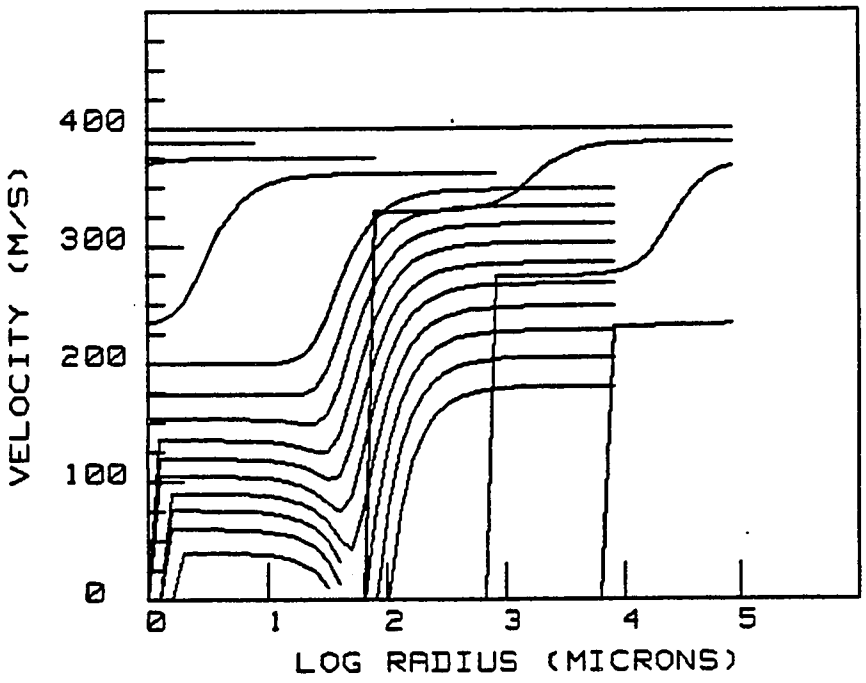

Figure 82. Effect of the standard deviation of the particulate distribution function with σ = 1.25 microns. Velocity contours of the pyroclastic particulates of the entire size distribution. Each line represents a contour of velocities at equal height intervals of 500 meters along the length of the established VCP.

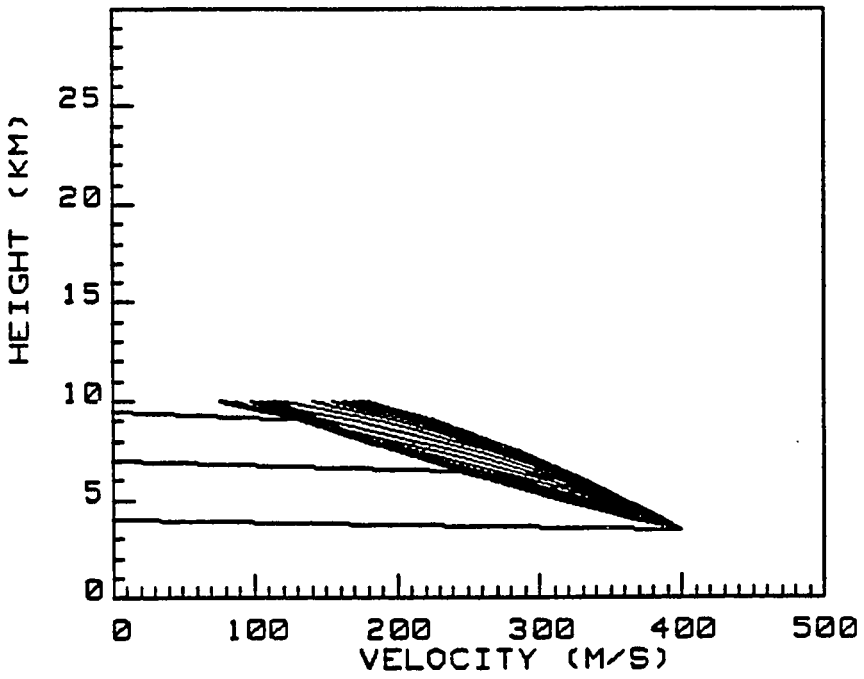

Figure 83. Effect of the standard deviation of the particulate distribution function with σ = 3.00 microns. Velocity - height profiles of the pyroclastic particulates (all 50 bins).

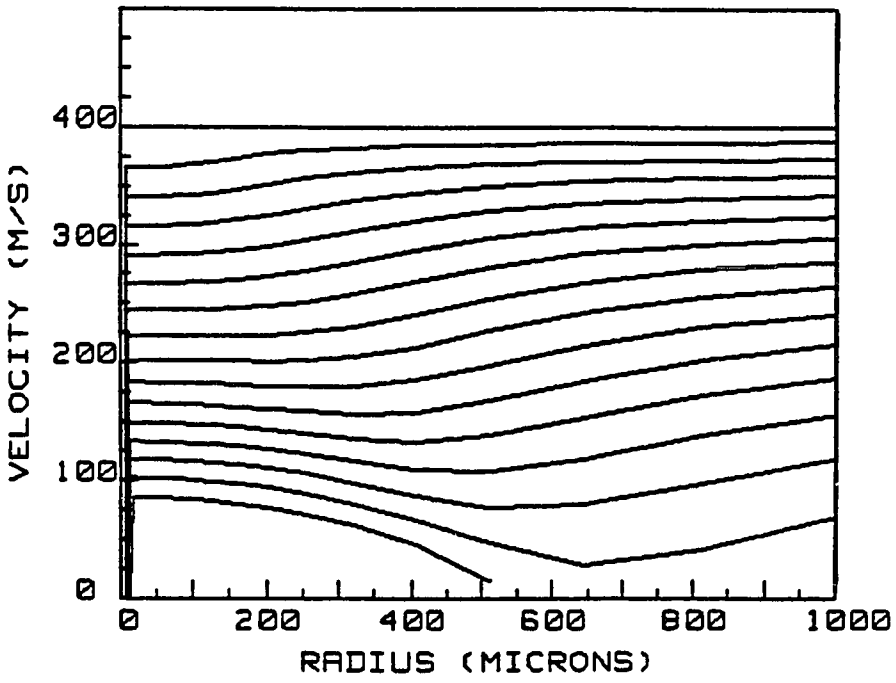

Figure 84. Effect of the standard deviation of the particulate distribution function with σ = 3.00 .microns. Velocity contours of the pyroclastic particulates within the sizes ranging below 1000 micron radius. Each line represents a contour of velocities at equal height intervals of 500 meters along the length of the established VCP.

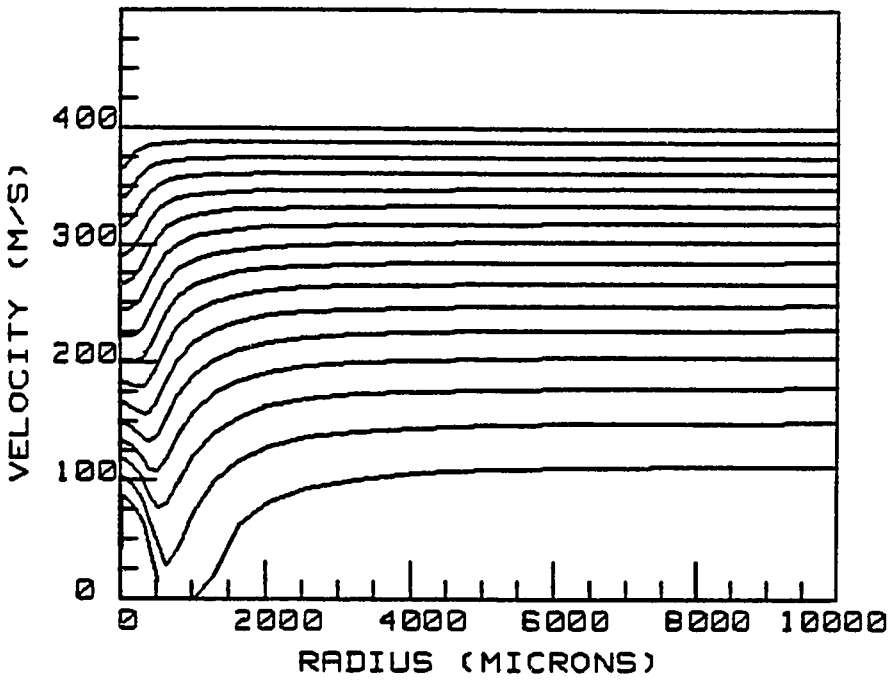

Figure 85. Effect of the standard deviation of the particulate distribution function with σ = 3.00 microns. Velocity contours of the pyroclastic particulates within the sizes ranging below 10,000 micron radius. Each line represents a contour of velocities at equal height intervals of 500 meters along the length of the established VCP.

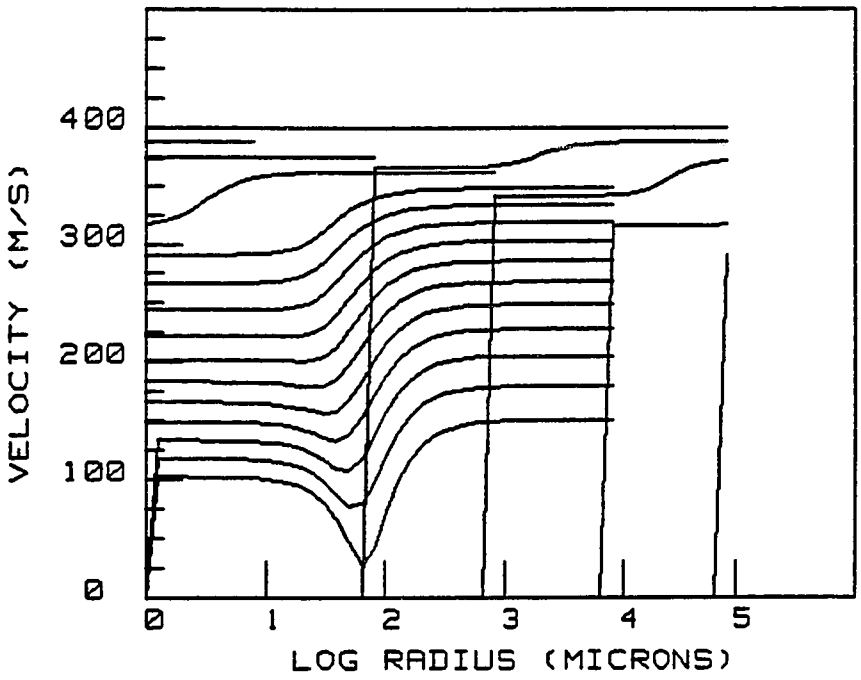

Figure 86. Effect of the standard deviation of the particulate distribution function with σ = 3.00 microns. Velocity contours of the pyroclastic particulates of the entire size distribution. Each line represents a contour of velocities at equal height intervals of 500 meters along the length of the established VCP.

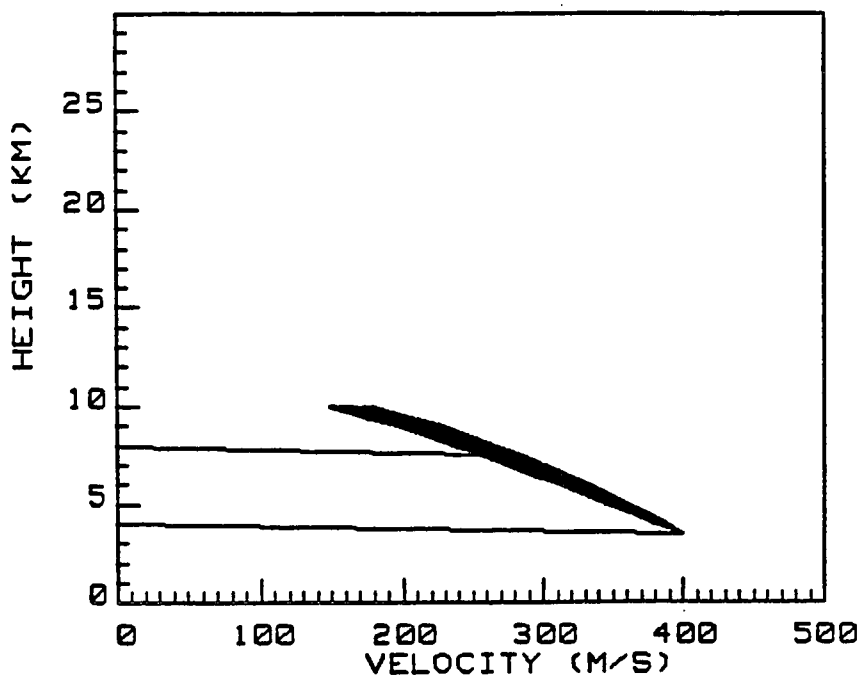

Figure 87. Effect of the standard deviation of the particulate distribution function with σ = 5.00 microns. Velocity - height profiles of the pyroclastic particulates (all 50 bins).

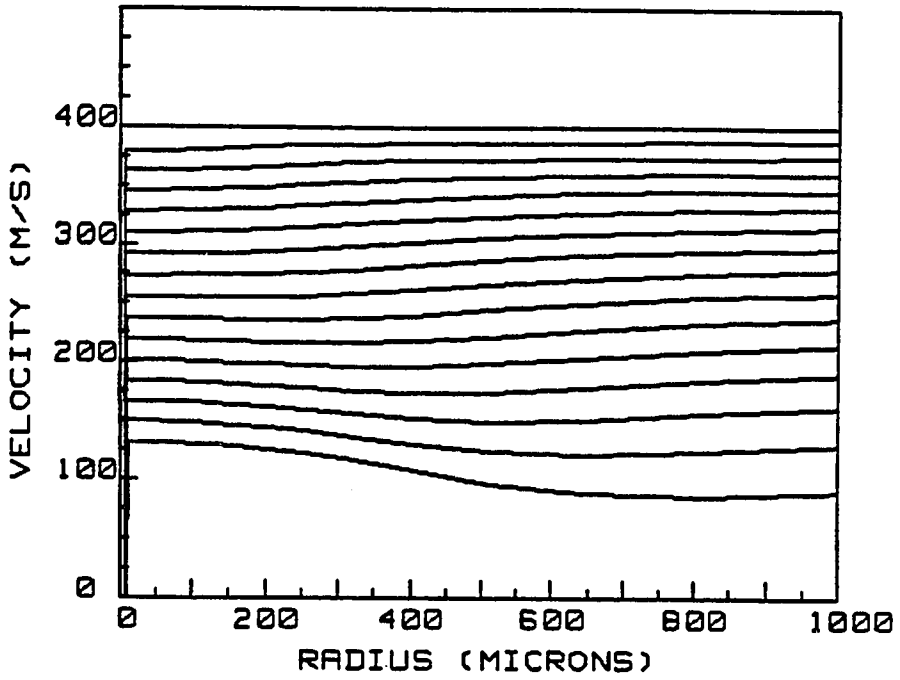

Figure 88. Effect of the standard deviation of the particulate distribution function with σ = 5.00 microns. Velocity contours of the pyroclastic particulates within the sizes ranging below 1000 micron radius. Each line represents a contour of velocities at equal height intervals of 500 meters along the length of the established VCP.

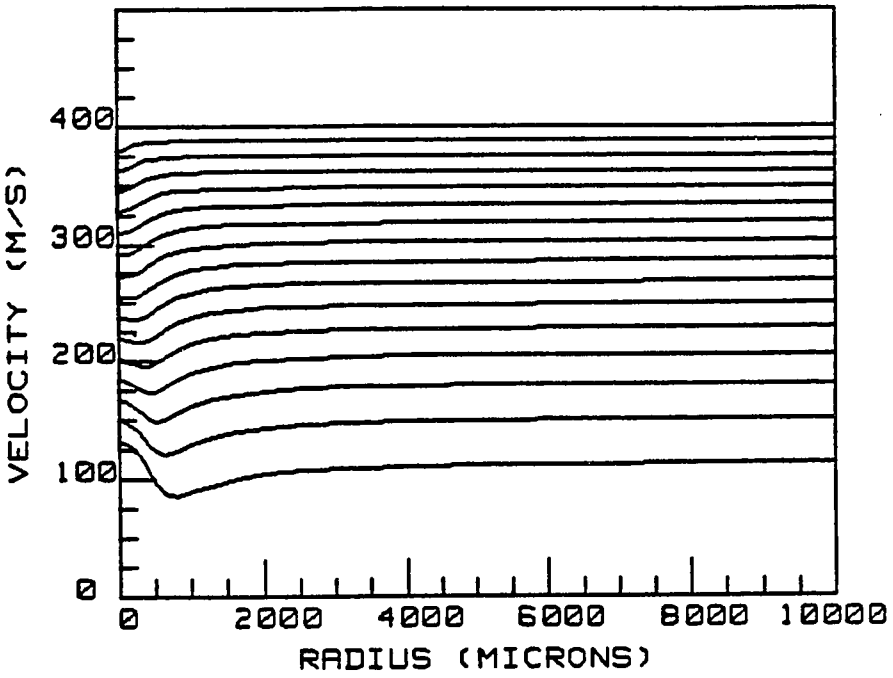

Figure 89. Effect of the standard deviation of the particulate distribution function with σ = 5.00 microns. Velocity contours of the pyroclastic particulates within the sizes ranging below 10,000 micron radius. Each line represents a contour of velocities at equal height intervals of 500 meters along the length of the established VCP.

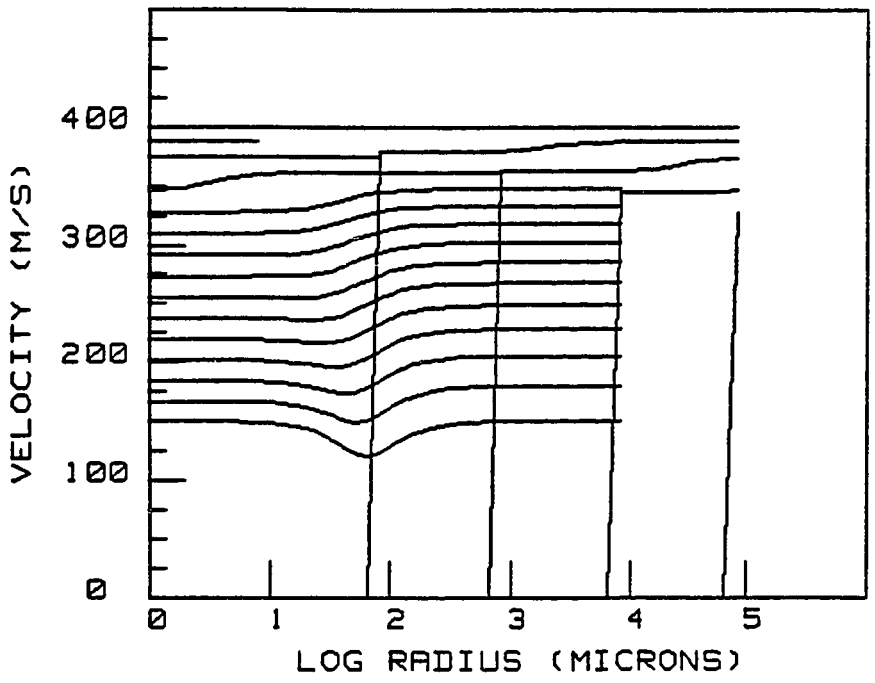

Figure 90. Effect of the standard deviation of the particulate distribution function with σ = 5.00 microns. Velocity contours of the pyroclastic particulates of the entire size distribution. Each line represents a contour of velocities at equal height intervals of 500 meters along the length of the established VCP.

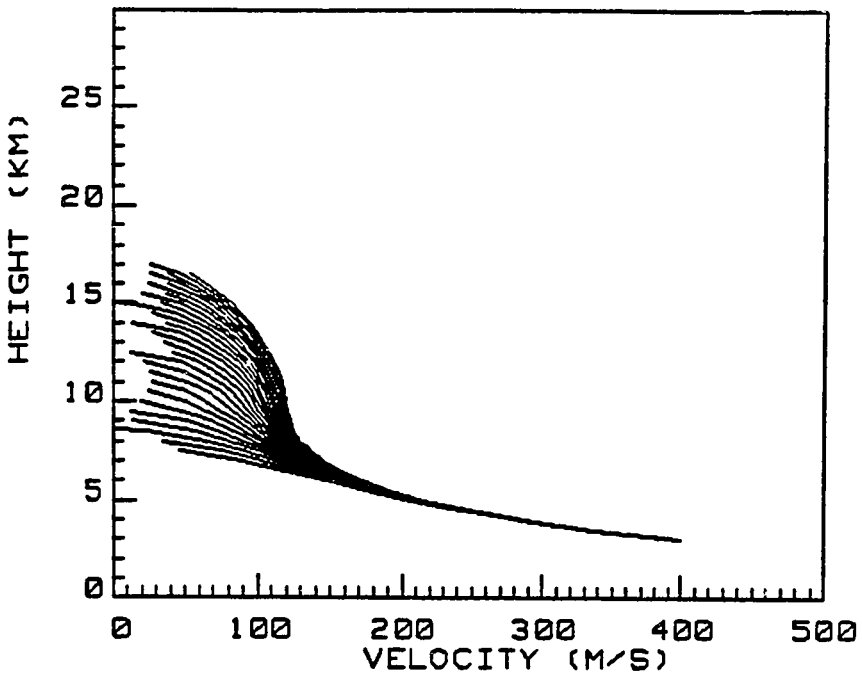

Figure 91. Effect of initial specific heat capacity of the VCP fluid upon the VCP velocity height profile. Initial specific heat capacity in the range from 500 to 3100 J/KgK in 50 J/KgK increments.

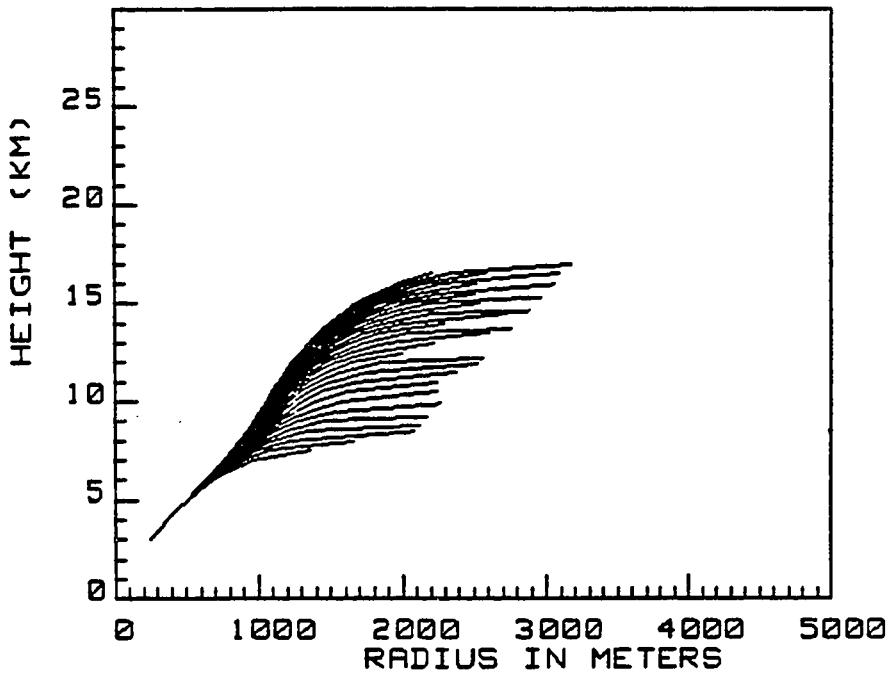

Figure 92. Effect of initial specific heat capacity of the VCP fluid upon the VCP radial profile. Initial specific heat capacity in the range from 500 to 3100 J/KgK in 50 J/KgK increments.

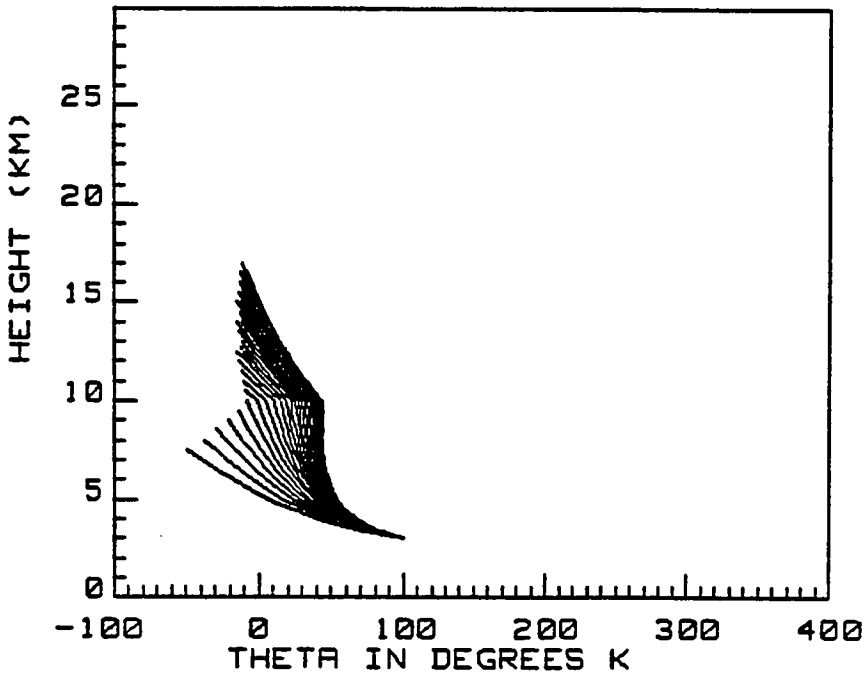

Figure 93. Effect of initial specific heat capacity of the VCP fluid upon the VCP differential temperature - height profile. Initial specific heat capacity in the range from 500 to 3100 J/KgK in 50 J/KgK increments.

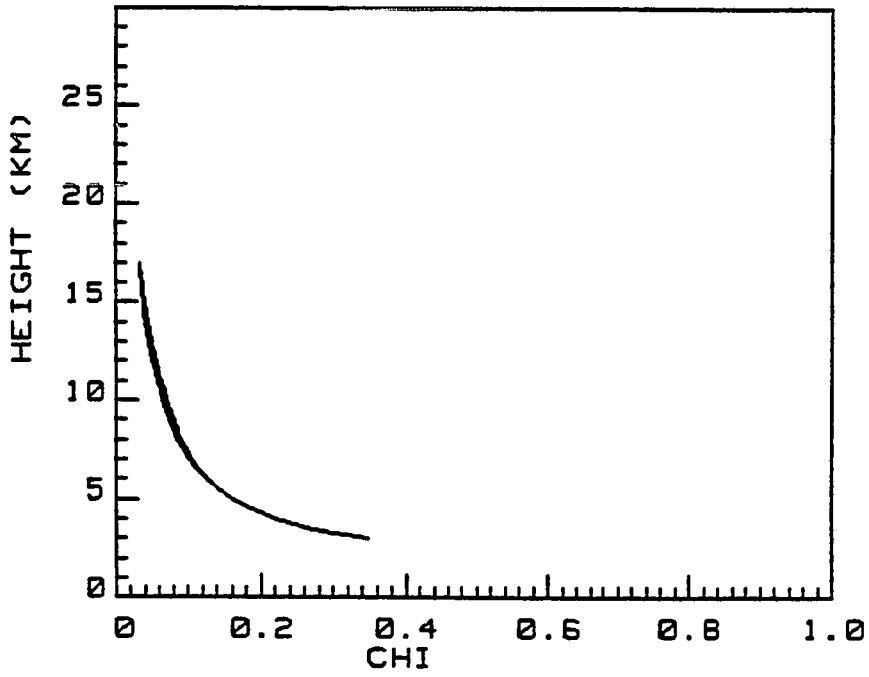

Figure 94. Effect of initial specific heat capacity of the VCP fluid upon the VCP ash fraction -height profile. Initial specific heat capacity in the range from 500 to 3100 J/KgK in 50 J/KgK increments.

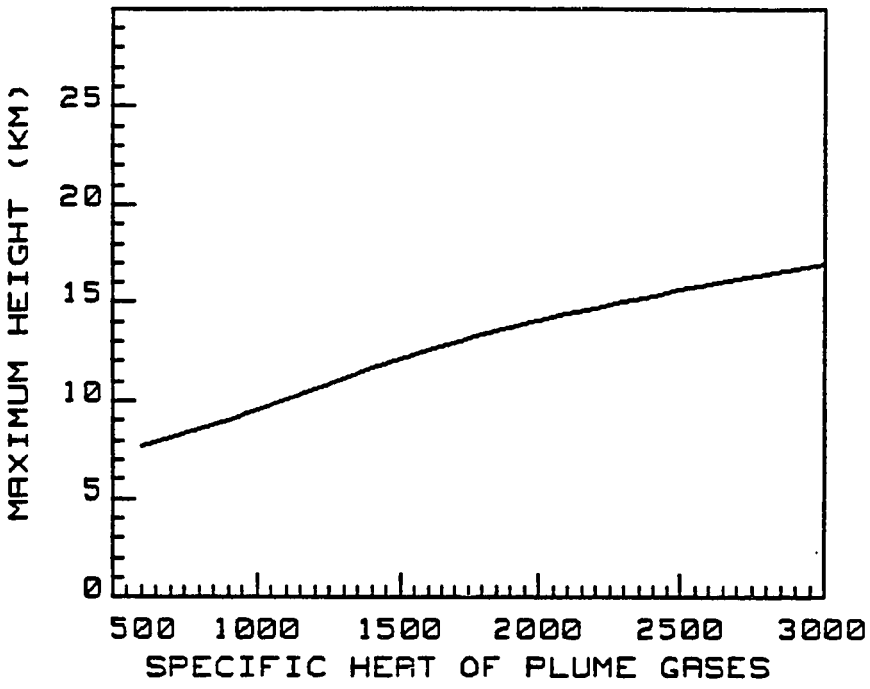

Figure 95. Effect of initial specific heat capacity of the VCP fluid upon the VCP maximum altitude. Initial specific heat capacity in the range from 500 to 3100 J/KgK in 50 J/KgK increments.

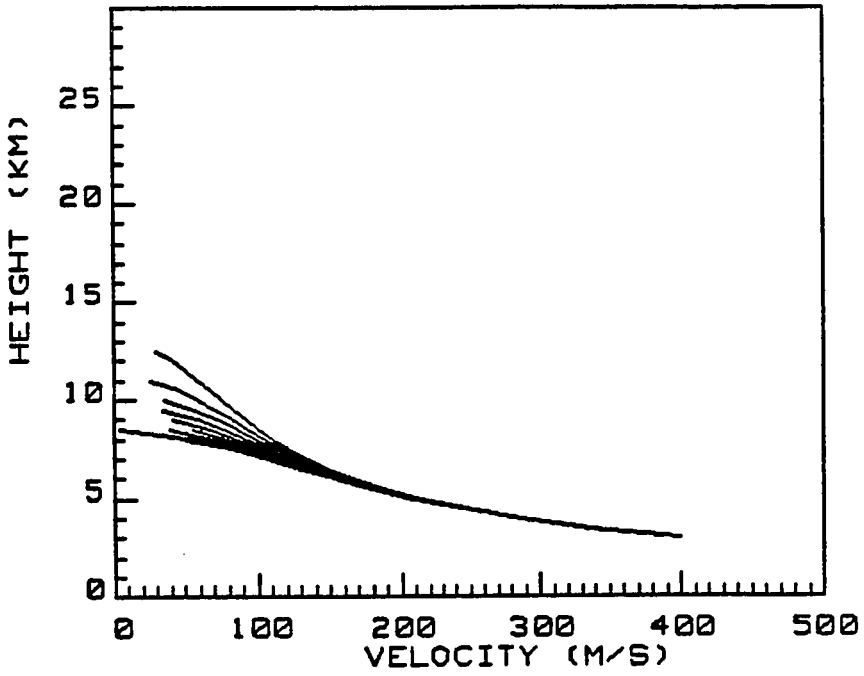

Figure 96. Effect of initial value of the stratification parameter Delta upon the VCP velocity - height profile. Initial Delta in the range from 0.10 to 0.95 in increments of 0.05.

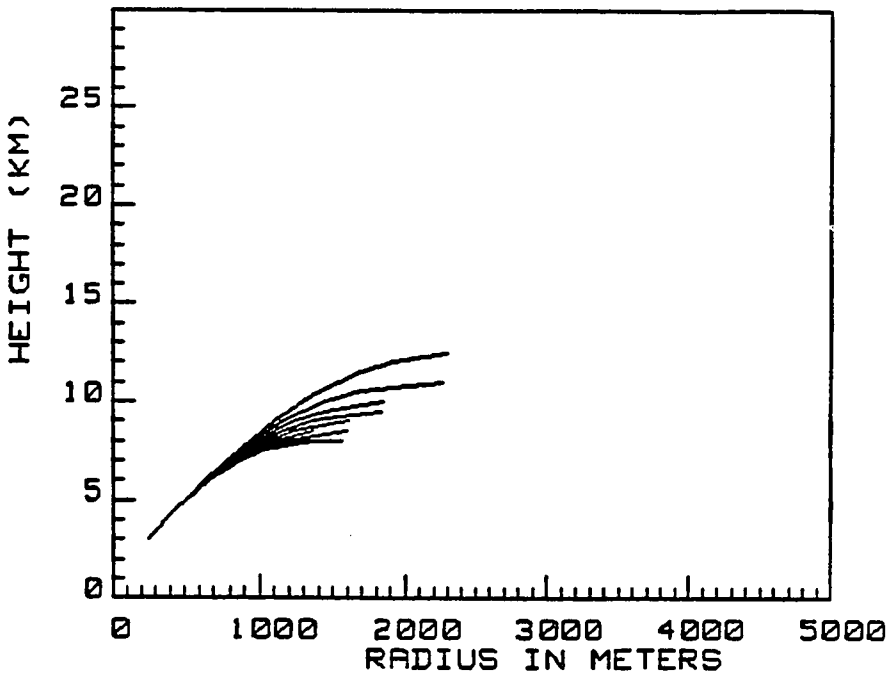

Figure 97. Effect of initial value of the stratification parameter Delta upon the VCP radial profile. Initial Delta in a range from 0.1 to 0.95 in increments of 0.05.

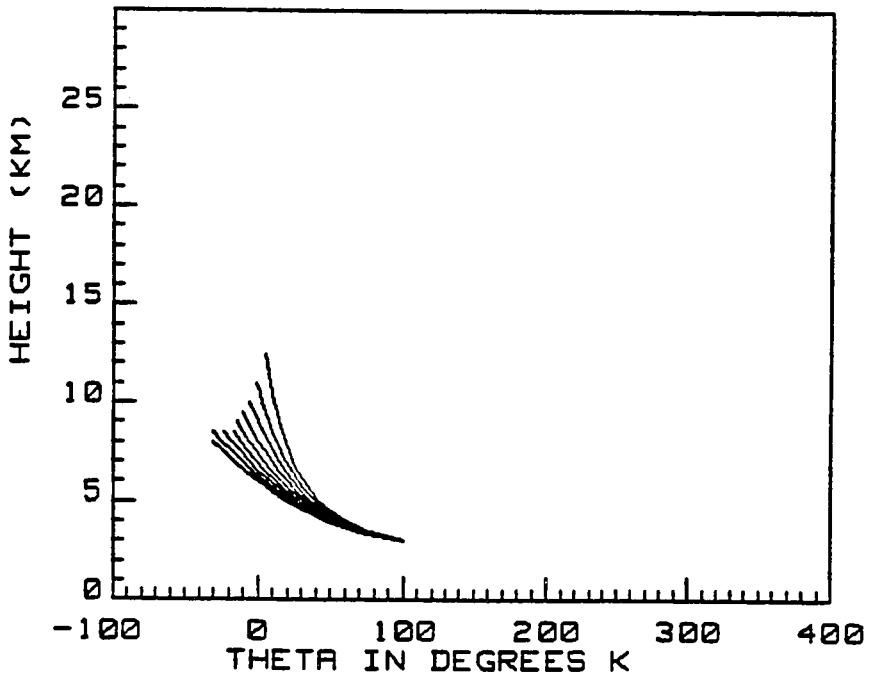

Figure 98. Effect of initial value of the stratification parameter Delta upon the VCP differential temperature - height profile. Initial Delta in a range from 0.1 to 0.95 in increments of 0.05.

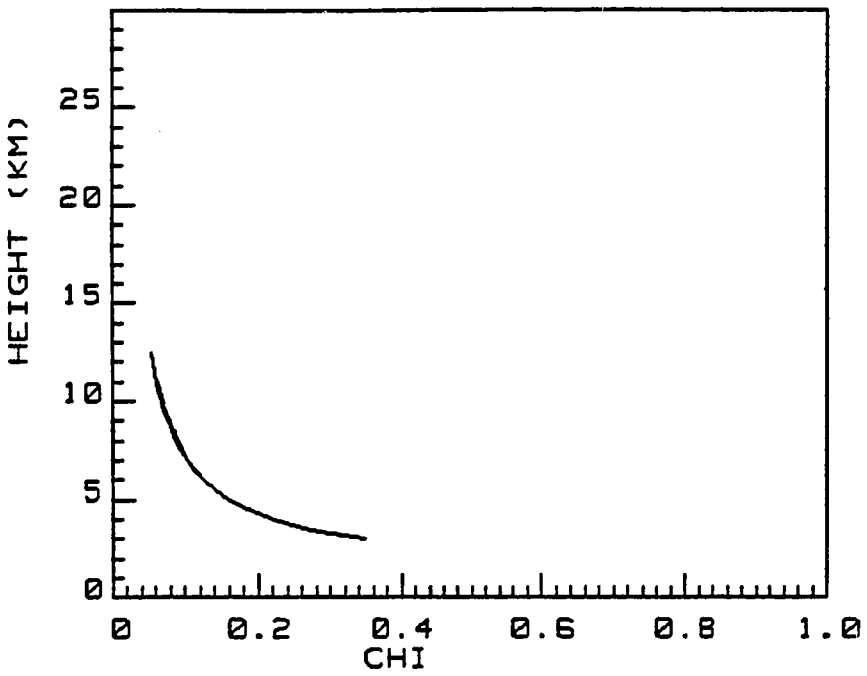

Figure 99. Effect of initial value of the stratification parameter Delta upon the VCP ash fraction - height profile. Initial Delta in a range from 0.1 to 0.95 in increments of 0.05.

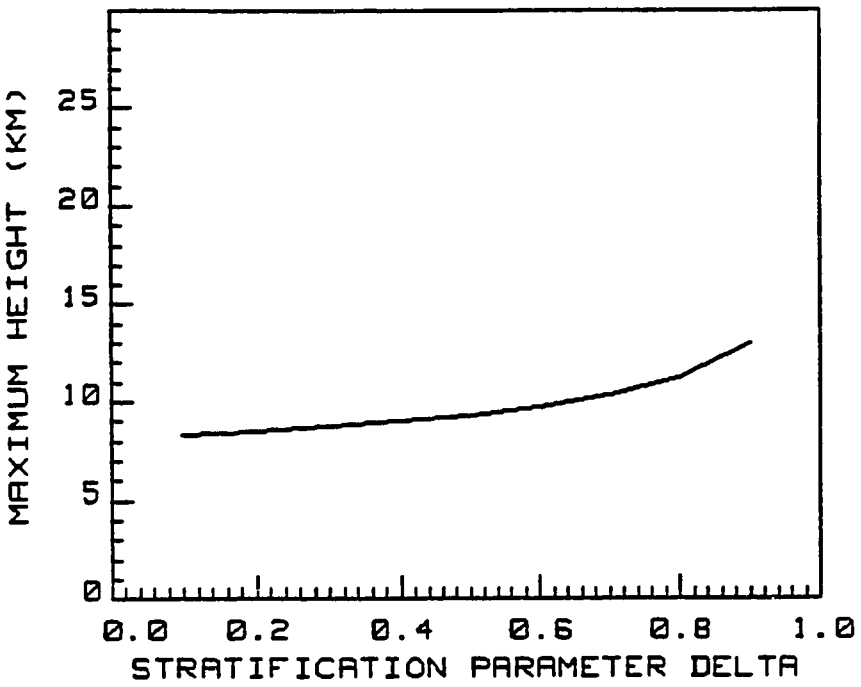

Figure 100. Effect of initial value of the stratification parameter Delta upon the VCP maximum height. Initial Delta in a range from 0.1 to 0.95 in increments of 0.05.

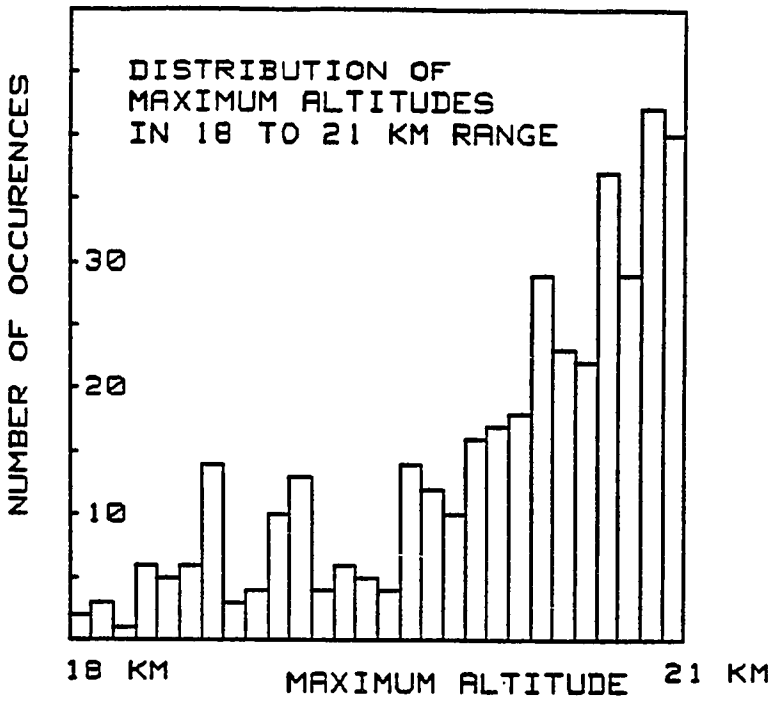

Figure 101. La Soufriere Simulation: Distribution of simulated maximum altitudes for the 449 cases. Number of occurrences plotted against the individual values for each case within the 18 to 21 kilometer maximum range.

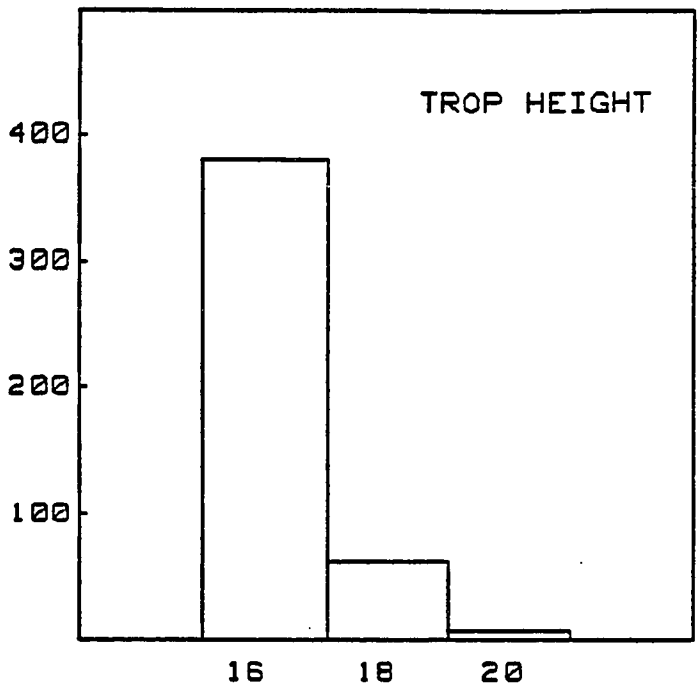

Figure 102. La Soufriere Simulation: Effect of tropopause height for the 449 cases similar to the La Soufriere event. Number of occurrences plotted against the individual values for each case within the 18 to 21 kilometer maximum range.

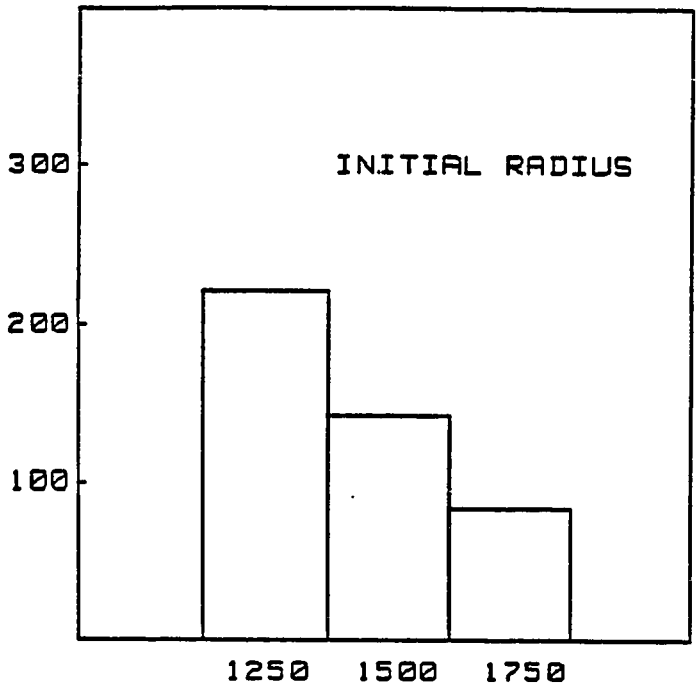

Figure 103. La Soufriere Simulation: Effect of initial radius for the 449 cases similar to the La Soufriere event. Number of occurrences plotted against the individual values for each case within the 18 to 21 kilometer maximum range.

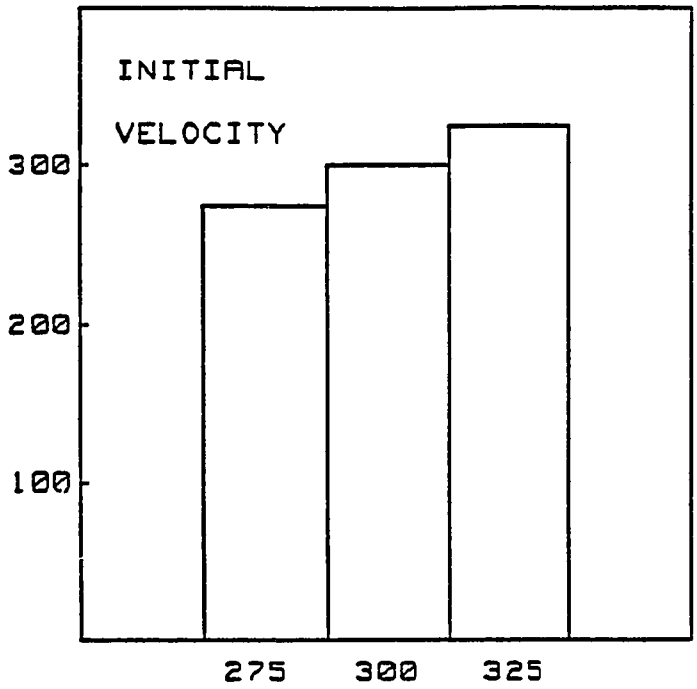

Figure 104. La Soufriere Simulation: Effect of initial velocity for the 449 cases similar to the La Soufriere event. Number of occurrences plotted against the individual values for each case within the 18 to 21 kilometer maximum range.

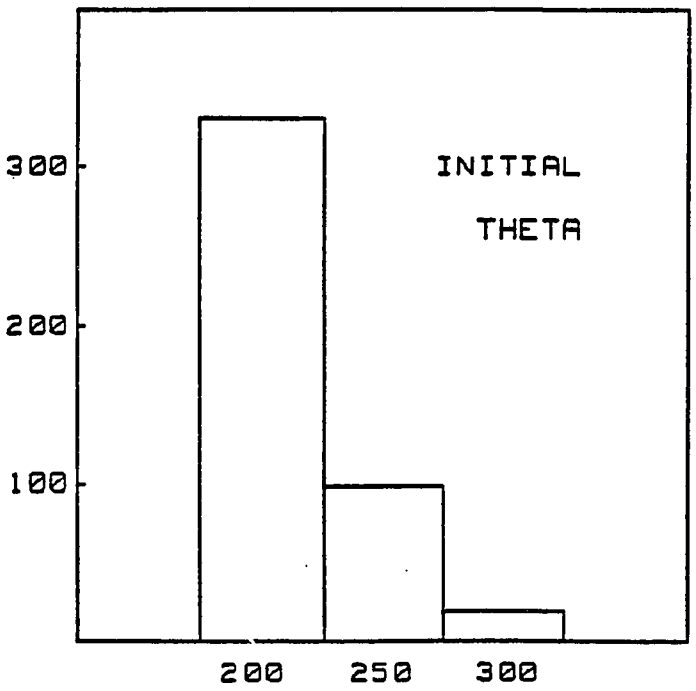

Figure 105. La Soufriere Simulation: Effect of initial differential temperature for the 449 cases similar to the La Soufriere event. Number of occurrences plotted against the individual values for each case within the 18 to 21 kilometer maximum range.

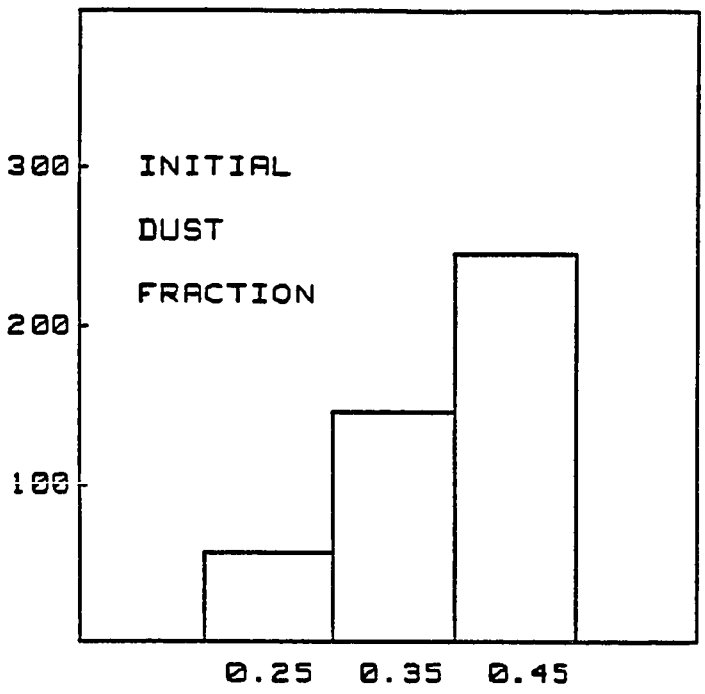

Figure 106. La Soufriere Simulation: Effect of initial ash fraction for the 449 cases similar to the La Soufriere event. Number of occurrences plotted against the individual values for each case within the 18 to 21 kilometer maximum range.

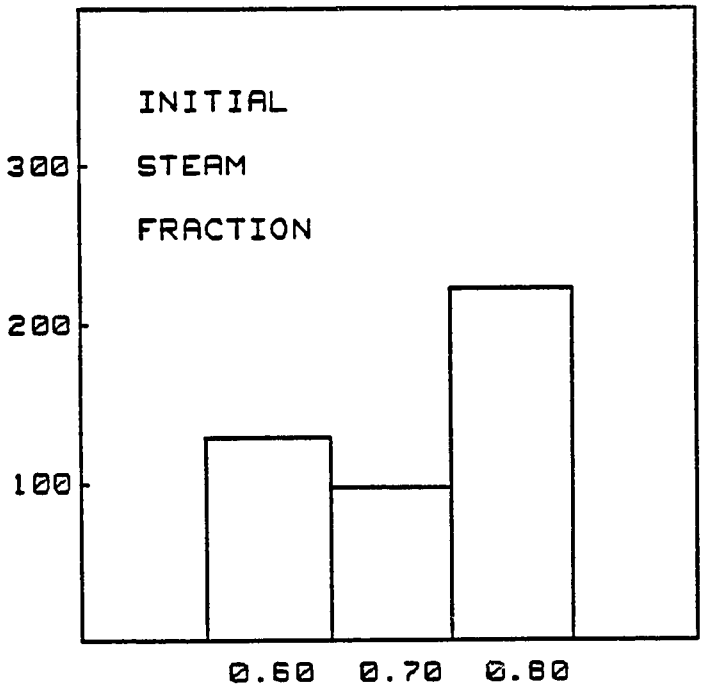

Figure 107. La Soufriere Simulation: Effect of initial steam fraction for the 449 cases similar to the La Soufriere event. Number of occurrences plotted against the individual values for each case within the 18 to 21 kilometer maximum range.

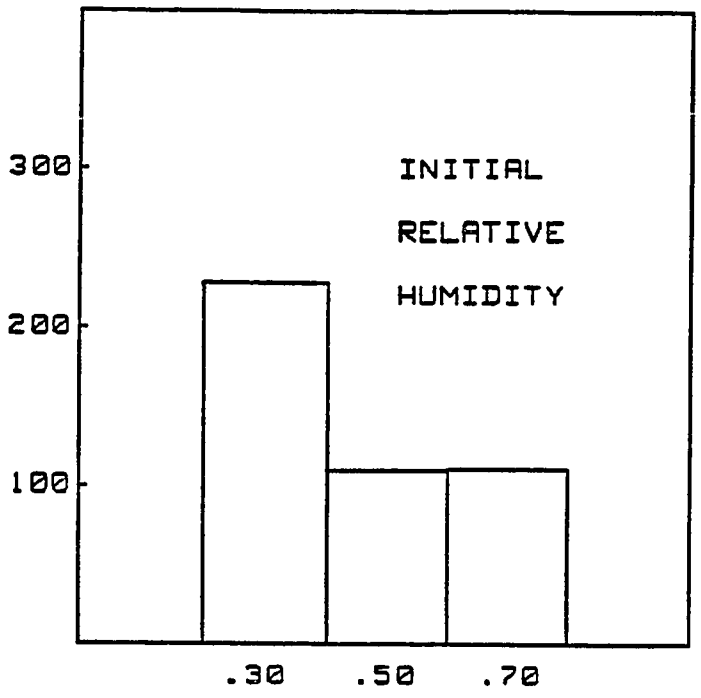

Figure 108. La Soufriere Simulation: Effect of ambient relative humidity for the 449 cases similar to the La Soufriere event. Number of occurrences plotted against the individual values for each case within the 18 to 21 kilometer maximum range.

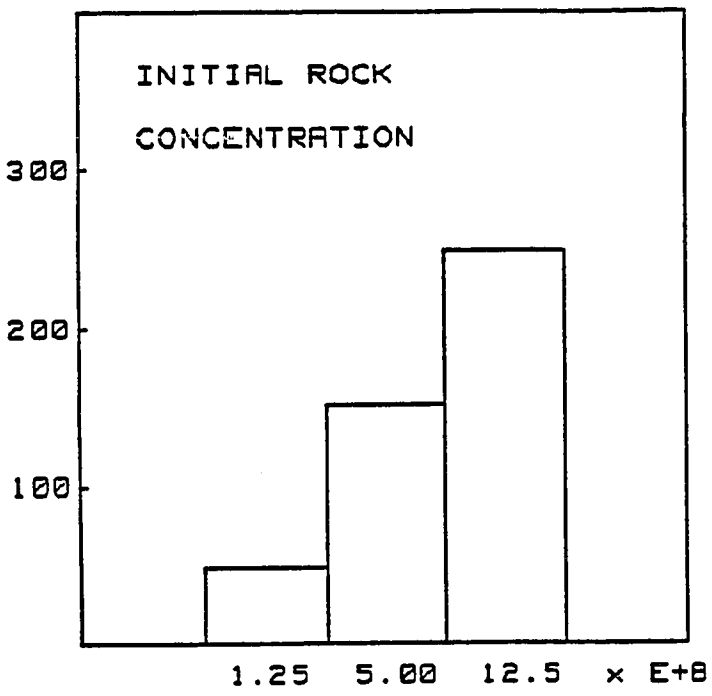

Figure 109. La Soufriere Simulation: Effect of initial pyroclastic number concentration (particles per cubic meter) for the 449 cases similar to the La Soufriere event. Number of occurrences plotted against the individual values for each case within the 18 to 21 kilometer maximum range.

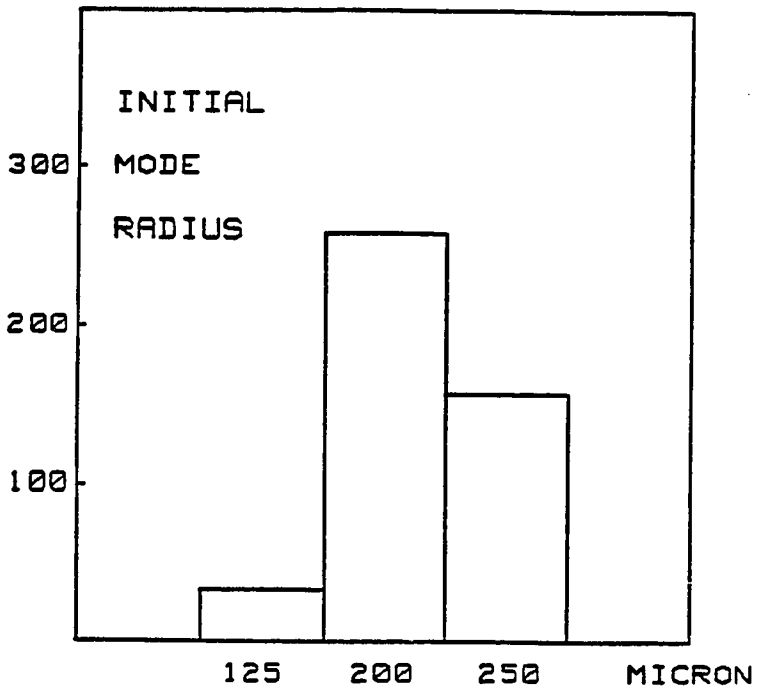

Figure 110. La Soufriere Simulation: Effect of initial mode radius of the particulate distribution for the 449 cases similar to the La Soufriere event. Number of occurrences plotted against the individual values for each case within the 18 to 21 kilometer maximum range.

References

Atkins, P. W. Physical Chemistry. San Francisco: W. H. Freeman and Company, 1978.

Barr, Sumner, and Jerome Heffter. "Meteorological analysis of the eruption of Soufriere in April 1979" Science, 216 (1982) pp 1109-1111.

Baum, Howard R., and George W. Mulholland. "Coagulation of smoke aerosol in a buoyant plume." Journal of Colloid and Interface Science, 22, No 1, (1979) pp 1-12.

Bennett, F. D. "Vaporization waves in explosive volcanism." Nature, 234 (1971)pp 538-539.

Blackburn, E. A. "Some aspects of explosive volcanism on the Earth, Moon and Mars." Ph.D. Dissertation, University of Lancaster, Lancaster U.K., 1977.

Blackburn, E. A. , L. Wilson, and R. S. J. Sparks. "Mechanisms and dynamics of strombolian activity."

Journal of the Geological Society of London, 132 (1976) pp. 429-440.

Corrsin, S. and M. S. Uberoi. "Further experiments on the flow and heat transfer in a heated air jet." National Advisory Committee for AeronauticsReport No. 998 (1950), n.p.

Crapper, P. F. "Forced plume characteristics." Tellus, 29 (1977) pp. 470-475.

Cronn, Dagmar R., and Winai Nutmagel. "Volcanic gases in the April 1979 Soufriere eruption." Science, 216 (1982) pp. 1121-1123.

Decker, Robert and Barbera Decker. Volcanoes. San Francisco: W. H. Freeman and Company, 1980.

Elder, John. The Bowels of the Earth. Oxford, London England: Oxford University Press, 1976.

Escher, B. G. "On a classification of central eruptions according gas pressure of the magma and viscosity of the lava." Liedse Geologische Medidelingen, 6 (1933) pp. 45-50.

Fox, Douglas G. "Forced plume in a stratified fluid." Journal of Geophysical Research, 75, no. 33 (1970) pp. 6818-6835.

Francis, Peter. "Giant volcanic calderas." The Scientific American, 248 no. 6 (1983) pp. 60-70.

Fudali, R. F. and W. G. Melson. "Ejecta velocities, magma chamber pressure and kinetic energy associated with the 1968 eruption of Arenal Volcano." Bulletin Volcanologique, 35-2, no.2 (1972) pp. 383-401.

Haltiner, G. J. and F. L. Martin. Dynamical and Physical Meteorology. New York: McGraw Hill Incorporated, 1957.

Hedervari, Peter. "on the energy and magnitude of volcanic eruptions." Bulletin Volcanologique, 25 (1963) pp. 373-385.

Hess, S. L. Introduction to Theoretical Meteorology. New York: Holt, Rhinehardand Winston (Henry Holt and Company), 1959.

Hinze, J. O. Turbulence. New York, New York: McGraw - Hill Incorporated, 1959.

Housley, R. M. "Modeling lunar volcanic eruptions." Proceedings of the Lunar and Planetary Society 9th Conference (1978) pp. 1473-1484.

Iribane, J. V. and W. L. Godson. Atmospheric Thermodynamics. Dordrecht,Holland: D.Riedel Publishing Company, 1981.

Kieffer, Susan Werner. "Sound speed in liquid-gas mixtures: water-air and water-steam." Journal of Geophysical Research, 82, no. 20 (1977) pp. 2895-2904.

Krauskopf, Konrad. Introduction to Geochemistry. San Francisco: McGraw -HillBook Company, 1967.

Krueger, Arther F. "Geostationary satellite observations of the April 1979 Soufriere eruptions." Science, 216 (1982) pp. 1108-1109.

List, E. J. and Jorg Imberger. "Turbulent entrainment in buoyant jets." Journal of the Hydraulics Division,

Proceedings of the American Society of Civil Engineers, 99, no. HY9 (1973) pp. 1461-1474.

McBirney, A. R. "Factors governing the intensity of explosive andesitic eruptions." Bulletin Volcanologique, 37 (1973) pp. 443-453.

McCormick, Patrick M. , G. S. Kent, G. K. Yue, and D. M. Cunnold."Stratospheric aerosol effects from Soufriere volcano as measured by the Sage Satellite System." Science, 216 (1982) pp. 1115-1118.

McGetchin, T. R. and G. W. Ullrich. "Xenoliths in maars and diatremes with inferences for the Moon, Mars, and Venus." Journal of Geophysical Research, 76 (1973) pp. 1833-1853.

Morton, B. R. "Forced plumes." Journal of Fluid Mechanics, 5 (1959) pp. 151-163.

Morton, B. R. "The ascent of turbulent forced plumes in a calm atmosphere." International Journal of Air Pollution, 1 (1959) pp. 184-197.

Morton, B. R. "The choice of conservation equations for plume models." Journal of Geophysical Research, 76, no. 30 (1971) pp. 7409-7416.

Morton, B. R. , Sir Geoffrey Taylor, and J. S. Turner. "Turbulent gravitational convection from maintained and instantaneous sources." Proceedings of the Royal Society of London A, 234 (1956) pp. 1-23.

Newhall, Christopher G. and Stephen Self. "The volcanic explosivity index (VEI): an estimate of explosive volcanism." Journal of Geophysical Research, 87, no. C2 (1982) pp 1231-1238.

Ollier, C. D. "Phreatic eruptions and maars" in Physical Volcanology, Developments in Solid Earth Geophysics Volume 6. Ed. L. Civetta, P. Gasparini,G. Luongo, and A. Rapolla. Amsterdam: Elsevier Scientific Publishing Company, 1974, pp. 289-311 (chapter 13).

Pai, S. I. , Y. Hsu, and John A. O'Keefe. "Similar explosive lunar and terrestrial volcanoes." Proceedings of the Lunar and Planetary Society 9th Conference (1979) pp. 1485-1508.

Pinnick, R. G. , J. M. Rosen and D. J. Hofmann. "Stratospheric aerosol measurements III: optical model calculations." Journal of the Atmospheric Sciences, 33 (1979) pp. 304-314.

Settle, Mark. "Volcanic eruption clouds and the thermal power output." Journal of Volcanology and Geothermal Research, 3 (1978) pp. 308-324.

Shepherd, J. B. , W. P. Aspinall, K. C. Rowley, J. Pereira, H. Sigurdsson, R.S. Fiske, and J. F. Tomblin." "The eruption of Soufriere volcano, St. Vincent, April - June 1979." Nature, 282 (1979) pp. 24-28.

Shepherd, J. B. and Haraldur Sigurdsson. "Mechanisms of the 1979 explosive eruption of Soufriere Volcano, St. Vincent." Journal of Volcanology and Geothermal Research, 13 (1982) pp. 119-130.

Sigurdsson, Haraldur. "Tephra from the 1979 Soufriere explosive eruption." Nature, 216 (1982) pp. 1106-1108.

Sigvaldason, G. E. "Chemical composition of Volcanic gases." in Physical Volcanology, Developments in Solid Earth Geophysics Volume 6. Ed. L. Civetta,P. Gasparini,

G. Luongo, and A Rapolla. Amsterdam: Elsevier Scientific Publishing Company, 1974 pp. 215-239 (chapter 6).

Singleton, O.P. and E. B. Joyce. "Cainozoic volcanicity in Victoria." Special Publication of the Geological Society of Australia, 2 (1969) pp. 145-154.

Sparks, R. S. J. and L. Wilson. "Explosive volcanic eruptions - v. observationsof plume dynamics during the 1979 Soufriere eruption, St. Vincent." Geophysical Journal of the Royal Astronomical Society, 69 (1982) pp. 551-570.

Tazieff, H. "New investigations on eruptive gases." Bulletin Volcanologique, 34 (1970) pp. 421-438.

Tennekes, H. and J. L. Lumley. A First Course in Turbulence. Cambridge, Massachussetts: The MIT Press, 1972.

Tsuya, H. "Geological and petrological studies of Volcano Fuji, 5. On the 1707 eruption of Volcano Fuji." Bulletin of the Earthquake Research Institute of Tokyo, 33 (1955) pp. 341-383.

Turner, J. S. Buoyancy Effects in Fluids. Cambridge, England: Cambridge University Press, 1979.

Walker, G. P. L. "Explosive volcanic eruptions - a new classification scheme." Geologische Rundscheau, 62 (1973) pp. 431-446.

Walker, G. P. L. "Plinian eruptions and their products." Bulletin Volcanologique, 44 - 2 (1981) pp. 223-240.

Walker, G. P. L. "Generation and dispersal of fine ash and dust by volcanic eruptions." Journal of Volcanology and Geothermal Research, 11 (1981) pp.81-92.

Walker, G. P. L. and R. Croasdale. "Grain-size characteristics of pyroclastic deposits." Journal of Geology, 79, no. 6 (1971) pp. 696-714.

Walker, G. P. L. and R. Croasdale. "Characteristics of some basaltic pyroclasts." Bulletin Volcanologique, 35 (1972) pp. 303-317.

Walker, G. P. L. , L. Wilson, and E. L. G. Bowell. "Explosive volcanic eruptions - I the rate of fall of pyroclasts." Geophysical Journal of the Royal Astronomical Society, 22 (1971) pp. 377-383.

Wilson, L. "Explosive volcanic eruptions - II the atmospheric trajectories of pyroclasts." Geophysical Journal of the Royal Astronomical Society, 30 (1972) pp. 381-392.

Wilson, L. "Explosive volcanic eruptions - III plinian eruption columns." Geophysical Journal of the Royal Astronomical Society, 45 (1976) pp. 543-556.

Wilson, L. "Relationships between pressure, volatile content, and ejecta velocity in three types of volcanic explosion." Journal of Volcanology and Geothermal Research, 8 (1980) pp. 297-313.

Wilson, L. , R. S. J. Sparks, T. C. Huang, and N. D. Watkins. "The control of volcanic column heights by eruption energetics and dynamics." Journal of Geophysical Research, 83, no. B4 (1978) pp. 1829-1835.

Wilson, L. , R. S. J. Sparks, and G. P. L. Walker. "Explosive volcanic eruptions - IV the control of magma properties and conduit geometry on eruption behavior." Geophysical Journal of the Royal Astronomical Society, 63 (1980) pp. 117-148.